Single Cell Proteomics Microchip to Profile Immune Function,

with Applications in Stem Cell Biology, Translational Disease Mechanism Study and Clinical Therapeutics Monitoring

Thesis by

Chao Ma

In Partial Fulfillment of the Requirements for the Degree of

Doctor of Philosophy

California Institute of Technology

Pasadena, California

2013

(Defended January 18th, 2012)

To my parents, and to my wife

Abstract

In response to infection or tissue dysfunction, immune cells develop into highly heterogeneous repertoires with diverse functions. Capturing the full spectrum of these functions requires analysis of large numbers of effector molecules from single cells. However, currently only 3-5 functional proteins can be measured from single cells. We developed a single cell functional proteomics approach that integrates a microchip platform with multiplex cell purification. This approach can quantitate 20 proteins from >5,000 phenotypically pure single cells simultaneously. With a 1-million fold miniaturization, the system can detect down to ~100 molecules and requires only ~10^4 cells. Single cell functional proteomic analysis finds broad applications in basic, translational and clinical studies. In the three studies conducted, it yielded critical insights for understanding clinical cancer immunotherapy, inflammatory bowel disease (IBD) mechanism and hematopoietic stem cell (HSC) biology.

To study phenotypically defined cell populations, single cell barcode microchips were coupled with upstream multiplex cell purification based on up to 11 parameters. Statistical algorithms were developed to process and model the high dimensional readouts. This analysis evaluates rare cells and is versatile for various cells and proteins. (1) We conducted an immune monitoring study of a phase 2 cancer cellular immunotherapy clinical trial that used T-cell receptor (TCR) transgenic T cells as major therapeutics to treat metastatic melanoma. We evaluated the functional proteome of 4 antigen-specific, phenotypically defined T cell populations from peripheral blood of 3 patients across 8 time points. (2) Natural killer (NK) cells can play a protective role in chronic inflammation and their surface receptor – killer immunoglobulin-like receptor (KIR) – has been identified as a risk factor of IBD. We compared the functional behavior of NK cells that had differential KIR expressions. These NK cells were retrieved from the blood of 12 patients with different genetic backgrounds. (3) HSCs are the progenitors of immune cells and are thought to have no immediate functional capacity against pathogen. However, recent studies

identified expression of Toll-like receptors (TLRs) on HSCs. We studied the functional capacity of HSCs upon TLR activation. The comparison of HSCs from wild-type mice against those from genetics knock-out mouse models elucidates the responding signaling pathway.

In all three cases, we observed profound functional heterogeneity within phenotypically defined cells. Polyfunctional cells that conduct multiple functions also produce those proteins in large amounts. They dominate the immune response. In the cancer immunotherapy, the strong cytotoxic and antitumor functions from transgenic TCR T cells contributed to a ~30% tumor reduction immediately after the therapy. However, this infused immune response disappeared within 2-3 weeks. Later on, some patients gained a second antitumor response, consisted of the emergence of endogenous antitumor cytotoxic T cells and their production of multiple antitumor functions. These patients showed more effective long-term tumor control. In the IBD mechanism study, we noticed that, compared with others, NK cells expressing KIR2DL3 receptor secreted a large array of effector proteins, such as TNF-α, CCLs and CXCLs. The functions from these cells regulated disease-contributing cells and protected host tissues. Their existence correlated with IBD disease susceptibility. In the HSC study, the HSCs exhibited functional capacity by producing TNF-α, IL-6 and GM-CSF. TLR stimulation activated the NF-κB signaling in HSCs.

Single cell functional proteome contains rich information that is independent from the genome and transcriptome. In all three cases, functional proteomic evaluation uncovered critical biological insights that would not be resolved otherwise. The integrated single cell functional proteomic analysis constructed a detail kinetic picture of the immune response that took place during the clinical cancer immunotherapy. It revealed concrete functional evidence that connected genetics to IBD disease susceptibility. Further, it provided predictors that correlated with clinical responses and pathogenic outcomes.

Table of Contents

Contents

Chapter 1

Introduction

The 21st century is the century of information. A transformation is taking place in almost every field. In biology and medicine, such a transformation leads to the emergence of "Systems Biology" and "Personalized Medicine", where massive valuable information is being generated and is starting to provide insights to understand the complexity of human biology.

Arguably, genomics is the first area in biology that benefits from this transformation. Nowadays, large scale genomics study has become commonplace in biology research. With the cost for genomic sequencing following the Moore law, it will not be long before whole genome sequencing become a common assay in the clinic. Advances in microfluidics and polymerase chain reaction (PCR) empowered this transformation. Just as what happened in the semiconductor industry, large scale integration and miniaturization enables assay replication at low cost.

Proteomics represent yet another layer of information of the cells, as cells execute the majority of their biological function by proteins. However, proteomics study poses additional challenges. Unlike DNA, protein exhibits flexible, complex three dimensional structures that is important for its function. There is still not a universal assay that can comprehensively characterize this structure. The best reagent available to specifically and sensitively target proteins is still antibody.

Immune cells protect the host against various pathogens and malignancy. They execute their functions and mediate immune response primarily by the expression and secretion of a myriad of functional proteins, collectively called cytokines. Although genetic and transcription analysis has

provided us with many insights, a direct measurement of immune functional proteomics has always been highly desirable. Traditionally, immunologists have been using surface markers characterized phenotypic information to imply immune cell function. Direct functional proteomics analysis has been limited to a very small number of cytokines, as one needs to related the measured secreted proteins back to their producer.

Motivated by this challenge, in my graduate research, we combined microfluidics and antibody microarray to develop a new single cell microchip platform, called the Single Cell Barcode Chip. This technology compares favorably to current cellular immunoassays in terms of sensitivity, multiplexing capacity, quantitation, sample size, cost and infrastructure requirements. For the first time, we are able to comprehensively visualize the T cell functional proteomics. We observed profound single cell functional heterogeneity and showed the power of our single cell proteomics approach to capture this immune functional information. We also developed analysis method to interpret the new data and showed the value of the technology in three different research directions, ranging from basic animal model studies, translational human disease mechanism study and clinical study of cancer therapy phase II clinical trial.

In the Chapter 2, I will review new technology that enables new understanding of single cell functional behavior. In Chapter 3, I will focus the Single Cell Barcode Chip, our solution for single cell proteomics analysis. I will also show proof-of-principle examples of its applications in this chapter. This work was published as a technical report in the journal Nature Medicine.

The next chapter will devote to a comprehensive study of a phase 2 cancer immunotherapy clinical trial, where we studied multiple aspects of single cell behavior of the therapeutically active antitumor T cells used in the therapy by integrating many different technical platforms. We investigated the changes in function, number, phenotype of single cells over time and time-dependent changes of blood marker abundance. This study showed that although the phenotype and frequency of these cells changed uniformly across patients over time, the function of the antitumor T cells showed dramatically

different dynamics between patients, and, the differences are associated with the differences observed in patient's clinical response. This study also points to interesting area to improve the antitumor therapy. The study is accepted as a research article in the journal Cancer Discovery.

I will show another application of our technology towards the study of cellular functional disease mechanism of inflammatory bowel disease (IBD) in Chapter 5. We started with the genetic risk factors and used those insights to draw our hypothesis that natural killer cells developed in a particular genetic environment would confer a pro-inflammatory functional trait that promote T cell activity, which in turn will lead to IBD susceptibility. Then we proved it using our single cell technology as well as other biological methods. I will talk about NK cells, their genetics, their functions, as well as their interaction with helper T cells. This study helped us establish a cellular functional mechanism that accounts for IBD susceptibility.

Finally, we will introduce the study of the hematopoietic stem cells and multi-potent progenitor cells in Chapter 6. We looked for immune effector functions of these cells and signaling pathways that lead to the cytokine production. We will also discuss the potential implications.

Chapter 2

Single Cell Proteomics for Monitoring Immune Response in Cancer Therapy: Technology, Methods and Applications

The field of targeted cancer therapeutics and immunotherapy has gone through significant maturation in recent years. For example, Ipilimumab, an antibody that blocks a T-cell function regulating surface receptor (CTLA-4) was approved by the Food & Drug Administration (FDA) for treatment of metastatic melanoma (1); Adoptive cell transfer therapy that utilizes T cells expressing transgenic T cell receptor (TCR) or chimeric antigen receptor (CAR) has demonstrated high objective response rate (>40%) in Phase II clinical trials (2); The newly approved small molecule drug, vemurafenib or PLX 4032, that targets BRAF oncogenic mutation (V600E), has been found to induce T-cell mediated antitumor response (3). Through these studies and other pre-clinical investigations, it has been increasingly recognized that immune cells play an important, yet paradoxical role in malignancy. Cytotoxic and helper T cells, natural killer cells and antigen presenting cells can mediate tumor destruction; whereas regulatory T cells, indoleamine-2.3-dyoxigenase (IDO) positive dendritic cells, and myeloid-derived suppressor cells (MDSCs) can protect malignancy (4, 5). Therefore, a deep understanding of the antitumor immune response and ways to control and maintain it are crucial for designing successful cancer therapeutics.

Immune cells execute their functions primarily through the secretion of effector or signaling proteins, jointly called cytokines. Hundreds of such molecules have been found and these cytokines can mediate a myriad of functions, from direct target killing, to self-renewal, to recruitment of other immune cell types, and to promotion or inhibition of local inflammation. Further, due to the variety of the pathogens it needs to target, cellular immunity is inherently heterogeneous at the single cell level. Individual immune cells can possess differential capacities in producing these cytokines. Therefore, a

survey of immune cell function would require the development of high-throughput, highly multiple, single-cell assays that can profile the immune functional proteomics of single cells. An additional technical difficulty, the assays should have the capacity to relate the released proteins back to their cellular producers.

In this review, we will focus on recent progresses in the development of single cell proteomics tools, with an emphasis to those that can be used as immune diagnostic and monitoring tools to cancer therapeutics. These technologies are necessarily sophisticated and generate large amounts of high-dimensional protein readouts. Therefore, advanced data modeling and analysis methods that can help interpret and visualize the readout is highly desirable. We will review these useful methods for data processing, analysis and presentation in the second section. It is exciting that several technologies have been used to study primary human samples. Pilot studies using these technologies have provided a fresh view on the functional heterogeneity of immune cells and the dynamics of antitumor immune response. Therefore we will review some of the recent applications and propose potential roles of these technologies in cancer therapy.

Single Cell Proteomics tools

Mass spectrometry in combination with liquid chromatography (MS-LC) was the first tool developed for proteomics studies. It is high-throughput and can potential reveal the full protein spectrum. Due to the limited amount of materials retrievable from single cells, the application of MS-LC towards single cells is challenging. Further, MS-LC requires input of fragmented or enzyme-digested samples and thus does not allow the recovery of viable cells for downstream usage. There have been exciting developments recently; however, the application of MS-LC in a clinical setting remains to be seen.

Flow cytometry, invented in the 1970s, is one of the most advanced, versatile tools for studying single cells in immunology. It utilizes photon detectors to measure laser-activated fluorescence signals that are emitted from cells stained by fluorophore labeled antibodies and uses fluidics to hand the individual cells. The technology can be used to profile cell surface markers, phosphorylation during intracellular signaling and, to a limited capacity, cytokine production. With the increasing number of fluorophores available, currently 20 parameters can be measured; of them, up to 5 can be cytokines. Cells can be measured at a rate of up 10,000 per second, so the technology is high-thoughput. The potentially complicated calibration procedure to compensate the spectrum overlap of fluorophores has been standardization and automated. Multiple clinical centers have established centralized flow cytometry facilities. A version of flow cytometery, called fluorescence activated cell sorting (FACS), allows retrieving live cells with desired surface properties. Currently, as many as four cell populations can be purified in parallel. However, when it comes to measuring cytokine production, this technology is less optimal, due to its limited multiplexcity (<5), the required un-physiological blockage of protein secretion and non-viability of cells analyzed.

One recent technical breakthrough along the direction of flow cytometry is mass cytometry, also known as cytometry by time-of-flight (cyTOF) (6). The technology is based on the detection of isotopes that do not naturally exist in biologically samples. Cells are stained by isotope-labeled antibodies and are then “evaporated” into clouds of molecules in the machine; thereby the isotope labeling is detected. The

application of this technology in immunology was first reported in 2011 (6). With proper combinatorial barcoding, the technology has been showed to detect 30 surface markers and 9 cytokines simultaneously. Unlike flow cytometry, whose multiplexity is limited by the overlap of fluorophore spectrum, mass cytometry can potentially detect a huge number of markers simultaneously (7). Currently, it is limited by a comparatively low-throughput and the low fraction of sample analyzable, but is expected to be improved (7). Because cells are "evaporated" during the assay, cells cannot be retrieved for downstream analysis. Thanks to many shared components and established experience available from flow cytometry, this technology grows very fast. It has been used to study the hierarchy of hematopoietic stem cell differentiation, the natural killer cell intracellular signaling and the T cell functional heterogeneity (6, 8, 9), as we will review in a later section.

The enzyme-linked immunosorbent spot (ELISpot) or fluorospot assay is a widely used quasi-single cell technique. In the assay, cells are cultured on a petri dish that is pre-coated with cytokine-specific antibodies. Cytokines released from individual cells are captured by surrounding antibodies. Subsequently, these captured cytokines are detected by applying secondary antibodies and fluorophore labels or through enzymatic reaction. After the assay, the number of spots on the petri dish, each relating to a cytokine producing cell, can be counted. It can achieve high sensitivity (<0.1%) and allows the detection of 3-5 cytokines at the same time. Because single cells are not separated when measured, the protein level cannot be quantitatively measured and single cannot be distinguished when cells are too close together.

Recent developments in microfluidics have revolutionized the traditional ELISpot assay. These microchip-based technologies utilize arrays of highly miniaturized nano- to pico-liter volume micro-chambers to achieve ultra-sensitive protein measurement and separation of single cells. Because single cells are separated in different micro-chambers, their protein levels can be quantitated in parallel. 1,000s to 10,000s micro-chambers can be integrated into one microchip, so the assay is high-throughput. The

amenability of these technologies to integrate with upstream cell purification and on-chip optical imaging further enhances their utility. Moreover, microchips are highly portable, low-cost and sample-efficient.

One version of these microchips is called the single cell barcode chip (10). It couples a microfluidics-generated antibody microarray substrate with a microfluidics chip containing a large array of micro-chambers. The antibody microarray serves to detect cytokines secreted and the microchip is designed so that there is a full panel of antibodies within each micro-chamber. During the assay, single cells are separated into these 100-picoliter size micro-chambers. Because of a 1-million fold miniaturization, the microchip can achieve ultra-sensitivity down to 100 molecules and only requires 10,000 cells as starting material. Currently, up to 20 – 40 proteins can be measured simultaneously from 5 to 10 thousand single cells (11, 12) (Fan, unpublished data). The technology has been applied across many fields, including studying adaptive, innate immune cells, hematopoietic stem cells and intracellular signaling in malignancy. In particular, this technology has been used to study the functional heterogeneity of human T cells and clinical immune responses in an adoptive cell transfer immunotherapy to metastatic melanoma.

Another version of the microchips employs the micro-engraving technique in fabricating micro-chambers (13). In this technology, 25,000 (?) nano-liter sized micro-chambers can be integrated into one chip, wherein up to 3 types of cytokines can be measured by antibody on the substrate and at the same time cells can be stained by three colors. Immune cell – target cell interaction can be measured by on-chip imaging and temporal cytokine production profile can be acquired by periodically switching the antibody substrate (13, 14). This technology also has the capacity to retrieve viable individual cells with desirable properties from the microchip, as has been showed in the case of T cell cloning (15). Moreover, it has also been used to show the discordant cytokine production dynamics in human T cells (14).

Clinical applications and future directions

The application of these new technologies has greatly advanced our understanding of the functional heterogeneity of immune cells. Initial studies (9, 10) on human T cells showed the existence of profound functional heterogeneity within a population of genetic and phenotypically similar T cells and that the level of functional heterogeneity reflects the functional activity of T cells. The functional heterogeneity has also been showed to be highly focused and the distribution of functional subsets is significantly different from a random distribution (9, 10). Thus, the functional heterogeneity contains valuable biological information, rather than pure noise.

A new insight emerges from flow cytometry and microchip analysis is that cells simultaneously secreting a large number of cytokines, called the polyfunctional cells, also secreted each of these cytokines in large amounts (11, 16, 17). Thus, they produced a predominant amount of cytokine in an immune response. One explanation of this phenomenon is that the cytokine functions are coordinated at the level of single cells. Therefore, new parameters have been defined to summarize this information of polyfunctionality (11, 16, 17). These parameters have been found to correlate with the quality of T response in human and animal models (11, 16, 17). For example, an index, named polyfunctional strength index (pSI), is developed to summarize the joint functional intensity from polyfunctional T cells and its distribution among cytokines. A recent study extensively monitored the temporal changes of antitumor T cells retrieved from metastatic melanoma patients participating in a transgenic TCR adoptive cell transfer immunotherapy. By comparing the changes in the frequency, phenotype and polyfunctionality (summarized by pSI) of these T cells, the study showed that only the functional changes are highly distinguishable among patients and that the changes correlated with the clinical outcome (11).

These studies demonstrated the importance to understand the functional heterogeneity of immune cells and its preliminary value in clinical diagnostics and monitoring. Because both the cellular immunity and tumor are heterogeneous at the single cell level, future successful cancer therapeutic scheme is necessarily personalized. Therefore, personalized diagnostic and monitoring tools, such as the single cell

functional analysis, are highly desirable and can be integrative components in different steps of cancer therapy. By understanding the functional characteristics of their immune cells, patients need to be stratified pre-treatment for the best available treatment; during the therapy, their immune response can be monitored and further intervention can be applied timely. The results obtained are feedbacks to guide further improvements of the therapy.

Chapter 3

A clinical microchip for evaluation of single immune cells reveals high functional heterogeneity in phenotypically similar T Cells (10)

Summary

Cellular immunity has an inherent high level of functional heterogeneity. Capturing the full spectrum of these functions requires analysis of large numbers of effector molecules from single cells. We report on a microfluidic platform designed for highly multiplexed (>10), reliable, sample-efficient (~10^4 cells) and quantitative measurements of secreted proteins from single cells. The platform was validated by assessment of multiple inflammatory cytokines from lipopolysaccharide-stimulated human macrophages, and comparison to standard immunotechnologies. We applied the platform towards the *ex vivo* quantitation of T cell polyfunctional diversity, via the simultaneous measurement of a dozen effector molecules secreted from tumor-antigen specific cytotoxic T lymphocytes (CTLs) that were actively responding to tumor, and compared against a cohort of healthy donor controls. We observed profound, yet focused, functional heterogeneity in active tumor-antigen specific CTLs, with major functional phenotypes quantitatively identified. The platform represents a novel and informative tool for immune monitoring and clinical assessment.

Introduction

In response to infection or tissue dysfunction, immune cells develop into highly heterogeneous repertoires with diverse functions (16, 18-24). A homeostatic makeup of these functional phenotypes dictates the overarching effect of an immune response (16, 25, 26). For example, tumor infiltrating macrophages are activated to be either pro-inflammatory or regulatory depending on their interactions with other cells within the local microenvironment (27-30). Viral infection leads to activated T cells with a large variety of effector functions as reflected by different cytokine profiles (31, 32). Thus, a comprehensive characterization of the multifunctional phenotypes of single immune cells could provide both fundamental immunobiological information and clinically relevant data (21, 33).

Common techniques for single cell protein assays include ELISpot (Fluorospot) and intracellular cytokine staining (ICS) flow cytometry (22). For ELISpot assays, typically 1-3 secreted proteins are detected at the single cell level. The approach can be quantitative for detecting cytokine secreting cells, but it is not quantitative for the secreted protein levels. ICS flow cytometry has enabled the detection of up to 5 cytokines from single cells. Measurements of polyfunctionality may provide a better indication of *in vivo* activity, relative to phenotypic classifications based upon cell surface markers (16). This implies the need for measurements of increasing numbers of functions, via multiplex protein assays, from single cells.

Herein, we report on the Single Cell Barcode Chip (SCBC), for the high-content assessment of functional heterogeneity at the single cell level. The chip is comprised of 1,040 3-nanoliter volume microchambers, and each loaded with single cells or small defined numbers of cells. Protein levels are measured using immuno-sandwich assays from a spatially encoded antibody barcode. A full barcode represents a complete panel of protein assays, and duplicate barcodes per microchamber enable measurement statistics at the single cell level. The SCBC permits on-chip, highly multiplexed detection of sub-thousand copies of proteins and requires only ~10^4 cells to perform the assay.

The technique was validated using a human macrophage cell line to demonstrate single cell detection of multiple cytokines. We then implemented it to assay the polyfunctionality of tumor-antigen-specific T cells in the setting of an adoptive cell transfer (ACT) therapy clinical trial for melanoma. We observed focused, yet highly heterogeneous, functional diversity compared to samples from healthy donor controls. The SCBC is a high-throughput, low-cost, and portable platform that can find a wide range of fundamental and clinical applications in understanding disease mechanism and therapeutics.

RESULTS

Single cell barcode chip: design rationale and detection limit

The SCBC system consists of four modules (**Figure 1**): microchannels that contain cells, control valves that isolate cells into microchambers, inlet and outlet ports for the introduction and depletion of reagents and cells, and a barcode-encoded glass substrate for protein detection. The chip itself consists of two PDMS layers, and fits onto a microscope slide (**Figure 1a**). The lower PDMS layer has inlets for the loading of reagents and cells which branch into 80 microchannels of 100 μm × 17 μm cross-section. Thirteen sets of vertical valves on the top PDMS layer divide those microchannels into 1,040 nanoliter-volume microchambers. For a microchamber containing 1-10 cells, the cell density is $0.3\text{-}3\times10^{6}$ cells ml^{-1}, falling into the normal range for culture conditions and physiological environments (34).

The barcode array is a pattern of parallel stripes, each coated with a distinctive antibody. The stripe width is 25 μm at a pitch of 50 μm. To achieve high and consistent antibody loading, and to prevent antibody denaturation during microfluidics assembly, the DNA-encoded antibody library (DEAL) approach (34), coupled with microchannel-guided flow patterning (35), was utilized (**Supplementary Figure 1**). The chemistry and reproducibility of the DNA barcode patterning process has been previously described (35-37). The SCBC barcodes contain 13 stripes, 12 for assaying a dozen different proteins, and one as a control and spatial reference. Two sets of barcodes are included per microchamber. Cells are randomly loaded so that each SCBC microchamber contains zero to a few cells, following a Gamma Poisson distribution (Goodness-of-Fit test: $P > 0.8$. **Supplementary Figure 2**). The numbers of cells in each chamber are counted via imaging (**Figure 1b**).

We determined the dynamic range and detection limit of our design by performing on-chip immunoassays with recombinant proteins (**Figure 1c**). The barcode array initially consists of 13 uniquely designed orthogonal DNA strands labeled in order as A through M (**Supplementary Table 1)**. Prior to loading recombinant proteins, a cocktail containing all capture antibodies conjugated to different complementary DNA strands (A'—L') is used to transform, via DNA-hybridization, the DNA barcode

into an antibody array (**Figure 1c**). As few as 10^2-10^3 copies (10^{-22}-10^{-21} mol) could be detected (3 standard deviations), with a dynamic range of 3-4 orders of magnitude (**Figure 1e, Supplementary Figure 3**), which is compatible with single cell secretion measurements (34). Antibody loading, and thus assay sensitivity, is uniform across the whole chip (coefficient of variation (C.V.) <10%) (**Figure 1d–e**).

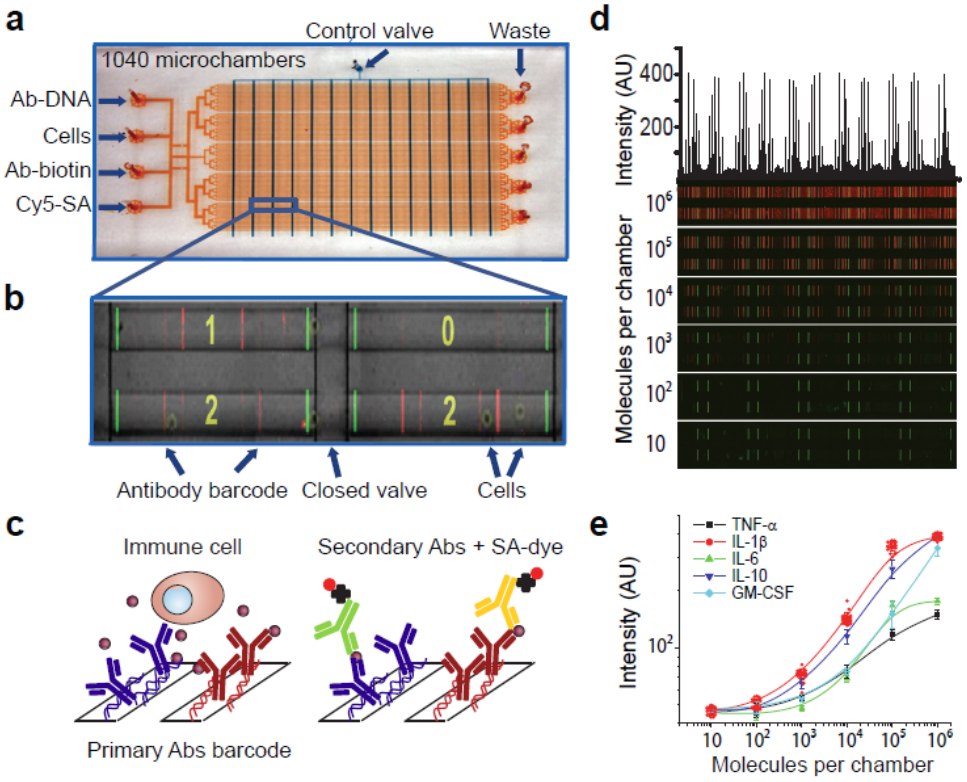

Figure 1 Design of the Single Cell Barcode Chip (SCBC) for single cell protein secretome analysis. (**a**) Image of an SCBC in which flow channels are shown in red and the control channels are shown in blue. Input and output ports are labeled. (**b**) An optical micrograph showing cells loaded and isolated within the microchambers, overlaid with the fluorescence micrograph of the developed assay barcode for those same microchambers. Numbers of cells per microchamber are indicated by the yellow numbers. (**c**) Drawing of the multiplex DEAL 1^o antibody barcode array used for capture of secreted proteins from single cells and then developed for the detection of those proteins. (**d**) Scanned fluorescent images used for the antibody barcode calibration measurements using spiked recombinant proteins. The protein concentrations (in numbers of molecules per chamber) are given to the left of each row of images. The

plot at the top is a line profile of the top row of images, and represents the reproducibility of the barcodes across the antibody array of an SCBC. (**e**) Recombinant protein calibration curves for TNF-α, IL-1β, IL-6, IL-10 and GM-CSF. Individual measurements (red) are shown for IL-1β. Other proteins measurements are represented by average intensity values and standard deviations.

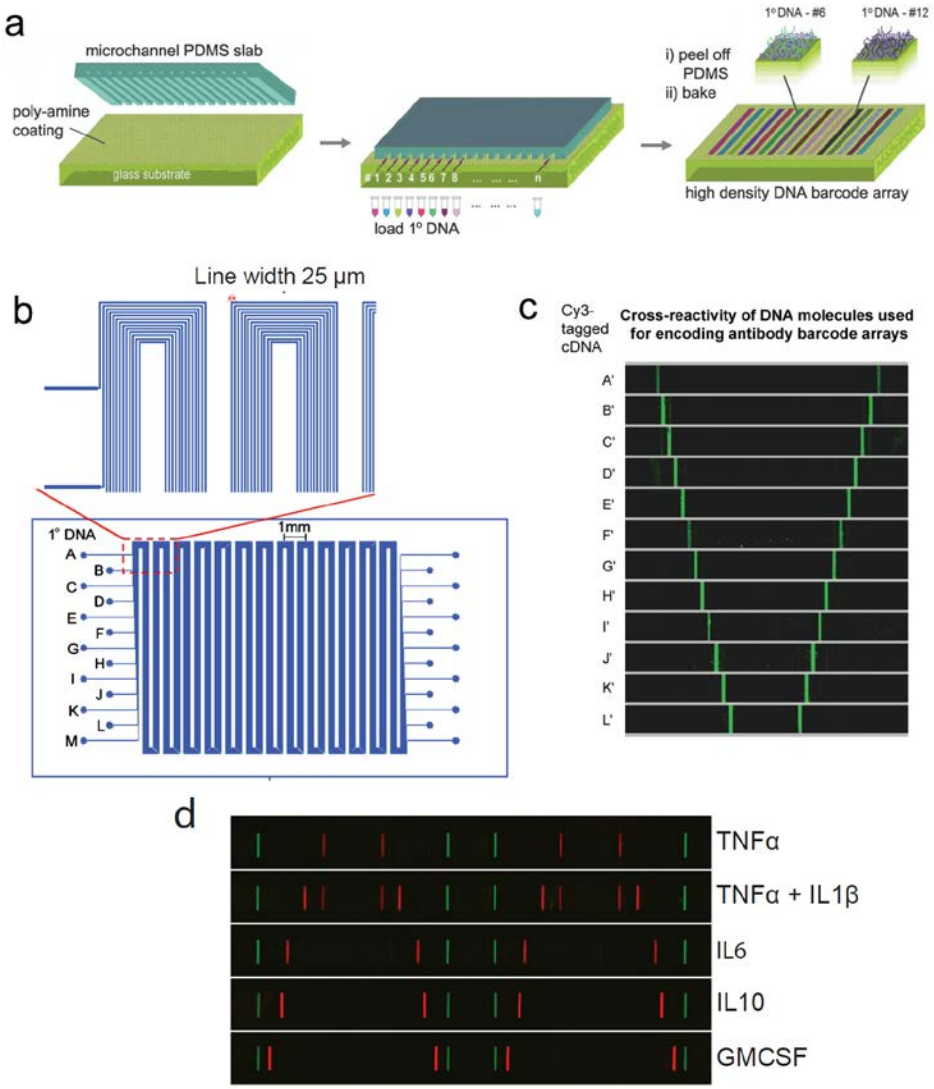

Supplementary Figure 1 Fabrication of the DNA barcode array. (a) Schematic illustration of the microchannel-guided flow patterning techniques. **(b)** AutoCAD design of the photolithographic mask

used for patterning a high-density DNA barcode array. A-M are the labels of primary DNA molecules. **(c)** Test result for hybridization to individual fluorescent Cy3-labeled complementary DNA showing negligible cross-reactivity (<1% in photon counts). **(d)** individual channels flowed by different recombinant proteins.

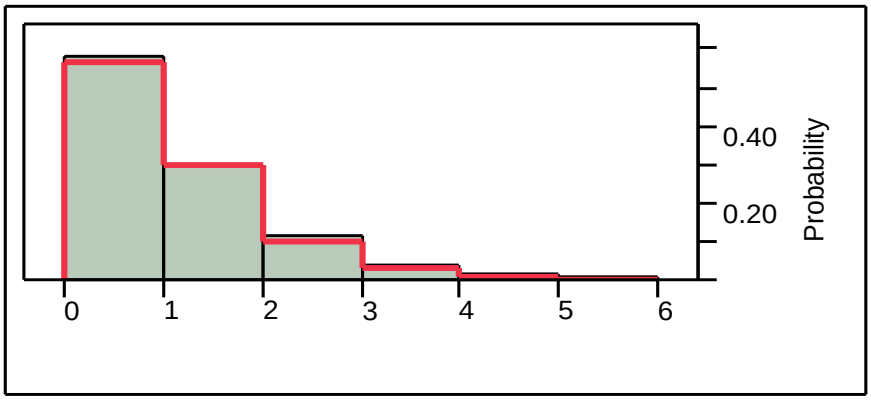

Gamma Poisson

(0.61912,1.17662)

Goodness-of-Fit Test p=0.9124

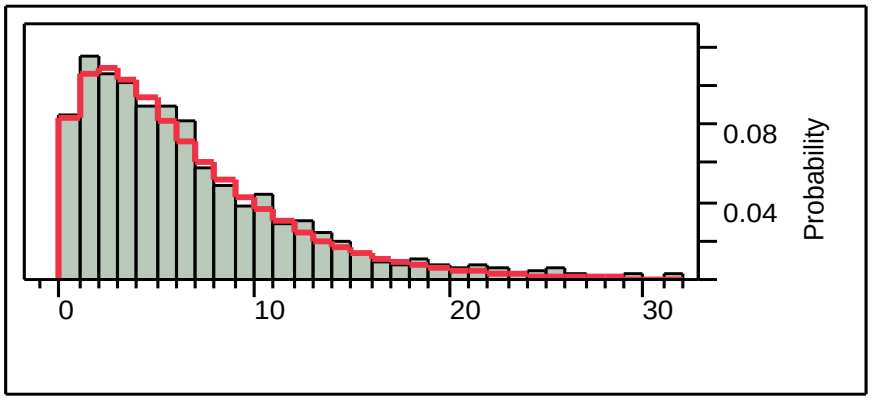

Gamma Poisson (5.89223,4.64461)

Goodness-of-Fit Test p=0.8482

Supplementary Figure 2 Distribution of number of cells across the whole chip, fitted to Gamma Poisson distribution.

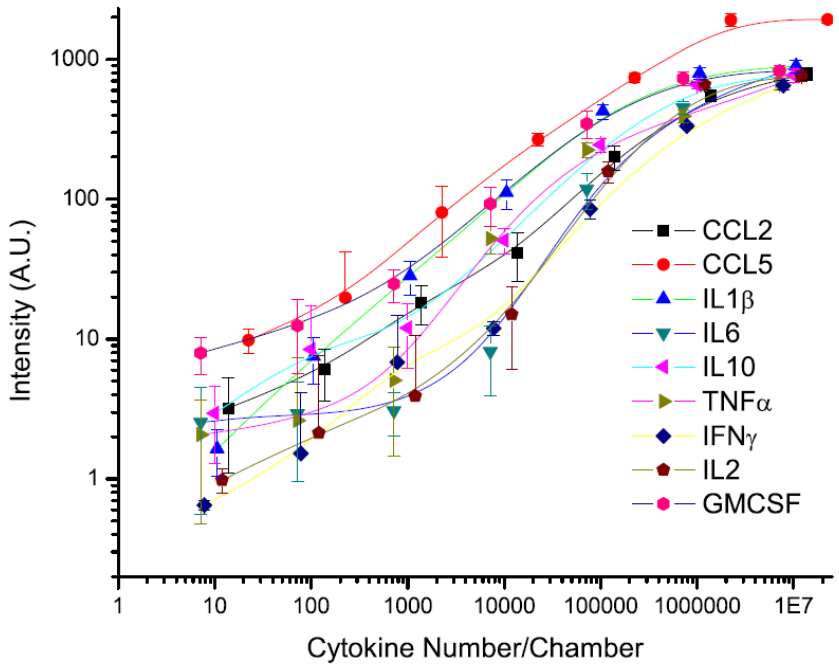

Supplementary Figure 3 Fluorescence quantitation curves for proteins measured from T cells.

Supplemental Table 1. Sequences and terminal functionalization of oligonucleotides*.

Name	Sequence	Melting Point
A	5'- AAA AAA AAA AAA AAT CCT GGA GCT AAG TCC GTA-3'	57.9
A'	5' NH3- AAA AAA AAA ATA CGG ACT TAG CTC CAG GAT-3'	57.2
B	5'-AAA AAA AAA AAA AGC CTC ATT GAA TCA TGC CTA -3'	57.4
B'	5' NH3AAA AAA AAA ATA GGC ATG ATT CAA TGA GGC -3'	55.9
C	5'- AAA AAA AAA AAA AGC ACT CGT CTA CTA TCG CTA -3'	57.6
C'	5' NH3-AAA AAA AAA ATA GCG ATA GTA GAC GAG TGC -3'	56.2
D	5'-AAA AAA AAA AAA AAT GGT CGA GAT GTC AGA GTA -3'	56.5

D'	5' NH3-AAA AAA AAA ATA CTC TGA CAT CTC GAC CAT -3'	55.7
E	5'-AAA AAA AAA AAA AAT GTG AAG TGG CAG TAT CTA -3'	55.7
E'	5' NH3-AAA AAA AAA ATA GAT ACT GCC ACT TCA CAT -3'	54.7
F	5'-AAA AAA AAA AAA AAT CAG GTA AGG TTC ACG GTA -3'	56.9
F'	5' NH3-AAA AAA AAA ATA CCG TGA ACC TTA CCT GAT -3'	56.1
G	5'-AAA AAA AAA AGA GTA GCC TTC CCG AGC ATT-3'	59.3
G'	5' NH3-AAA AAA AAA AAA TGC TCG GGA AGG CTA CTC-3'	58.6
H	5'-AAA AAA AAA AAT TGA CCA AAC TGC GGT GCG-3'	59.9
H'	5' NH3-AAA AAA AAA ACG CAC CGC AGT TTG GTC AAT-3'	60.8
I	5'-AAA AAA AAA ATG CCC TAT TGT TGC GTC GGA-3'	60.1
I'	5' NH3-AAA AAA AAA ATC CGA CGC AAC AAT AGG GCA-3'	60.1
J	5'-AAA AAA AAA ATC TTC TAG TTG TCG AGC AGG-3'	56.5
J'	5' NH3-AAA AAA AAA ACC TGC TCG ACA ACT AGA AGA-3'	57.5
K	5'-AAA AAA AAA ATA ATC TAA TTC TGG TCG CGG-3'	55.4
K'	5' NH3-AAA AAA AAA ACC GCG ACC AGA ATT AGA TTA-3'	56.3
L	5'-AAA AAA AAA AGT GAT TAA GTC TGC TTC GGC-3'	57.2
L'	5' NH3-AAA AAA AAA AGC CGA AGC AGA CTT AAT CAC-3'	57.2
M	5'-Cy3-AAA AAA AAA AGT CGA GGA TTC TGA ACC TGT-3'	57.6
M'	5' NH3-AAA AAA AAA AAC AGG TTC AGA ATC CTC GAC-3'	56.9

* all oligonucleotides were synthesized by Integrated DNA Technology (IDT) and purified via high performance liquid chromatography (HPLC).

Analysis of cytokine production by LPS-stimulated macrophages

We validated the SCBC by using the human monocyte cell line, THP-1. The THP-1 cells were differentiated into cytokine-producing macrophages using phorbol 12-myristate 13-acetate (PMA). Before loading into the device, lipopolysaccharide (LPS) was added to activate the Toll-like Receptor-4 (TLR4) signaling (38, 39), a process that mimics the innate immune response to Gram-negative bacteria (**Supplementary Figure 4**). For these experiments, the antibody barcode was designed to measure 12 proteins: tumor necrosis factor-α (TNF-α), interferon-γ (IFN-γ), interleukin-2 (IL-2), IL-1α, IL-1β, IL-6, IL-10, IL-12, granulocyte macrophage-colony stimulating factor (GM-CSF), chemokine (C-C motif) ligand-2 (CCL-2/MCP-1), transforming growth factor-β (TGF-β), and prostate specific antigen (PSA) (**Supplementary Table 2**).

The microchambers contained between 0-40 cells so that both single cell behavior and signals from a population could be measured. Through an automated image processing algorithm, we quantified the fluorescence intensities for each protein from each microchamber. For chambers with cells centered between the two barcodes, measurements from the barcode replicates are consistent (C.V. < 15%, **Figure 2**). Un-centered cells contribute to variance between replicates (C.V. up to 50%); however, averages of the barcode replicates from chambers with centered and un-centered cells are indistinguishable ($P > 0.2$, **Supplementary Figure 5**). Furthermore, measurements between chips displayed good consistency ($P > 0.2$).

The intensities of the individual proteins, averaged over many individual SCBC microchamber measurements, agreed with measurements of those same proteins from cell culture supernatants (**Figure 2a**). Secretome data, when binned according to the numbers of cells per chamber, yielded statistically distinct protein signals ($P < 0.05$, **Figure 2b and Supplementary Figure 6**). However, the reference signal was insensitive to the numbers of cells ($P > 0.2$, **Figure 2b and Supplementary Figure 6**). Most notably, single cell protein signals can be clearly detected ($P < 0.0001$, **Figure 2b and Supplementary Figure 6**). Clear separation of secreting and non-secreting cells is also visualized by multiple peaks in the

histograms provided in **Figure 2c**.

The fraction of cells detected to secrete a given protein was gated using background signals from empty chambers. The frequency of TNF-α, IL-1β, IL-10 and GM-CSF producing cells were measured to be similar by both SCBC and by ICS flow cytometry (**Figure 2c and Supplementary Figure 6**). Furthermore, the measured fraction of cells in each quadrant also shows a good similarity between the two techniques (**Figure 2c and Supplementary Figure 6**). Thus, the SCBC platform can efficiently provide a functional profiling of single immune cells.

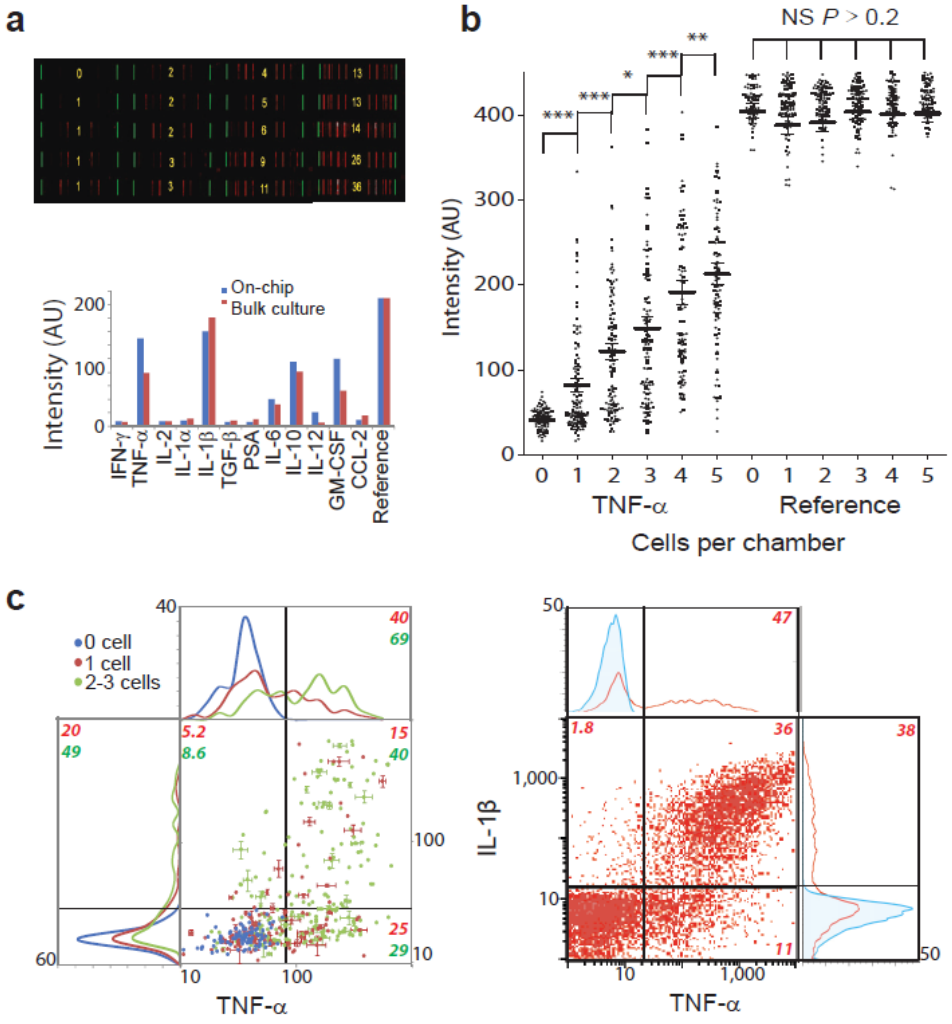

Figure 2. On chip secretion measurements of macrophage differentiated from THP-1 monocyte cell. (**a**) Left. Representative scanned images of barcode signals from individual chambers. Green bars

represent microchamber boundaries, red bars are protein signals, and the yellow numbers indicate the number of cells. Right. Comparison of averaged intensity from SCBC measurements and bulk culture supernatant. Data is normalized so that references have the same intensity. (**b**) Scatterplots of measured levels of TNF-α and the reference control, for individual microchambers containing n = 0,1,2,3,4,5 cells. P values are calculated by comparing neighboring columns (* $P < 0.005$; ** $P < 0.001$; *** $P < 0.0001$; NS not significant.). (**c**) Scatterplots of TNF-α v.s. IL-1β derived from SCBC measurements (left) and from ICS coupled with flow cytometry (right). Histograms (frequency v.s. intensity) for the individual protein are provided at the top and sides of the scatterplots. All y-axis units are fluorescence intensity. For the SCBC data, each quadrant is labeled with numbers that reflect the % of single cells (red) and 2-3 cells (green) in that section. The gates separating cytokine secreting and non-secreting cells are determined from 0 cell microchamber (background) measurements (blue). Standard deviations from barcode replicates of the same chamber are provided for selected points (see text for selection criteria). For the ICS measurements the gates were determined by isotype control staining.

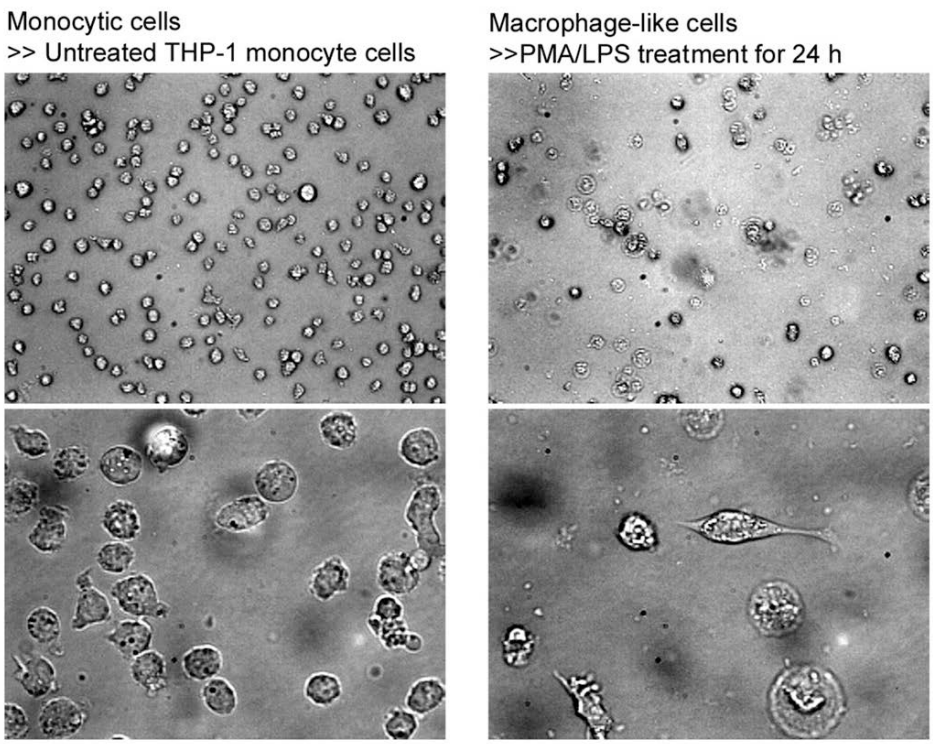

Supplementary Figure 4 Morphology change of THP-1 cell upon PMA/LPS activation. The upper panels are lower magnification optical images and the lower panels are viewed at a higher magnification. The morphological change from non-adherent to adherent phenotypes was observed upon PMA/LPS treatment.

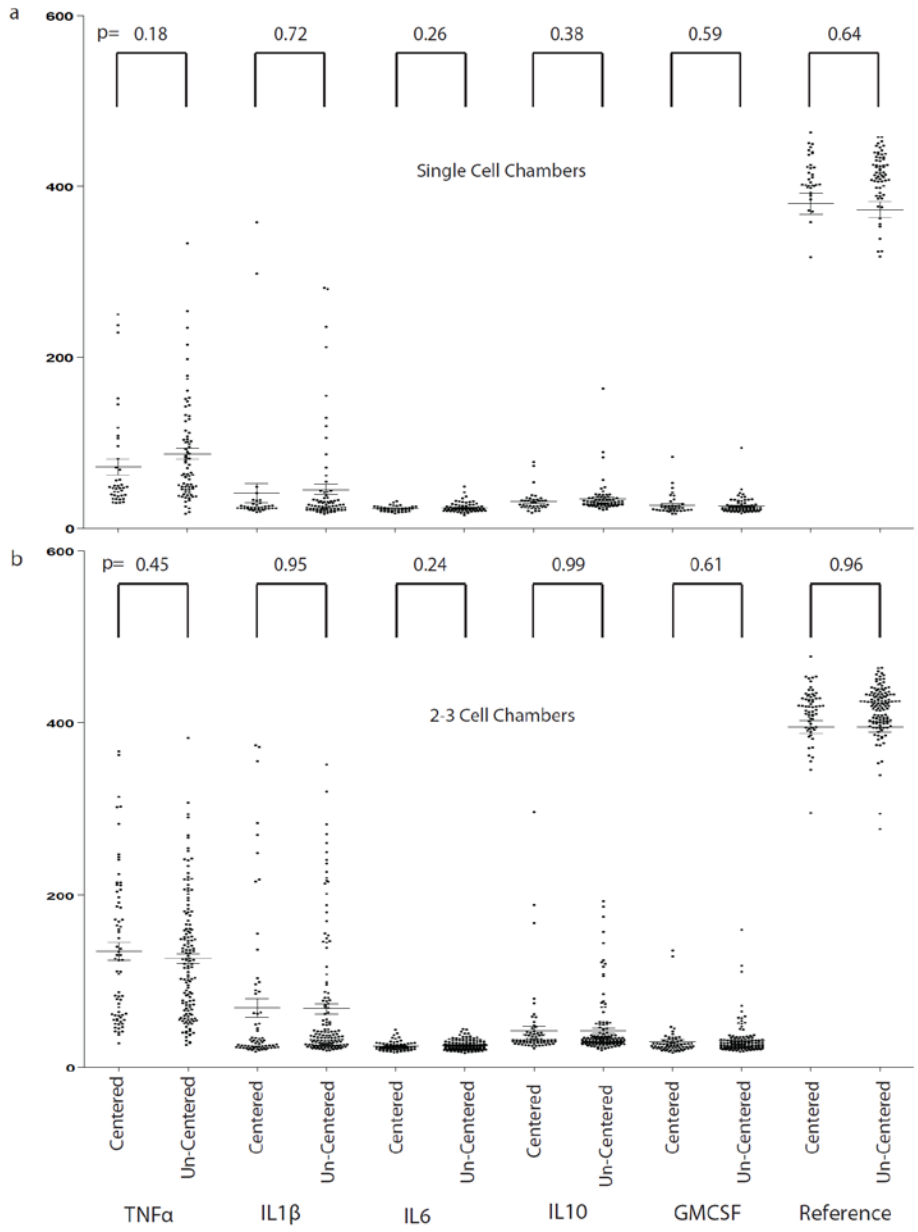

Supplementary Figure 5 Averaged signals detected from cells located in middle of the chamber vs. cells on the edge (p>0.2).

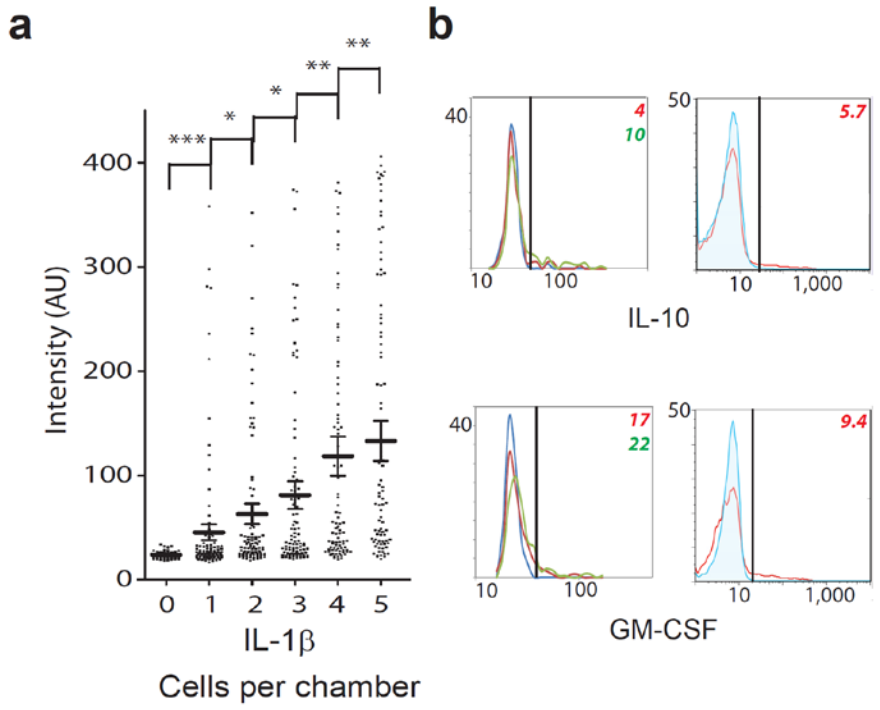

Supplementary Figure 6 On chip secretion measurements of macrophage differentiated from THP-1 monocyte cell. (**a**) Scatterplots of measured levels of IL-1β, for individual microchambers containing *n* = 0,1,2,3,4,5 cells. *P* values are calculated by comparing neighboring columns (* $P < 0.005$; ** $P < 0.001$; *** $P < 0.0001$; NS not significant.). (**b**) Histogram comparisons of SCBC and ICS for IL10 and GMCSF.

Supplementary Table 2. Summary of antibodies used for macrophage experiments.

DNA label	primary antibody (vendor: clone)	secondary antibody (vendor: clone)
A'	mouse anti-hu IFN-γ (eBio: MD-1)	biotin-labeled mouse anti-hu IFN-γ (eBio: 4S.B3)
B'	mouse anti-hu TNF-α (eBio: Mab1)	biotin-labeled mouse anti-hu TNF-α (eBio: Mab11)
C'	mouse anti-hu IL-2 (eBio: MQ1-17H12)	biotin-labeled mouse anti-hu IL-2 (eBio: polyclonal)
D'	mouse anti-hu IL-1α (eBio: CRM8)	biotin-labeled mouse anti-hu IL-1α (eBio: CRM6)
E'	mouse anti-hu IL-1β (eBio: CRM56)	biotin-labeled mouse anti-hu IL-1β (eBio: CRM57)
F'	mouse anti-hu TGF-β (eBio: TB2F)	biotin-labeled mouse anti-hu TGF-β (eBio: 16TFB)
G'	mouse anti-hu PSA (BioDesign: S6)	biotin-labeled mouse anti-hu PSA (BioDesign: S2)
H'	mouse anti-hu IL-6 (eBio: MQ2-13A5)	biotin-labeled mouse anti-hu IL-6 (eBio: MQ2-39C3)
I'	mouse anti-hu IL-10 (eBio: JES3-9D7)	biotin-labeled mouse anti-hu IL-10 (eBio: JES3-12G8)

J’	mouse anti-hu IL-12(p70) (eBio: BT21)	biotin-labeled mouse anti-hu IL-12 (eBio: C8.6)
K’	mouse anti-hu GM-CSF (BD)	biotin-labeled mouse anti-hu GM-CSF-γ (BD) **
L’	mouse anti-hu MCP-1(eBio: 5D3-F7)	biotin-labeled mouse anti-hu MCP-1(eBio: 2H5)

**** BD OptEIA ELISA Set, Catalog No. 555126.**

Analysis of poly-cytokine production by human cytotoxic T lymphocytes

We now turn towards utilizing the SCBC to functionally profile antigen specific CTLs, which are the main effector cell type of an adaptive immune response targeting intracellular pathogens and tumors (40). CTLs can exhibit a great diversity of antigen specificities, phenotypic surface proteins, and functions. Capturing this diversity is a significant challenge. Previous data suggests that the ability of CTLs to produce multiple cytokines (polyfunctionality) correlates with protective immune responses *in vivo* (16, 41, 42).

We assayed the functional diversity of healthy donor CD8+ T cells (n = 3), MART-1-specific T cell receptor (TCR) transgenic cells harvested from the peripheral blood of a patient with metastatic melanoma participating in an adoptive cell transfer (ACT) immunotherapy clinical trial, and of *ex vivo* expanded tyrosinase-specific T cells. TCR engineering provides a means to generate large quantitites of antigen-specific T cells amenable to use for the therapy of cancer (43). The TCR transgenic cells collected from peripheral blood of a patient had been previously generated *in vitro* by retroviral vector transduction to insert the two chains of a TCR specific for MART-1, then expanded *ex vivo* for two days followed by re-infusion into the patient after a lymphodepletion conditioning regimen. The patient then received three vaccinations with dendritic cells pulsed with a MART-1 peptide and high dose IL-2 to further activate and expand the cells *in vivo*. Peripheral blood mononuclear cells (PBMCs) were harvested on day 30 following re-infusion by leukapheresis, at a time when multiple metastatic melanoma lesions were responding to this therapy. The tyrosinase-specific T cell culture was generated *ex vivo* from a tyrosinase-specific cell culture obtained by peptide/HLA-A0201 tetramer based selection followed by non-specific expansion with CD3 antibody and IL-2 to obtain a population of non-transgenic but uniform antigen-specific T cells.

PBMCs were enriched for CD3 markers by negative magnetic beads selection before sorting on DEAL-based CD8 antibody or peptide/HLA-A0201 tetramer coated microarrays (44). Then $CD3^+CD8^+$ or $CD3^+tetramer^+$ cells were released from the microarrays. The released T cells underwent activation

either by polyclonal TCR engagement of CD3 and CD28 antibody binding or antigen-specific TCR engagement via tetramer and CD28 antibody, respectively. Activation and SCBC loading was completed within 5 minutes. To maximize the percentage of single cell measurement to 25-40%, ~10^4 sorted T cells in 5μl media were loaded into the device. Protein heat maps and plots that compare and contrast these different T cell groups are presented in **Figure 3**. Multiple markers that indicate functions such as cytoxicity (perforin), T cell growth and differentiation (IL-2), apoptosis promotion (TNF-α, IFN-γ), inflammation (IL-1β, IL-6, TNF-β), anti-inflammation (IL-10), and the stimulation and recruitment of other immune compartments (CCL-2/MCP-1, CCL-3/MIP-1α, CCL-5/RANTES, GM-CSF) (42), were included in the T cell panel (**Figure 3 and Supplementary Table 3**).

More than 20% (median) of the healthy donor $CD3^+CD8^+$ T cells produced TNF-α, IL-6 and three chemokines CCL-2, CCL-3 and CCL-5. The MART-1-specific TCR transgenic cells that were inducing an objective tumor response *in vivo* exhibited a wide range of positive functions demonstrated by the release of perforin, IL-1β, IL-10, IFN-γ, IL-2 and CCL-5 upon *ex vivo* antigen restimulation with the MART-1/HLA-A0201 tetramer. The functionality of the antigen-specific patient-derived TCR transgenic cells was higher compared to the healthy donor lymphocytes in terms of both signal intensity and fraction of positive cells (**Figure 3a-b, e**). The frequency of cytokine-producing cells among the patient-derived TCR transgenic cells was consistent with Fluorospot results (**Figure 3d**). Phenotyping results identified by flow cytometry on surface markers of T cell phenotype (**Figure 3c**) illustrated that the population of patient-derived TCR transgenic MART-1-specific cells was mostly homogeneous; the principal (>90%) population these cells was $CD8^+$ and had a phenotype consistent with effector T_{EMRA} cells at a late differentiation stage (**Figure 3c**) (31). In comparison, the *ex vivo* expanded tyrosinase-specific T cells exhibited decreased production of CCL-3, IL-6 and TNF-α. Consistent with the notion that *ex vivo* expansion of T cells by IL-2 and CD3 antibody results in terminal differentiation of T cells, the tyrosinase-specific T cell clone had elevated release of perforin, IL-1β and IL-2, compared to healthy control samples, upon exposure to their cognate antigen (**Figure 3e and Supplementary Figure 7**).

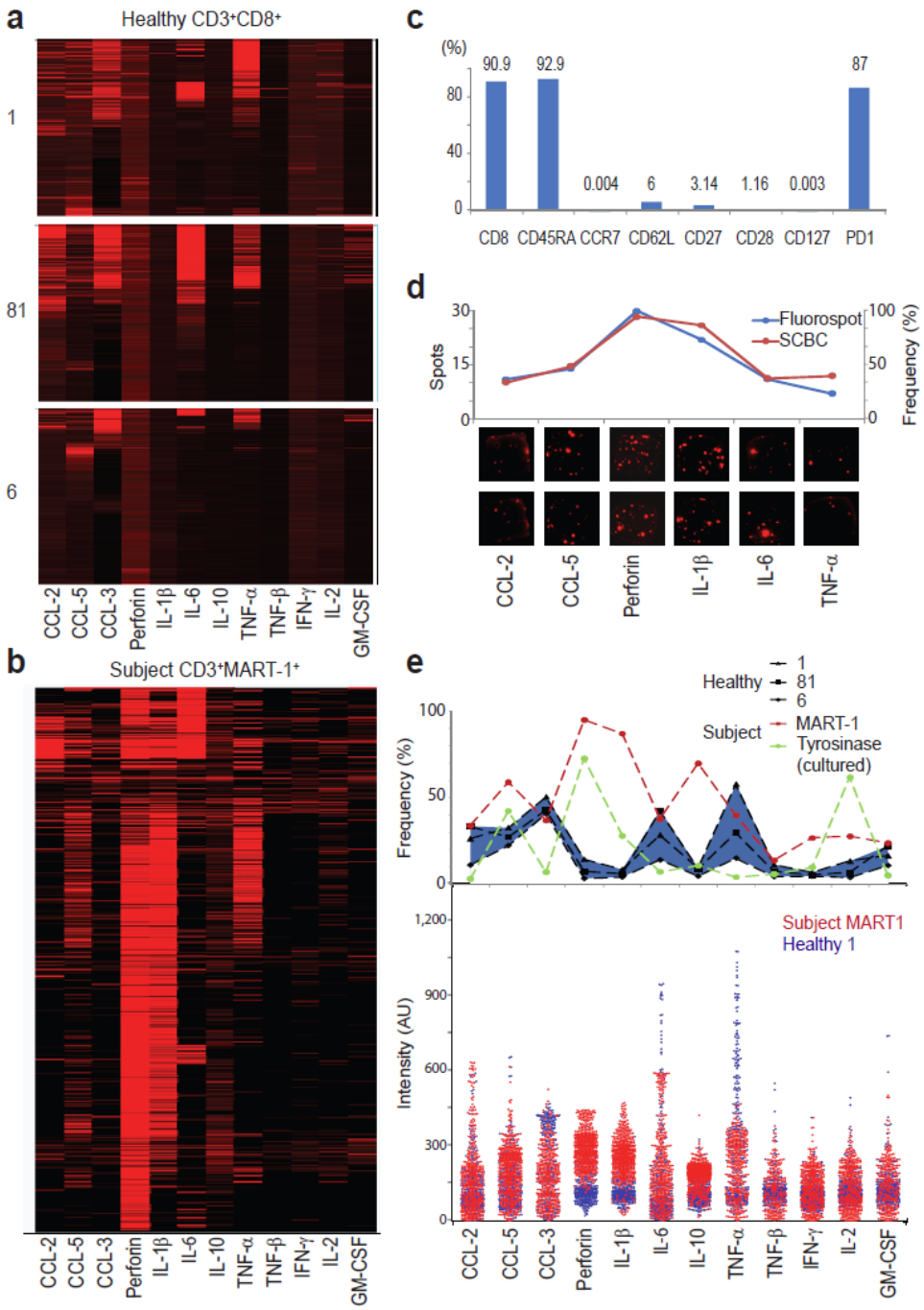

Figure 3 Single cell secretion measurements of CTLs from melanoma patients and healthy donors. (**a**) Unsupervised clustering of CD8+ T cells from three healthy donors, presented as a heat map. Each row represents a measurement of 12 secreted cytokines from a single cell, with protein labels provided at the bottom. (**b**) Data from MART-1-specific TCR transgenic CTLs single cell experiments, presented as a heat map organized via unsupervised clustering. The fluorescence intensity scale for all 4 heat maps is the

same. (**c**) Phenotyping data from flow cytometry for MART-1-specific TCR transgenic CTLs. Each bar shows the percentage of cells positive for the specific surface marker. (**d**) Fluorospot analysis of the MART-1-specific TCR transgenic T cell population. The curves on top compare SCBC and Fluorospot measurements on fraction (or number) of cells secreting CCL-2, CCL-5, perforin, IL-1β, IL-6 and TNF-α. Representative Fluorospot images are provided below. (**e**) Univariate comparison of patient-derived antigen specific TCR transgenic T cells and healthy donor CD8+ T cell culture controls. The lines of the top plot represent the percentage of cytokine producing cells from each sample. Blue area shows the range detected from healthy donor samples. The one-dimensional scatter plot on the bottom compares the signal intensities measured from the patient's MART-1-specific TCR transgenic T cells and the CD8+ T cell background from one representative healthy donor.

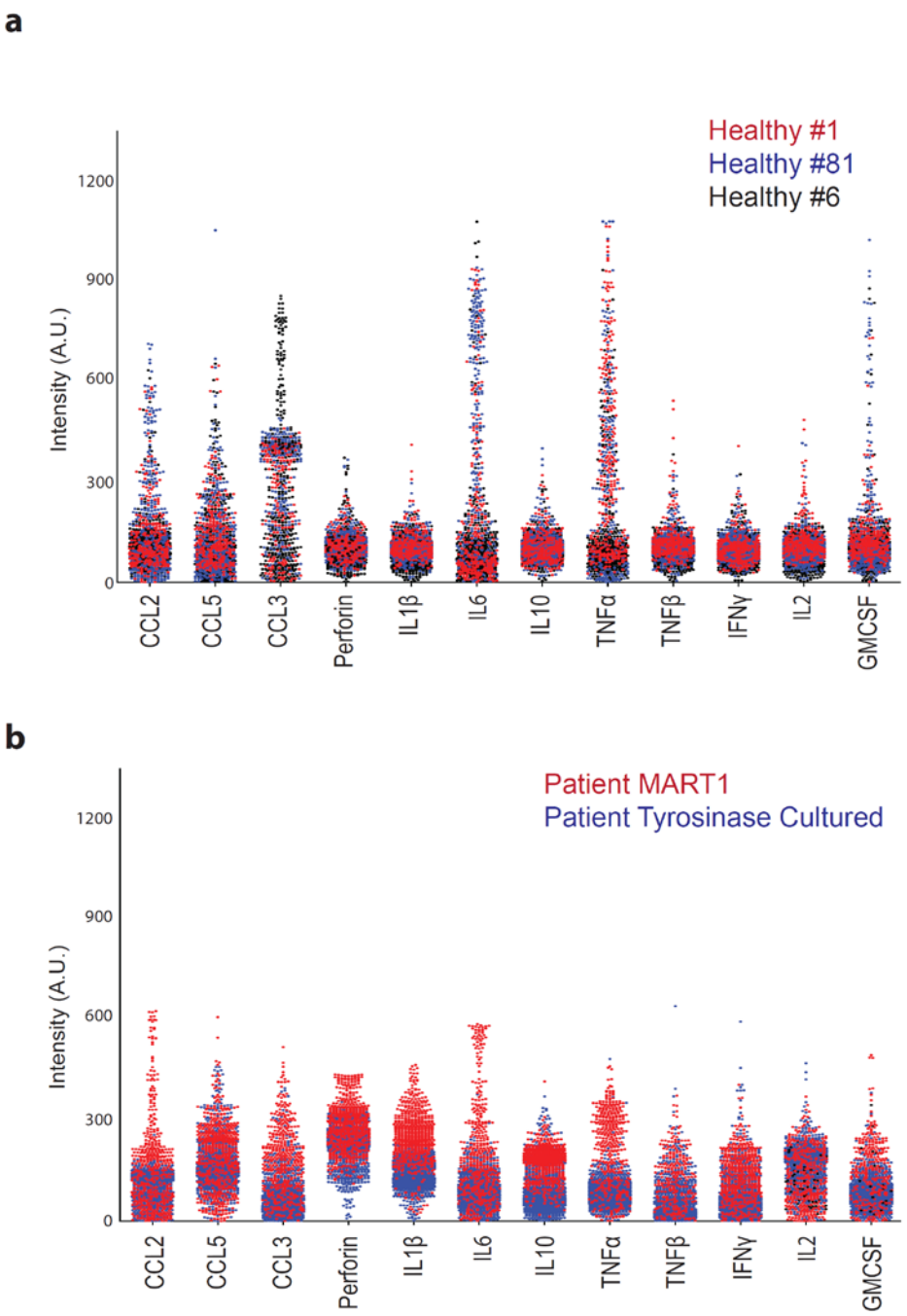

Supplementary Figure 7 Univariate comparison among CTLs from healthy donors (a), CD3+ MART-1-specific CTLs and CD3+ Tyrosinase-specific CTLs from melanoma patients (b).

Supplementary Table 3. Summary of antibodies used for patient T cell experiments.

DNA label	primary antibody (vendor: clone)	secondary antibody (vendor: clone)
A’	mouse anti-hu IFN-γ (R&D)	biotin-labeled mouse anti-hu IFN-γ (R&D)
B’	mouse anti-hu TNF-α (R&D)	biotin-labeled mouse anti-hu TNF-α (R&D)
C’	mouse anti-hu IL-2 (R&D)	biotin-labeled mouse anti-hu IL-2 (R&D)
D’	mouse anti-hu TNF-β (eBio: 359-238-8)	biotin-labeled mouse anti-hu TNF-β (eBio: 359-81-11)
E’	mouse anti-hu CCL5 (R&D)	biotin-labeled mouse anti-hu CCL5 (R&D)
F’	mouse anti-hu Perforin (Abcam)	biotin-labeled mouse anti-hu Perforin (Abcam)
G’	mouse anti-hu IL-1β (R&D)	biotin-labeled mouse anti-hu IL-1β (R&D)
H’	mouse anti-hu IL-6 (R&D)	biotin-labeled mouse anti-hu IL-6 (R&D)
I’	mouse anti-hu IL-10(R&D)	biotin-labeled mouse anti-hu IL-10 (R&D)
J’	mouse anti-hu MCP-1(eBio: 5D3-F7)	biotin-labeled mouse anti-hu MCP-1(eBio: 2H5)
K’	mouse anti-hu GM-CSF (eBio: BVD2-23B6)	biotin-labeled mouse anti-hu GM-CSF (BVD2-21C11)
L’	mouse anti-hu CCL3 (R&D)	biotin-labeled mouse anti-hu CCL3 (R&D)

Evaluation of polyfunctionality

We analyzed the multivariate features of these T cell populations by studying the protein-protein correlations for 2 and 3 proteins. Pseudo-3D plots (**Figure 4a—c**) of markers representing different functions revealed that certain functions of the MART-1-specific cell population were highly coordinated compared to the healthy donor cells. For example, 70% of IL-6^+ cells produce CCL-5, whereas for CTLs from healthy donors the frequency is around 50%. TNF-α and IFN-γ production are anti-correlated in MART-1-specific cells (**Figure 4c**), with >90% of the population expressing at most one of these effector molecules. However, for the small fraction of MART-1-specific TCR transgenic cells that were TNF-α^+IFN-γ^+, secretion of IL-2 is often an additional function (75%, **Figure 4**). A full set of protein-protein correlations is provided in **Supplementary Figure 8**.

We defined functional subsets of the various T cells by identifying groups of cells that secrete the same combination of proteins (**Figure 4d—e**). At least 45 distinct sub-populations are required to account for 60% of the MART-1-specific TCR transgenic cells (**Figure 4e and Table 1**). A similar accounting for the healthy donor CD8+ T cells and the tyrosinase-specific T-cells yields 4-17 sub-populations (**Figure 4d and Table 1**). Furthermore, for the MART-1-specific TCR transgenic cells, the major functional subsets averaged more than 5 active functions. By contrast, both healthy donor and tyrosinase-specific cells averaged only 1-2 functions (**Table 1**). This demonstrates the ability of SCBC to visualize and discriminate different levels of functional heterogeneity.

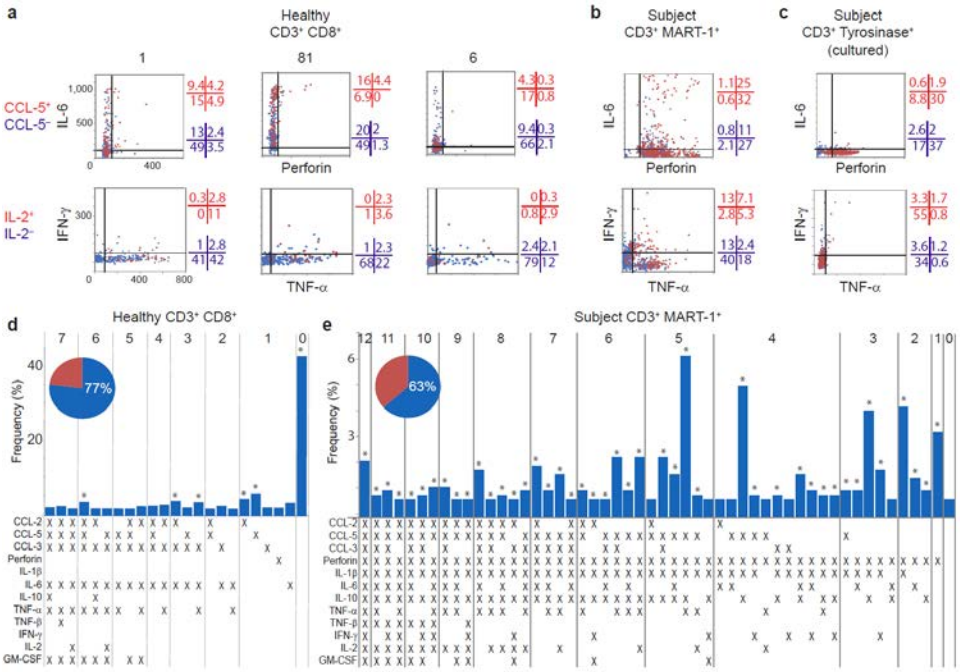

Figure 4 Polyfunctional diversity analysis for CTLs from a patient with metastatic melanoma and from healthy donors. (**a—c**) Pseudo three dimensional scatterplots for representative single cell cytokine measurements from CD8+ T cells. Upper and lower rows are correlations for perforin vs. IL-6 and TNF-α vs. IFN-γ, respectively. The third dimension (CCL-5 or IL-2) is projected to the 2D plot by using red for positive cells and blue for negative cells. Numbers on the right show percentage in each quadrant. Samples are labeled on the left. (**d—e**) Functional diversity plots for patient's MART-1-specific TCR transgenic cells and CD8+ T cells from a representative healthy donor. Each major functional subset identified (with frequency >0.5%) is shown by an individual bar. The bar heights represent population percentages. 53 major subsets were identified from the MART-1-specific TCR transgenic cells; 23 were identified from the healthy donor. The number on top of the plot shows number of functions associated with each subset. The matrix below provides the function detail (X: positive). The pie charts give the percentage of cells that fell into one of the major functional subsets. Asterisks above the blue bars denote those subsets within the most frequent 60% of the population.

Table 1 Summary of functional diversity of assayed samples

Sample		Major functional subsets identified	Percentage of total populations	Number of function		Functional subsets in top 60% populations	Number of function	
				Range	Mean		Range	Mean
Healthy	1	33	70.3	0-7	1.68	17	0-5	1.32
$CD3^+$	81	23	77.4	0-7	1.44	6	0-6	1.34
$CD8^+$	6	21	80.2	0-7	0.89	4	0-2	0.36
Subject $CD3^+$ $MART1^+$		53	63.4	0-12	5.17	45	1-12	5.27
Subject $CD3^+$ $Tyrosinase^+$ (Cultured)		27	80.1	0-5	2.25	8	0-4	2.11

Scatterplot for CTLs from healthy donor controls (n=3)

#1

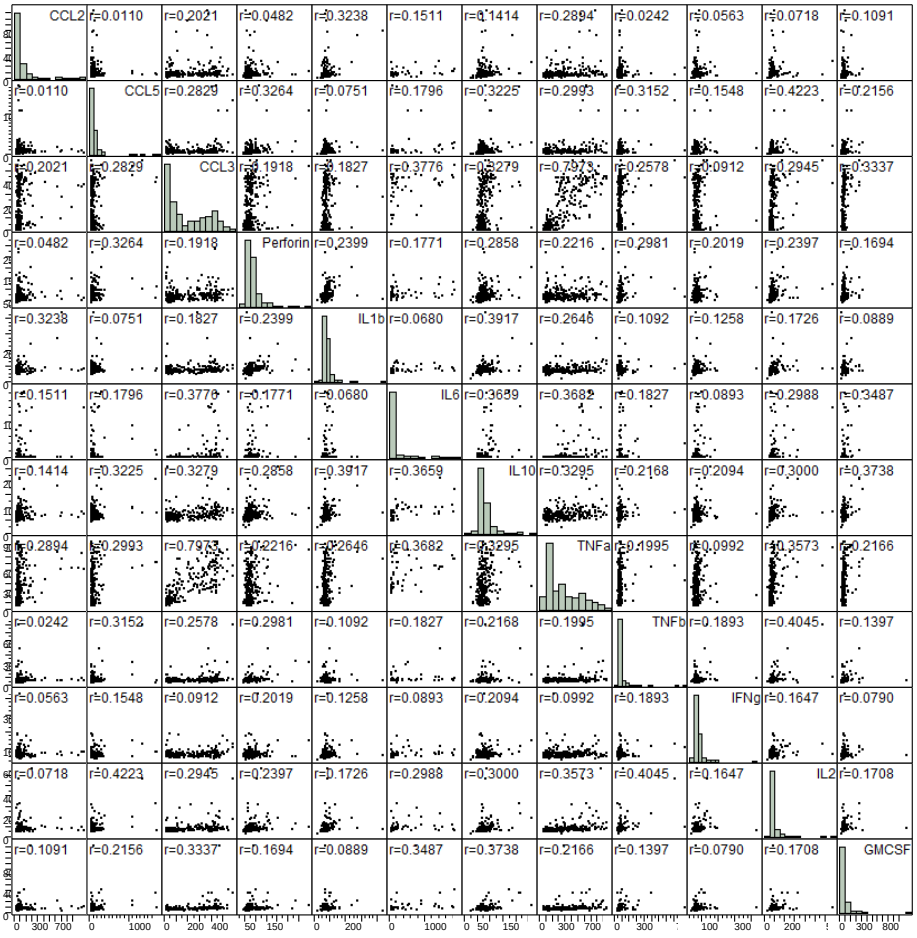

#81

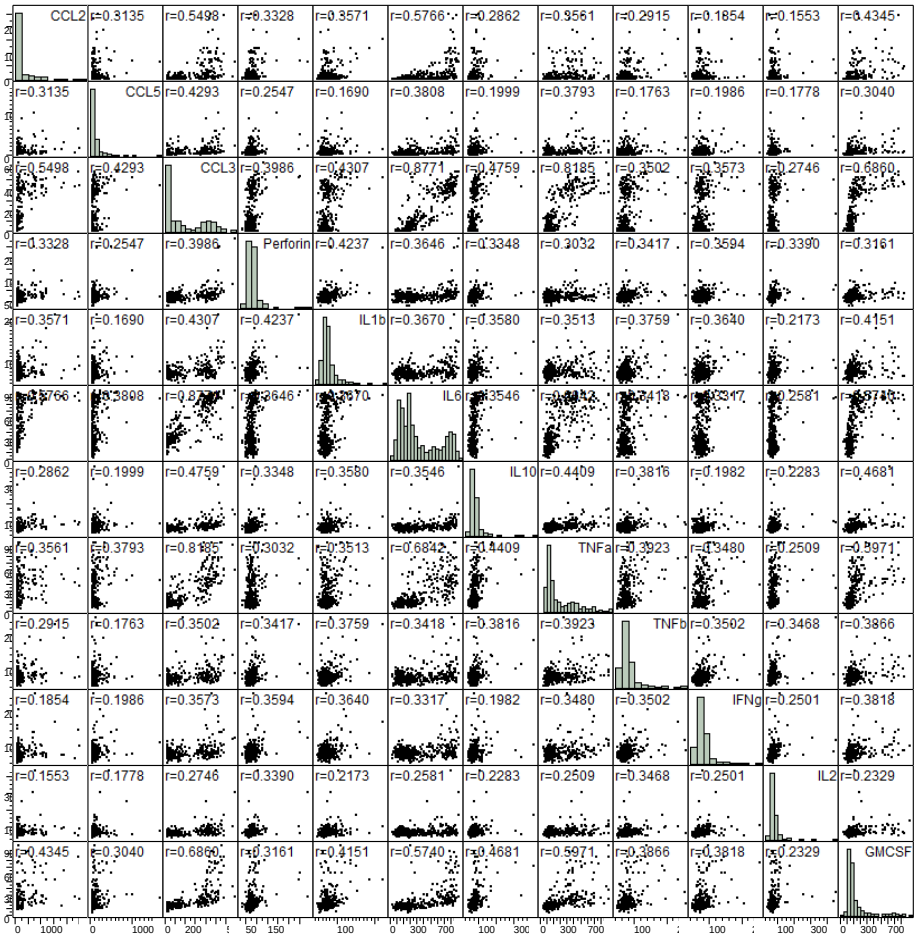
CCL2
CCL5
CCL3
Perforin
IL1b
IL6
IL10
TNFa
TNFb
IFNg
IL2
GMCSF

#6

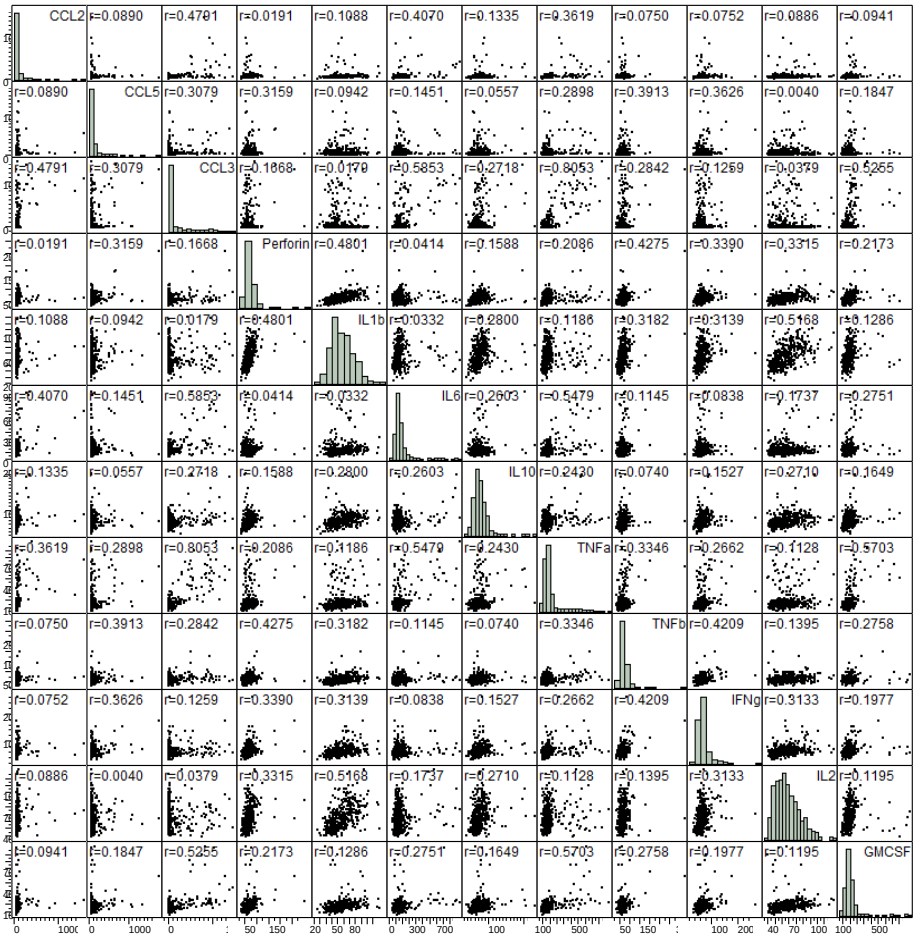
CCL2
r=0.0890
r=0.4791
r=0.0191
r=0.1088
r=0.4070
r=0.1335
r=0.3619
r=0.0750
r=0.0752
r=0.0886
r=0.0941
r=0.0890
CCL5
r=0.3079
r=0.3159
r=0.0942
r=0.1451
r=0.0557
r=0.2898
r=0.3913
r=0.3626
r=0.0040
r=0.1847
r=0.4791
r=0.3079
CCL3
r=0.1668
r=0.0179
r=0.5853
r=0.2718
r=0.8053
r=0.2842
r=0.1259
r=0.0379
r=0.5255
r=0.0191
r=0.3159
r=0.1668
Perforin
r=0.4801
r=0.0414
r=0.1588
r=0.2086
r=0.4275
r=0.3390
r=0.3315
r=0.2173
r=0.1088
r=0.0942
r=0.0179
r=0.4801
IL1b
r=0.0332
r=0.2800
r=0.1186
r=0.3182
r=0.3139
r=0.5168
r=0.1286
r=0.4070
r=0.1451
r=0.5853
r=0.0414
r=0.0332
IL6
r=0.2603
r=0.5479
r=0.1145
r=0.0838
r=0.1737
r=0.2751
r=0.1335
r=0.0557
r=0.2718
r=0.1588
r=0.2800
r=0.2603
IL10
r=0.2430
r=0.0740
r=0.1527
r=0.2710
r=0.1649
r=0.3619
r=0.2898
r=0.8053
r=0.2086
r=0.1186
r=0.5479
r=0.2430
TNFa
r=0.3346
r=0.2662
r=0.1128
r=0.5703
r=0.0750
r=0.3913
r=0.2842
r=0.4275
r=0.3182
r=0.1145
r=0.0740
r=0.3346
TNFb
r=0.4209
r=0.1395
r=0.2758
r=0.0752
r=0.3626
r=0.1259
r=0.3390
r=0.3139
r=0.0838
r=0.1527
r=0.2662
r=0.4209
IFNg
r=0.3133
r=0.1977
r=0.0886
r=0.0040
r=0.0379
r=0.3315
r=0.5168
r=0.1737
r=0.2710
r=0.1128
r=0.1395
r=0.3133
IL2
r=0.1195
r=0.0941
r=0.1847
r=0.5255
r=0.2173
r=0.1286
r=0.2751
r=0.1649
r=0.5703
r=0.2758
r=0.1977
r=0.1195
GMCSF

Scatterplot for MART-1 T Cells

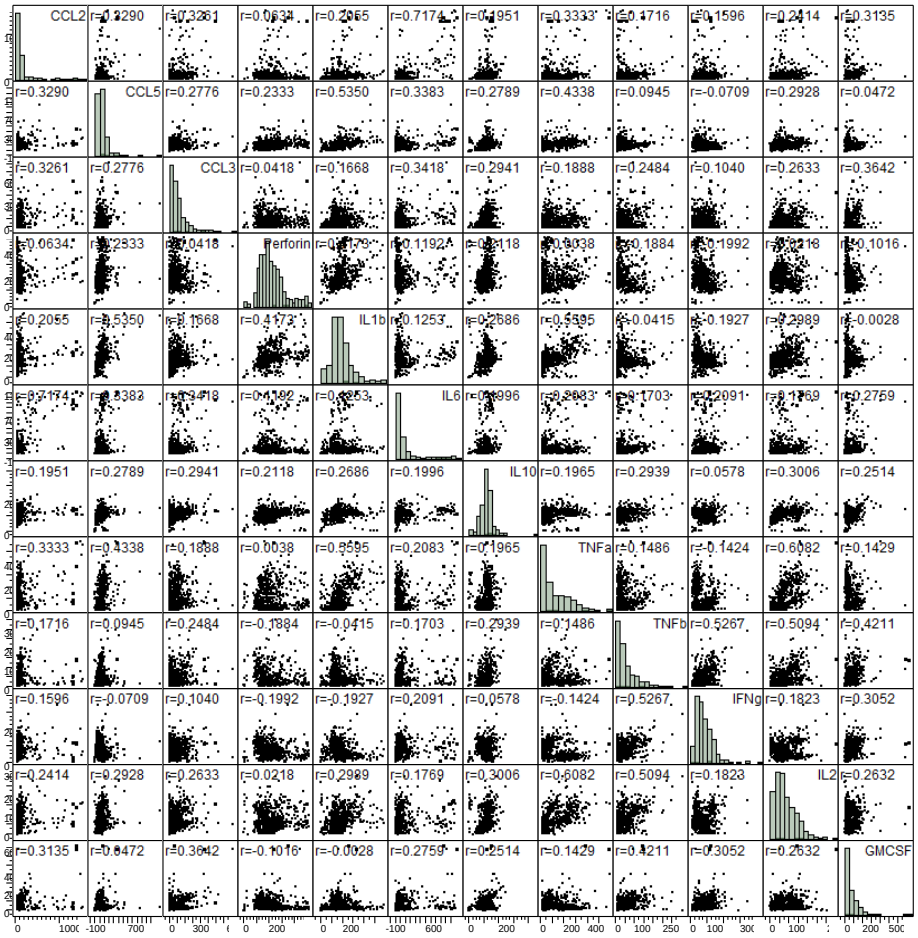

Scatterplot for Tyrosinase T Cells

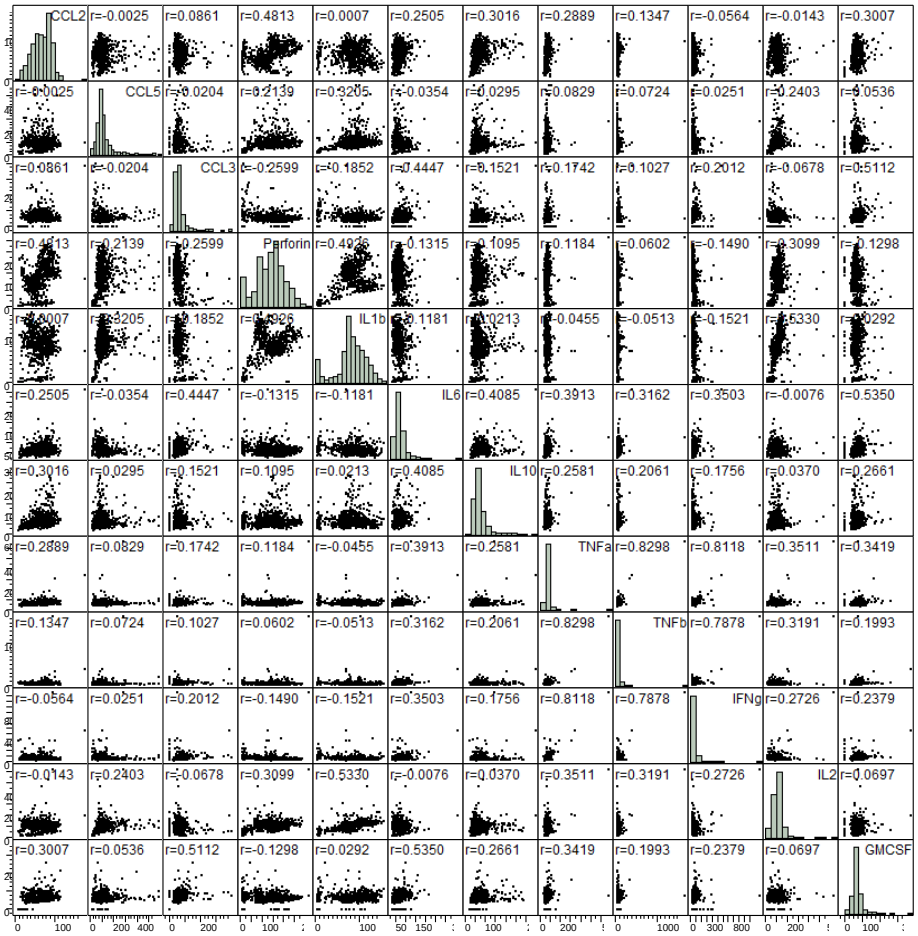

Supplementary Figure 8. Protein-protein correlation plot matrices from single cell experiments of CTLs from healthy donor controls, MART1 T cells and Tyrosinase T cells.

DISCUSSION

The SCBC permits highly multiplexed (> 10) measurements of effector molecules from single cells by detecting the natural protein secretome from macrophages and T cells upon activation. The multiplex capacity can be further expanded beyond what was explored here, as will be showed in later chapters. The ability to use small sample size (~10^4 cells) implies that the SCBC can be integrated with other upstream multiplexed analysis, such as flow cytometry or, as demonstrated, microarray sorting, to enable a detailed functional study of phenotypically defined sets of cells selected from heterogeneous populations. Analysis of signals from chambers containing different numbers of cells may also provide information relevant to cell-cell interactions.

The MART-1-specific TCR transgenic CTLs had stronger perforin, IFN-γ and interleukin secretion and higher level functional heterogeneity compared with the healthy donor CTL controls. This functional status is also indicated by their identity as effector T cells ($CD45RA^+$, $CCL7^-$, $CD27^-$, $CD28^-$, $CD62L^-$) (31, 45, 46). Previous vaccination studies identified that polyfunctional T cells are better cytokine producers, and that the quality of a polyfunctional T cell response is a good predictor of clinical outcome (16, 47). We found that the MART-1-specific TCR transgenic CTLs exhibit favorable features compared against CTLs from healthy donors (e.g. polyfunctional subset frequency 62% v.s. 6-25% and **Supplementary Figure 9**). These data are consistent with the observation that, at the time the CTLs were harvested, there was active inflammation and the tumors were responding to the ACT therapy in this patient.

We observed signs of T cell terminal effector differentiation and exhaustion, as indicated by the anti-correlation of TNF-α and IFN-γ secretion, high $IL\text{-}10^+$ cell frequency, and high PD1 and CD127 expression (31). However, the quality of the T cell response at a single time point within a vaccination trial may not provide an indicator of long term vaccination or therapy response (16). A similar multi-parametric SCBC analysis, but carried out at multiple time points throughout the course of a cancer immunotherapy treatment, will be described in later chapters.

We saw a high level of functional heterogeneity within a population defined as relatively homogeneous by surface markers (40, 48), and that heterogeneity is also focused. For example, the top 60% of the MART-1-specific TCR transgenic cells fell into 45 out of >4000 (2^{12}) possible functional subsets. The observed high level of polyfunctionality (up to 12 functions per cell, with an average of >5 functions) exceeds current multiplexing capacity by most existing single cell secretion assays. Moreover, we note that none of the proteins being profiled were interchangeable with others within the panel (with $R^2 < 0.6$, **Supplementary Figure 8**). These findings indicate that a high dimensional analysis is in fact required for comprehensively profiling of T cell effector functions.

The SCBC provides a novel platform for analyzing the functional activity of immune cells immediately following short term *ex vivo* activation. This technology compares favorably to current cellular immunoassays in terms of sensitivity, multiplexing capacity, quantitation, sample size, cost and infrastructure requirements, and thus has potential for a thorough, cost-effective characterization of patient immune cell responses.

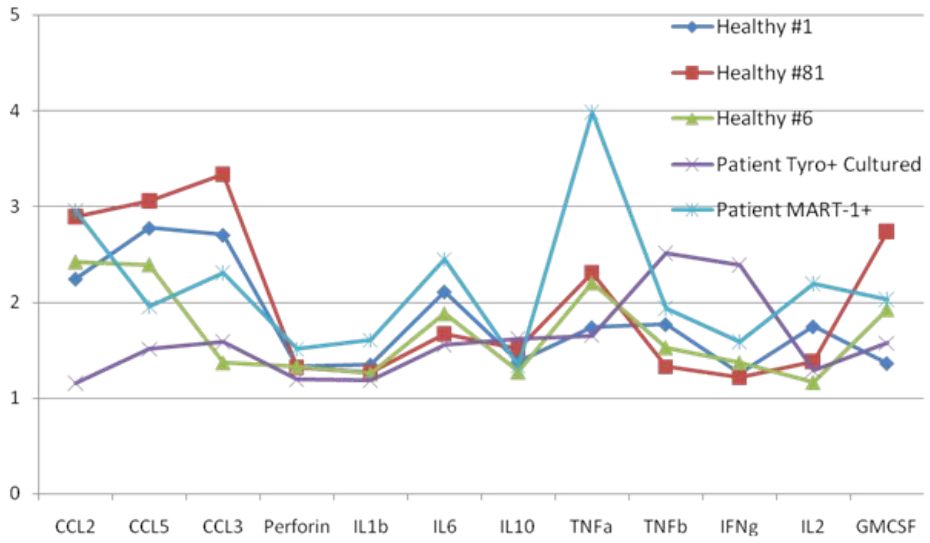

Supplementary Figure 9 Ratio of averaged functional intensity of polyfunctional T cells ($n > 4$) to non-polyfunctional T cells ($n \leq 4$).

METHODS

Microchip Fabrication. The SCBCs were assembled from a DNA barcode microarray glass slide and a PDMS slab containing a microfluidic circuit. The DNA barcode array was created with microchannel-guided flow patterning (**Supplementary Fig. 1**). Each barcode was comprised of thirteen stripes of uniquely designed ssDNA molecules. PDMS microfluidic chip was fabricated using a two-layer soft lithography approach(49) (**Supplementary Methods**).

Human samples. Human samples were obtained from patients with metastatic melanoma enrolled in a T cell receptor (TCR) transgenic ACT protocol clinical trial registration number (NCT00910650). The study using Human sample were approved by the appropriate human use committees (UCLA IRB# 08-02-020, IND# 13859), and informed consent was obtained from all subjects studied.

Isolation, purification and expansion of T cells. PBMC were collected from patients receiving TCR engineering ACT immunotherapy by leukapheresis and periodic peripheral blood draws as previously described(50). Aliquots of cryopreserved PBMC thawed and immediately diluted with RPMI complete media containing 5% human AB serum (Omega Scientific). Cells were washed and subjected to enzymatic treatment with DNase (Sigma) for 1 hour at 37°C, washed and rested overnight in a 5% CO_2 incubator. Antigen-specific MART-1 T cells were purified sequentially by magnetic negatively enrichment for CD3 (Stemcell) and by MART-1/HLA-A0201 tetramer microarray that have been previously described(44) (**Supplementary Methods**). Purified cells were collected, washed, stimulated with MART-1 tetramer/CD28 antibody and loaded into SCBC chip. PBMC from healthy donor were negatively enriched in the same way and were further purified by CD8 antibody microarray, followed by stimulation with CD3/CD28 antibody. Sorted cells was checked to be >95% pure.

On-chip secretion profiling. Prior to loading cells on chip, the DNA barcode array was transformed into an antibody microarray through the following steps. The chip is then ready for cell loading. Chips with

cells were incubated and then assays were developed with secondary antibodies and fluorescent markers (**Supplementary Methods**).

Intracellular cytokine staining of THP-1 cells. Brefeldin A (eBioscience) was added in the presence of PMA and LPS at recommended concentration in the final 4h of stimulation. Standard intracellular staining was performed as described by supplier's protocol (eBioscience) with additional blocking with human serum (Sigma) and washes. Cells were fixed and permeabilized by using a fixation and permeabilization kit (eBioscience) and then were stained intracellularly with αTNFα (MAb11), αIL-1β (H1b-98), αIL-10 (JES3-9D7) and αGM-CSF (BVD2-21C11). Isotype control staining was used as negative control and 2 x 10^4 events were collected for each condition. Samples were analyzed on a FACSCalibur (BD Biosciences) machine with CellQuest Pro software (BD Biosciences).

Flow cytometry analysis of antigen specific T cells. Cryopreserved PBMC samples from peripheral blood draws or leukapheresis were thawed and analyzed by HLA-A*0201 tetramer assay (Beckman Coulter) with flow cytometric analysis as previously described(50, 51). In brief, PBMCs were resuspended in 100 µl of adult bovine serum (Omega Scientific) and stained for 15 minutes at room temperature using a cocktail of antibodies: CD45RA, CCR7, CD62L, CD27, CD28, PD-1, CD127 in replicate aliquots. For all flow cytometry experiments, anti-mouse Igk/Negative Control FBS compensation particles (BD Biosciences) were used for compensation purpose, and 5 x 10^5 to 1 x 10^6 lymphocytes were acquired for each condition. In order to correctly gate the flow cytometry data, the fluorescent minus one (FMO) approach was used. Samples were acquired on a LSR II systems (BD Biosciences) and data was analyzed using FlowJo software (TreeStar).

Fluorospot assay for sorted antigen specific T cells. Antigen specific T cells were captured by tetramer microarray. Primary cytokine capture antibody was co-localized on the same array. The captured cells were then incubated at 37 degree/5% CO_2 for 12 hours in 10% FBS/RPMI 1640 media. PE labeled

secondary antibody was applied after incubation. Then slides were washed and imaged by EZ-C1 confocal microscope systems (Nikon).

Data analysis and statistics. We used GenePix 4400 (Axon Instruments) to obtained the scanned fluoresce image for both Cy3 and Cy5 channels. All scans were performed at constant instrument settings: laser power 80% (635 nm) and 15% (532 nm), optical gains 600 (635 nm) and 450 (532nm), brightness 80 and contrast 83 for T cell experiment and laser power 100% (635 nm) and 33% (532 nm), optical gains 800 (635 nm) and 700 (532nm), brightness 87 and contrast 88 for macrophage experiment. All the barcodes were processed in PhotoShop (Adobe) and ImageJ software (NIH) to generate fluorescence line profiles. A home-developed Excel (MicroSoft) macro was employed for automatic extraction of average fluorescence signal for all bars in each set of barcode, and all the barcode profiles were compared to the number of cells by using the same program. Based on this data, heat maps were generated by using the software Cluster and *Treeview(52)*. Flow cytometry data is analyzed in FlowJo software . P-values are calculated from two tail student's T-test assuming unequal variance.

Microchip Fabrication. The control layer was molded from a SU8 2010 negative photoresist (~20um in thickness) silicon master using a mixture of GE RTV 615 PDMS prepolymer part A and part B (5:1). The flow layer was fabricated by spin-casting the pre-polymer of GE RTV 615 PDMS part A and part B (20:1) onto a SPR 220 positive photoresist master at ~2000rpm for 1minute. The SPR 220 mold was ~17 μm in height after rounding via thermal treatment at 80 degree for 60 mins. The control layer PDMS chip was then carefully aligned and placed onto the flow layer, which was still situated on its silicon master mold, and an additional 60 mins thermal treatment at 80^{o}C was performed to enable bonding. Afterward, this two-layer PDMS chip was cut off with access holes drilled. Finally, the microfluidic-containing PDMS slab was thermally bonded for 2 hours at 80 degree onto the barcode-patterned glass slide to give a fully assembled microchip.

Isolation, sorting and expansion of T cells. Briefly, enriched PBMC were applied onto a MART-1 tetramer microarray. After 20 minutes incubation at 37 degree, unbounded cells were washed off and then attached MART-1 specific T cells were released from the array. In order to characterize low frequency antigen-specific T cells, 5 x 10^6 PBMC were expanded with irradiated and tumor antigen peptide-pulsed HLA-A*0201-transfected K562 (K562A2.1) used as antigen presenting cells (APC) at a ratio of 5:1 (51, 53). The PBMC were cultured in AIM-V media plus IL-2 (300IU/ml) and CD3 antobidy (OKT3, 50ng/ml) on day 1, and then kept in culture for 24 days with IL-2 but without OKT-3. Irradiated (75 Gy) K562A2.1 cells were pulsed with 10μg of peptide tyrosinase$_{368-376}$ (YMDGTMSQV). The peptide-pulsed APCs were added weekly. After 30 days, expanded cells were sorted based on the same technique described above with Tyrosinase$_{368-376}$/HLA-A0201 tetramer.

On-chip secretion profiling. First, 200 ul 3% bovine serum albumin (BSA, Sigma) in phosphate buffer saline (PBS, Irvine Scientific) was flowed and dead-end filled into the chip to block non-specific binding. Second, a 200-μl cocktail containing all 12 DNA-antibody conjugates at 5 ug/ml in 3% BSA/PBS buffer was flowed through all microfluidic channels in 1 h at 37 degree. Then, 100μl of 3% BSA/PBS buffer was flowed into the device to wash unbounded DNA conjugated primary antibody solutions. THP-1 Cells were washed, stimulated with PMA/LPS or purified T cells acitivated with tetramer/anti-CD28 antibody or anti-CD3/anti-CD28 antibody in 10% FBS/RPMI-1640 media (ATCC) and loaded on chip within 5 min in order to minimize pre-chip secretion. Then, the pneumatic valves were pressed down by applying 20 psi constant pressure to divide 80 microfluidic channels into 1000 isolated microchammbers. Next, the chip was placed in a cell incubator (~37^{o}C and 5% CO_2) for 24 h (THP-1) or 12 h (T cells) to perform on chip secretion. Afterwards, the chip was removed from incubator and cells were quickly washed of the chip. A 200-μl cocktail containing all biotinylated detection antibodies was then flowed through the microchannels. The antibody concentrations are 5 ug/mL. Then, 200ul of the fluorescent probe solution (100 ng/ml Cy5-labeled straptavidin and 20 ng/ml C3-labeld M' ssDNA) were flowed through to

complete the immuno-sandwich assay. Finally, the PDMS slab was peeled off and the microarray slide was rinsed with 1x PBS, 0.5xPBS and DI water twice, sequentially, and spin-dried.

Culture and stimulation of THP-1 cells. THP-1 monocyte cells were (clone TIB 202) cultured in RPMI-1640 (ATCC) medium supplemented with 10% fetal bovine serum (FBS) and 10 μM 2-mercaptoethanol. Cells grown close to the maximum density ($0.8x10^6$ cells/mL) were chosen for the experiment in order to minimize variation of cell cycles. Cells were washed and resuspended in fresh media at $2\text{-}4x10^6$ cells/ml. Aliquots each containing 100 μL of cell suspension were prepared. 1μL of 1mg/mL PMA and 1μL of 20μg/ml LPS were sequentially added into each aliquot to induced monocytic differentiation and stimulate TLR-4 activation. THP-1 cells activated with PMA and LPS exhibited a characteristic morphological change (**Supplementary Figure 2**).

Melanoma adoptive transgenic T cell transfer clinical trial. Peripheral blood samples were obtained from patients with metastatic melanoma enrolled in a T cell receptor (TCR) transgenic ACT protocol (UCLA IRB# 08-02-020, IND# 13859, clinical trial registration number NCT00910650). A single baseline unmobilized leukapheresis processing two plasma volumes was performed to obtain PBMC, which were isolated by Ficoll-Hypaque (Amersham-Pharmacia) gradient centrifugation, for the generation of TCR transgenic cells and dendritic cell (DC) vaccines. Freshly collected PBMC were activated for 2 days by clinical grade anti-CD3 antibody OKT3 (50 ng/ml, anti-human CD3 FG purified OKT3, eBioscience) and human interleukin-2 (IL-2, 300 IU/ml, aldesleukin, Novartis). Following activation, cells are transduced in two consecutive days with a retroviral vector expressing the MART-1 F5 TCR (MSGV1-F5AfT2AB vector), in plates coated with retronectin (Takara Bio Inc.) as previously described(54). The clinical grade retroviral vector MSGV1-F5AfT2AB was generated at the Indiana University Viral Production Facility starting from the master cell bank provided by Dr. Steven A. Rosenberg (Surgery Branch, NCI) as previously described(54). Patients were then admitted to the hospital and conditioned with a non-myeloablative, lymphocyte depleting chemotherapy regimen consisting of cyclophosphamide (60 mg/kg/day for two days, Mead Johnson & Company) and fludarabine (25

mg/m^2/day i.v. daily for five days, Berlex). On study day 0 patients received up to 10^9 MART-1 F5 TCR transgenic T cells infused. MART-1_{26-35} peptide pulsed DC were generated from cryopreserved PBMC following a one-week *ex vivo* differentiation culture in RPMI 1640 medium supplemented with 5% heat inactivated autologous plasma, 256 IU/ml of GM-CSF (Bayer) and 160 IU/ml of IL-4 (CellGenix) as previously described(55). On the day after TCR transgenic ACT, patients received an i.d. administration of up to 10^7 MART-1_{26-35} peptide pulsed DC vaccines at a site close to a lymph node basin, and were started on systemic high dose IL-2 at 600,000 IU/kg i.v. every 8 hours for up to 14 doses as tolerated. Thereafter, patients stayed in the hospital until they had recovered from the chemotherapy-induced pancytopenia (median of 11 days).

Synthesis of DNA-1^o antibody conjugates. As-received antibodies were desalted, buffer exchanged to pH 7.4 PBS and concentrated to 1 mg/mL using Zebba protein desalting spin columns (Pierce). Succinimidyl 4-hydrazinonicotinate acetone hydrazone in *N*,*N*-dimethylformamide (DMF) (SANH, Solulink) was added to the antibodies at variable molar excess of (85:1) of SANH to antibody. Separately, succinimidyl 4-formylbenzoate in DMF (SFB, Solulink) was added at a 20-fold molar excess to 5‘aminated 28mer oligomers in PBS. After incubation for 4 h at room temperature, excess SANH and SFB were removed and both samples buffered exchanged to pH 6.0 citrate buffer using protein desalting spin columns. A 20-fold excess of derivatized DNA was then combined with the antibody and allowed to react overnight at room temperature. Noncoupled DNA was removed using a Pharmacia Superdex 200 gel filtration column (GE) at 0.5 mL/min isocratic flow of PBS.

Fabrication of microfluidic-patterning chips. The microfluidic-patterning chips were made by molding a polydimethylsiloxane (PDMS) elastomer from a master template, which was prepared using photolithography to create a photoresist pattern on a Si wafer. An alternative was to make a silicon “hard” master by transferring the photolithographically-defined pattern into the underlying silicon wafer using a deep reactive ion etching (DRIE) process(56). The first method offers rapid prototyping, while the second method yields a robust and reusable mold, permitting higher throughput chip fabrication. The typical line

width and height are 20μm and 20μm, respectively. The PDMS elastomer-based microfluidic patterning chips were fabricated via a molding process. The mixture of Sygard PDMS (Corning) prepolymer and curing agent (10:1) was stirred, and poured onto the silicon mold which was pre-treated with trimethyl-chloro-silane vapor to facilitate mold release. Next the PDMS poured on the mold was degassed for 30 min via a house vacuum line, and then cured at 80^{o}C for 1 h. The solidified PDMS slab was cut off the mold, assess holes drilled and then bonded onto a glass slide. Prior to bonding, the glass surface was pre-coated with the polyamine polymer, poly-L-lysine (Sigma-Aldrich), to increase DNA loading. The coating process is described elsewhere[18]. The number of microfluidic channels determines the size of the barcode array. The completely microfluidic patterning chip contained of 13 parallel microchannels designed to cover a large area (3cm×2cm) of the glass slide for creating the DNA barcode microarray.

Patterning of DNA barcode arrays. Using the microchannel-guided flow-patterning approach, we fabricated DNA barcode arrays that were at least 10-fold denser than conventional microarrays. Microcontact printing can generate high density arrays of biomolecules with spot sizes of a few micrometers (μms) **(57, 58),** but extending stamping to large numbers of biomolecules is awkward because of the difficulty in aligning multiple stamps precisely to produce a single microarray. Direct microfluidics-based pattering of proteins has been reported, but DNA flow-patterning with sufficient loading remains less successful compared to conventional spotting methods **(59, 60).** During the patterning of a DNA barcode array, solutions, each containing a different strand of primary DNA oligomers prepared in 1x PBS buffer, were flowed into each of the microfluidic channels. Then, the solution-filled chip was placed in a desiccator to allow solvent (water) to evaporate completely through the gas-permeable PDMS, leaving the DNA molecules behind. This evaporation process took from several hours to overnight to complete. Last, the PDMS elastomer was removed from the glass slide, and the barcode-patterned DNA was fixed to the glass surface by thermal treatment at 80^{o}C for 4 hours. Potassium phosphate crystals precipitated during solution evaporation, but were readily removed by

rapidly dipping the slide in deionized water prior to bonding the blood-assay chip to the slide. This did not affect the quality of the DNA barcode arrays.

References

1. Gordon, S. & Taylor, P.R. Monocyte and macrophage heterogeneity. *Nat Rev Immunol* **5**, 953-964 (2005).

2. O'Shea, J.J., Hunter, C.A. & Germain, R.N. T cell heterogeneity: firmly fixed, predominantly plastic or merely malleable? *Nat Immunol* **9**, 450-453 (2008).

3. Kaech, S.M. & Wherry, E.J. Heterogeneity and cell-fate decisions in effector and memory CD8(+) T cell differentiation during viral infection. *Immunity* **27**, 393-405 (2007).

4. Darrah, P.A., *et al.* Multifunctional T(H)1 cells define a correlate of vaccine-mediated protection against Leishmania major. *Nature Medicine* **13**, 843-850 (2007).

5. Lee, P.P., *et al.* Characterization of circulating T cells specific for tumor-associated antigens in melanoma patients. *Nature Medicine* **5**, 677-685 (1999).

6. Seder, R.A., Darrah, P.A. & Roederer, M. T-cell quality in memory and protection: implications for vaccine design (vol 8, pg 247, 2008). *Nat Rev Immunol* **8**(2008).

7. Re, F. & Strominger, J.L. Heterogeneity of TLR-induced responses in dendritic cells: from innate to adaptive immunity. *Immunobiology* **209**, 191-198 (2004).

8. Chattopadhyay, P.K., Yu, J. & Roederer, M. A live-cell assay to detect antigen-specific CD4(+) T cells with diverse cytokine profiles. *Nature Medicine* **11**, 1113-1117 (2005).

9. Zak, D.E. & Aderem, A. Systems biology of innate immunity. *Immunological Reviews* **227**, 264-282 (2009).

10. Precopio, M.L., *et al.* Immunization with vaccinia virus induces polyfunctional and phenotypically distinctive CD8(+) T cell responses. *Journal of Experimental Medicine* **204**, 1405-1416 (2007).

11. Mantovani, A., Allavena, P., Sica, A. & Balkwill, F. Cancer-related inflammation. *Nature* **454**, 436-444 (2008).

12. Coussens, L.M. & Werb, Z. Inflammation and cancer. *Nature* **420**, 860-867 (2002).

13. Medzhitov, R. Origin and physiological roles of inflammation. *Nature* **454**, 428-435 (2008).

14. Hagemann, T., Balkwill, F. & Lawrence, T. Inflammation and cancer: A double-edged sword. *Cancer Cell* **12**, 300-301 (2007).

15. Appay, V., van Lier, R.A.W., Sallusto, F. & Roederer, M. Phenotype and Function of Human T Lymphocyte Subsets: Consensus and Issues. *Cytometry Part A* **73A**, 975-983 (2008).

16. Song, K.M., *et al.* Characterization of subsets of CD4(+) memory T cells reveals early branched pathways of T cell differentiation in humans. *Proceedings of the National Academy of Sciences of the United States of America* **102**, 7916-7921 (2005).

17. Kotecha, N., *et al.* Single-cell profiling identifies aberrant STAT5 activation in myeloid malignancies with specific clinical and biologic correlates. *Cancer Cell* **14**, 335-343 (2008).

18. Bailey, R.C., Kwong, G.A., Radu, C.G., Witte, O.N. & Heath, J.R. DNA-encoded antibody libraries: A unified platform for multiplexed cell sorting and detection of genes and proteins. *Journal of the American Chemical Society* **129**, 1959-1967 (2007).

19. Fan, R., *et al.* Integrated barcode chips for rapid, multiplexed analysis of proteins in microliter quantities of blood. *Nature Biotechnology* **26**, 1373-1378 (2008).

20. Shin, Y.S., *et al.* Chemistries for Patterning Robust DNA MicroBarcodes Enable Multiplex Assays of Cytoplasm Proteins from Single Cancer Cells. *Chemphyschem* **11**, 3063-3069 (2010).

21. Wang, J., *et al.* A self-powered, one-step chip for rapid, quantitative and multiplexed detection of proteins from pinpricks of whole blood. *Lab Chip* **10**, 3157-3162 (2010).

22. Aderem, A. & Ulevitch, R.J. Toll-like receptors in the induction of the innate immune response. *Nature* **406**, 782-787 (2000).

23. Fan, J. & Malik, A.B. Toll-like receptor-4 (TLR4) signaling augments chemokine-induced neutrophil migration by modulating cell surface expression of chemokine receptors. *Nature Medicine* **9**, 315-321 (2003).

24. Attig, S., *et al.* Simultaneous Infiltration of Polyfunctional Effector and Suppressor T Cells into Renal Cell Carcinomas. *Cancer Res* **69**, 8412-8419 (2009).

25. De Rosa, S.C., *et al.* Vaccination in humans generates broad T cell cytokine responses. *J Immunol* **173**, 5372-5380 (2004).

26. Makedonas, G. & Betts, M.R. Polyfunctional analysis of human t cell responses: importance in vaccine immunogenicity and natural infection. *Springer Semin Immun* **28**, 209-219 (2006).

27. Morgan, R.A., *et al.* Cancer regression in patients after transfer of genetically engineered lymphocytes. *Science* **314**, 126-129 (2006).

28. Kwong, G.A., *et al.* Modular Nucleic Acid Assembled p/MHC Microarrays for Multiplexed Sorting of Antigen-Specific T Cells. *Journal of the American Chemical Society* **131**, 9695-9703 (2009).

29. Bachmann, M.F., Wolint, P., Schwarz, K., Jager, P. & Oxenius, A. Functional properties and lineage relationship of CD8(+) T cell subsets identified by expression of IL-7 receptor alpha and CD62L. *J Immunol* **175**, 4686-4696 (2005).

30. van Lier, R.A.W., ten Berge, I.J.M. & Gamadia, L.E. Human CD8(+) T-cell differentiation in response to viruses. *Nat Rev Immunol* **3**, 931-938 (2003).

31. Pantaleo, G. & Koup, R.A. Correlates of immune protection in HIV-1 infection: what we know, what we don't know, what we should know. *Nature Medicine* **10**, 806-810 (2004).

32. Ribas, A., *et al.* Dendritic Cell Vaccination Combined with CTLA4 Blockade in Patients with Metastatic Melanoma. *Clinical Cancer Research* **15**, 6267-6276 (2009).

33. Thorsen, T., Maerkl, S.J. & Quake, S.R. Microfluidic large-scale integration. *Science* **298**, 580-584 (2002).

34. Comin-Anduix, B., *et al.* Detailed analysis of immunologic effects of the cytotoxic T lymphocyte-associated antigen 4-blocking monoclonal antibody tremelimumab in peripheral blood of patients with melanoma. *Journal of Translational Medicine* **6**(2008).

35. Comin-Anduix, B., *et al.* Definition of an immunologic response using the major histocompatibility complex tetramer and enzyme-linked immunospot assays. *Clin Cancer Res* **12**, 107-116 (2006).

36. Eisen, M.B., Spellman, P.T., Brown, P.O. & Botstein, D. Cluster analysis and display of genome-wide expression patterns. *Proceedings of the National Academy of Sciences of the United States of America* **95**, 14863-14868 (1998).

Supplementary References

1. Thuillier, G. & Malek, C.K. Development of a low cost hybrid Si/PDMS multi-layered pneumatic microvalve. *Microsystem Technologies-Micro-and Nanosystems-Information Storage and Processing Systems* **12**, 180-185 (2005).

2. Michel, B., *et al.* Printing meets lithography: Soft approaches to high-resolution patterning. *Chimia* **56**, 527-542 (2002).

3. Lange, S.A., Benes, V., Kern, D.P., Horber, J.K.H. & Bernard, A. Microcontact printing of DNA molecules. *Analytical Chemistry* **76**, 1641-1647 (2004).

4. Delamarche, E., Bernard, A., Schmid, H., Michel, B. & Biebuyck, H. Patterned delivery of immunoglobulins to surfaces using microfluidic networks. *Science* **276**, 779-781 (1997).

5. Bernard, A., Michel, B. & Delamarche, E. Micromosaic immunoassays. *Analytical Chemistry* **73**, 8-12 (2001).

Chapter 4

Multifunctional T Cell Analyses to Study Response and Progression in Adoptive Cell Transfer Immunotherapy

Summary

Adoptive cell transfer (ACT) of genetically engineered T-cells expressing cancer-specific T cell receptors (TCR) is a promising cancer treatment. Here we investigate the *in vivo* functional activity and dynamics of the transferred cells by analyzing samples from three representative patients with melanoma enrolled in a clinical trial of ACT with TCR transgenic T cells targeted against the melanosomal antigen MART-1. The analyses included evaluating 19 secreted proteins from individual cells from phenotypically defined T cell subpopulations, and the enumeration of T cells with TCR antigen specificity for 36 melanoma antigens. These analyses revealed the coordinated functional dynamics of the adoptively transferred, as well as endogenous, T cells, and the importance of highly functional T cells in dominating the anti-tumor immune response. This study points to the need to develop approaches to maintain antitumor T cell functionality in order to increase the long term efficacy of TCR engineered ACT immunotherapy.

In summary, a longitudinal functional study of adoptively transferred T cell receptor engineered lymphocytes yielded revealing snapshots for understanding the changes of antitumor responses over time in an adoptive cell transfer immunotherapy of patients with advanced melanoma.

Introduction

A small percentage of patients with widely metastatic cancers can be cured with a variety of immune activating approaches. These dramatic, but infrequent, clinical responses are generally mediated by cytotoxic T lymphocytes (CTLs) that recognize tumor antigens through their T cell receptor (TCR). Adoptive cell transfer (ACT)-based therapies bypass many limitations of other cancer immunotherapies by generating *ex vivo* and then administering to patients large numbers of activated, tumor antigen-specific effector cells. These cellular immune responses to cancer are mediated by CTLs specifically recognizing tumor antigens through their TCR. There are several classes of tumor antigens, including tumor-specific mutations, re-expressed cancer-testis antigens and lineage-specific antigens. Melanoma frequently expresses proteins of the pigmented pathway, reminiscent of its normal counterpart, the melanocytes, representing lineage-specific antigens such as tyrosinase, MART-1/Melan-A or gp100, which have been validated as targets for T cell responses to melanoma (61).

Several groups have demonstrated that the treatment of patients with ACT therapy results in a high frequency of initial tumor responses (4, 62-66). When using T cells with multiple antigen specificities, such as when tumor infiltrating lymphocytes (TIL) are used for ACT transfer, tumor responses tend to be durable, sometimes lasting years (67). But TIL therapy is only feasible in a minority of patients who can undergo surgical resection of a metastatic lesion and have T cells in the biopsy that can be expanded in the laboratory. A potentially more widely applicable approach is the genetic modification of T cells obtained from peripheral blood. These blood cells can be modified to express natural TCRs or chimeric antigen receptors (CARs) that allow the specific recognition of tumor antigens. Early clinical experiences demonstrate that ACT using TCR-engineered T cells has antitumor activity in patients with metastatic melanoma and sarcoma (68-70). However, most of those responses have been transient, despite the persistence of circulating TCR transgenic cells in many cases (68, 69). This observation raises the question of whether these cells lose their antitumor functions, or if other components of the immune system are detrimentally influencing the therapy. As described in patients

with HIV infection, the quality of a T cell response is related to the functional performance of the T cells (17, 71, 72), which can be informatively analyzed at a single cell level with multiplexed technologies (10). Therefore, we conducted a detailed time-course analysis of patient-derived samples using newly developed multidimensional and multiplexed immune monitoring assays in selected patients receiving TCR engineered ACT therapy (10, 73). Our analyses revealed that coordinated, time-dependent functional changes of the adoptively transferred TCR transgenic cells and T cells with other antigen specificities, exhibiting changes that paralleled the clinical outcomes of the patients. This study points to the need to develop therapeutic approaches to maintain and foster antitumor T cell functionality in order to increase the long term efficacy of ACT immunotherapy.

Results

Clinical protocol and patient characteristics

In order to perform a detailed multidimensional analysis of immune function changes over time, and to study the response and resistance to ACT immunotherapy, we selected three out of 14 patients enrolled in a phase 2 clinical trial of MART-1 TCR transgenic ACT therapy. These three cases were selected based on their clinical course that are representative of the whole group, i.e. an initial transient tumor response followed by progression, and also based on the adequacy of samples to be analyzed in different assay platforms. All patients underwent a baseline leukapheresis to collect peripheral blood mononuclear cells (PBMCs), which were stimulated with anti-CD3 antibodies and IL-2 *ex vivo* for two days before undergoing two rounds of transduction with a retroviral vector carrying the high affinity MART-1-specific TCR termed F5 (69). With this approach, both CD4+ and CD8+ T cells were genetically engineered to express the MART-1-specific TCR. Cells were then cultured in IL-2 for three more days and were cryopreserved after lot release testing following the approved investigator new drug (IND) application #13859. Once the TCR transgenic cells were generated, patients were admitted to the hospital to receive conditioning chemotherapy with cyclophosphamide and fludarabine (69). This lymphodepletion procedure is designed to provide 'space' within the immune system for the TCR transgenic cells to expand, and is followed on day 0 with the reinfusion of up to 1 x 10^9 MART-1 TCR transgenic cells. On the next day, and on days 14 and 30 post-ACT, patients received three subcutaneous injections of 1 x 10^7 MART-1_{26-35} peptide-pulsed dendritic cell (DC) vaccine generated from the same baseline leukapheresis product. They also received up to 14 doses of high dose-IL-2 at 600,000 IU/kg every 8 hours within the first five days post-ACT (**Figure 1a and Table 1**). The lymphodepleting chemotherapy and IL-2 administration were designed to maximize the ability of the infused TCR transgenic lymphocytes to homeostatically expand *in vivo*. The MART-1_{26-35} peptide-pulsed DC vaccine was designed to provide antigen-specific stimulation based on our prior protocol optimization studies in mouse models (74). The above four components form a combined therapy approach that provides a

unified effector mechanism – the activated tumor-specific CTLs. Details on the patient characteristics, treatment delivery and outcomes for the three patients (F5-1, F5-2 and F5-8) studied herein are provided in **Table 1**.

The adoptively transferred TCR transgenic lymphocytes undergo a rapid *in vivo* expansion and repopulate the peripheral immune system (peak frequency of >50%, 90 day persistence of >10%, **Table 1**), with evidence of target specificity and antitumor activity (tumor reduction of 13-33%, **Table 1**). The repopulation of the immune system with the MART-1 TCR transgenic T cells resulted in an initial skin rash frequently centered on moles, systemic vitiligo (skin depigmentation) due to attack on MART-1 specific melanocytes in the skin and hair follicles, and diffuse infiltration of CTLs into melanoma metastases (**Table 1 and Figure 1b**).

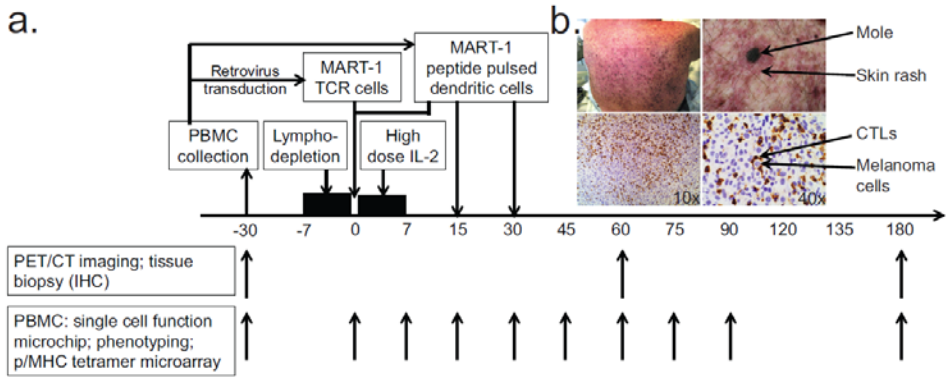

Figure 1. The MART-1-TCR transgenic T cell ACT therapy. a. The boxes above the timeline show different modules of the therapy, with arrows pointing to the time they are administrated relative to day 0 (the day of the infusion of the TCR-engineered T cells). Arrows below the timeline demonstrate the dates when blood samples are collected for different assays. **b.** Photo of one representative patient's back with skin rash surrounding moles (top). In the immunohistochemistry staining of a tumor biopsy (bottom), CD8+ CTLs are stained as dark brown and melanoma cells are blue.

Table 1: Patient Demographics and Treatment

Pt Study #	Sex	Age	Prior Treatments	Active Metastasis Sites	Stage	% MART-1+ cells	IFN-γ with K562-A2-MART-1 (pg/ml/10^6)	Peak % of MART-1+ T cells	Persistence of MART-1+ T cells	# IL2 doses administered	Best % decrease of tumor sizes from baseline	Toxicities	Response at EOS (day 90)	Skin and/or hair depigmentation	Increased TIL infiltrates
F5-1	M	60	No	Lung, Stomach, Liver, Pancreas, Peritoneum, Soft tissues	M1c	84.3	2.2 x 10^5	57% at Day 9	18.5% at 3 months	12	-33	Grade 3 rash, NPF	PD	Yes	Yes
F5-2	F	46	MKC prime-boost vaccine, HD IL-2	Skin, LN, Bone	M1c	74.1	1.5 x 10^5	59% at Day 9	11% at 6 months	6	-22	Grade 3 rash, NPF	SD	Yes	Yes
F5-8	M	44	No	LN, Liver	M1c	66.7	7.8 x 10^5	51% at Day 7	15.5% at 5 months	11	-13	Grade 3 rash, NPF	SD	Yes	NA

Legend: M: Male; F: Female; LN: Lymph nodes; EOS: end of study; PD: progressive disease; SD: stable disease; NA: not available. NPF, Neutropenic fevers.

Integrated single cell functional analyses and antigen-specific CTL population enumerations

To capture the time-dependent functional changes of the MART-1 TCR transgenic T cells and certain other T cell populations that could influence the therapy, we coupled our newly developed single cell barcode chip (SCBC) (10) with multi-parametric fluorescence activated cell sorting (FACS) (**Figure 2a and Supplementary Figure 1**). This approach allowed us to interrogate the functional performance of phenotypically defined, antigen-specific T cells at the single cell level. We segregated CD4+ and CD8+ T cells with MART-1 specificity, as well as MART-1-negative T cells with a non-naïve phenotype, based on 10 cell surface parameters (**Figure 2a**). We then quantitated 19 cytokines and chemokines produced from single cells under stimulation using the SCBC microchip platform (**Supplementary Figure 1**), expanding on the 12-cytokine panel that we had used as a pilot panel for a previous paper (10). As an initial example of the potential of our SCBC chip, in that paper we reported the functionality of MART-1+ T cells from patient F5-2 from study day 30 only, compared to blood lymphocytes from three healthy donors. The expanded and modified new panel used herein includes cytokines specific to CTL function (e.g. granzyme B), as well as cytokines characterizing T helper 1 (IFN-γ, IL-2), T helper 2 (IL-4, IL-5), T helper 17 (IL-17) and regulatory T (IL-10, TGF-β) cell functions (**Supplementary Tables 1 and 2**).

We first compared the approach of FACS/SCBC with our previously described approach that coupled single-parameter NACS cell sorting (73) with SCBC functional analysis (10). The prior approach allowed for analysis of the MART-1 antigen-specific T cells, but did not permit the separation of the CD8+ and CD4+ components from the mixed population. The FACS/SCBC analysis permits such separation, but the FACS step requires a longer time prior to SCBC loading, which could lead to the loss of protein signal. Therefore, we tested the use of both antigen-specific and mitogen-based T cell reactivation in FACS/SCBC assays relative to antigen-specific reactivation in NACS/SCBC analyses (**Supplementary Figure 2 and Methods**) using MART-1+ T cells from a patient (F5-8) who had few CD4+ MART-1+ T cells. Both protocols revealed similar cytokine secretion profiles and time-dependent

functional changes, within the range of error bars. Thus, although there may be some signal loss associated with the FACS/SCBC assays, much of the critical information content is retained, and the significantly refined phenotype selection is a powerful advantage.

The CD8+ MART-1-negative T cell population may contain populations that are specific to melanoma antigens other than MART-1. The detection of such populations has been attributed to epitope spreading, where T cells with antigen specificity other than the one induced by vaccination or ACT appear after tissue damage by the driver clone (75). Thus, we also monitored the frequency of 35 antigen specific sub-populations against previously described putative melanoma tumor antigens (**Supplementary Table 3**) using the NACS peptide/MHC tetramer assays (73). We also conducted multiplexed blood molecular marker assays based on samples from this clinical trial (**Supplementary Figure 1**). The blood assay results will be reported separately.

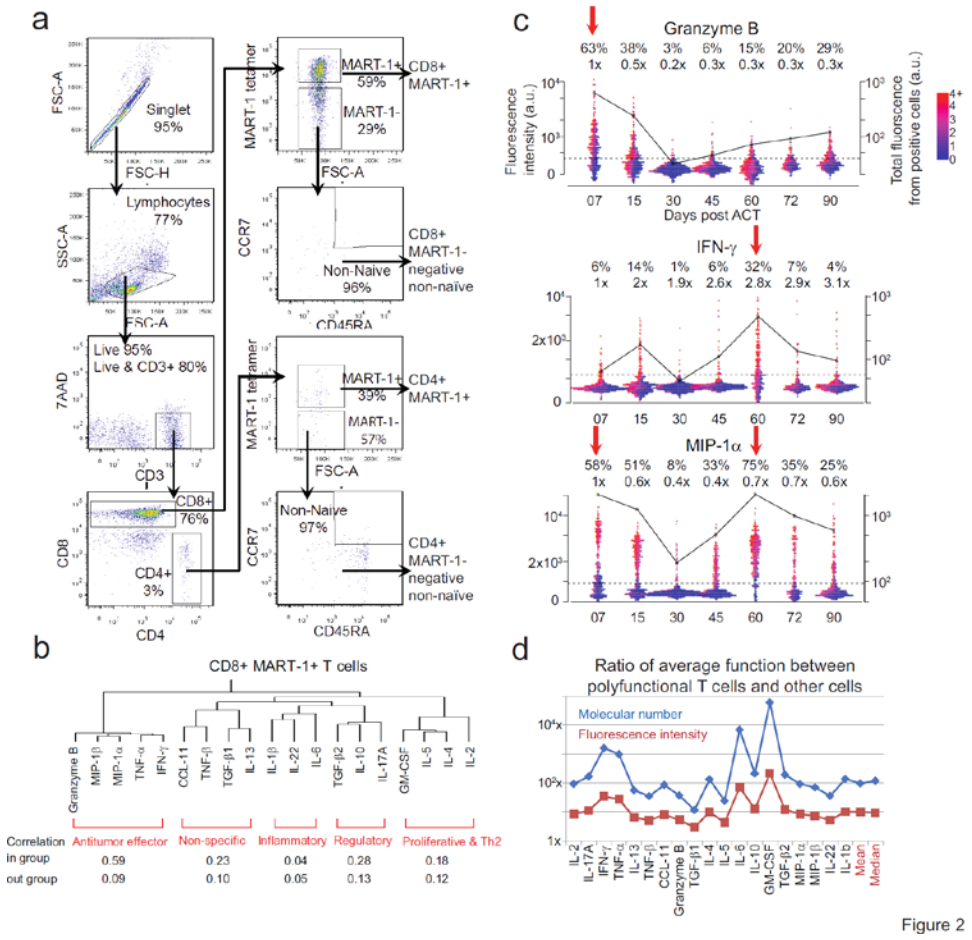

Figure 2

Figure 2. FACS scheme for purifying phenotypically defined T cells, and general properties of T cell functions. a. Multi-parametric FACS purification for selecting phenotypically defined T cell populations. A representative set of scatterplots are shown with the surface markers used and the cell frequency for each gating. **b.** Hierarchical clustering of the 19 functional cytokines studied based on the single cell cytokine secretion measurement of CD8+ MART-1+ T cells from all three patients, and across all time points. Each functional group is identified and labeled (red). Protein-protein correlations for proteins within the same group and across groups are given below the clustering map. **c.** One-dimensional scatterplots of three representative cytokines produced by single cells, separated by time points. The dotted line represents the gate that separates cytokine-producing and non-producing cells. The percentages given above the plots denote the frequency of positive cells and the relative mean fluorescence intensity (MFI) of those cells relative to day 7. Each point represents a single cell assay. The

points are color encoded (from purple to red) to represent the number of different proteins produced by each cell. The black trend line shows the total functional intensity of the positive cells for the specific cytokine plotted, computed as the frequency of positive cells, times their MFI. **d.** Ratio between the MFI (red line) and the molecular number of cytokines (blue line) for the polyfunctional T cells (cells with 5 or more functions) and all other cells, for each cytokine. At far right are the mean and median values, averaged over all cytokines.

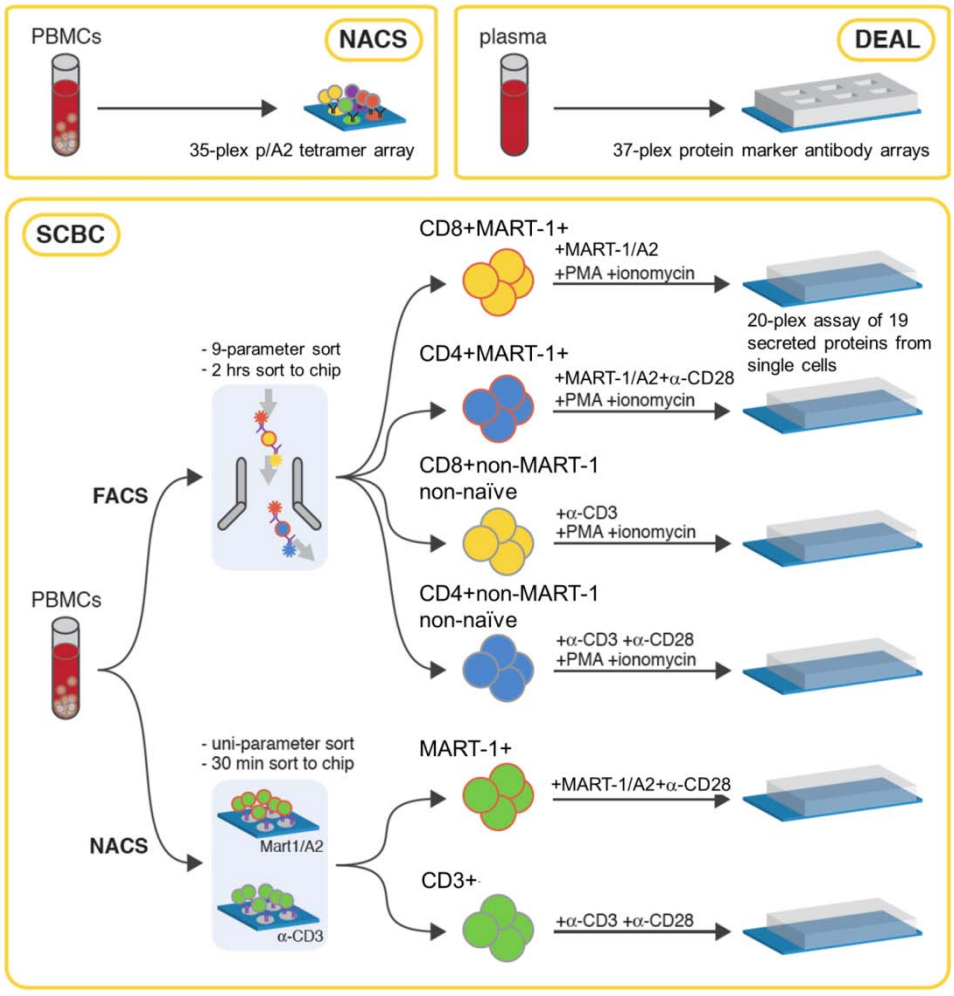

Supplementary Figure 1. Scheme for the multiplexed immune monitoring study. a. NACS peptide/MHC tetramer microarray assays are used to enumerate the abundance of 35 melanoma-antigen specific T cell populations in PBMCs. b. DEAL antibody microarrays are utilized to quantitatively

measure the levels of 37 blood protein markers from blood plasma. c. SCBC microchips are coupled with multi-parameter FACS (top) or with NACS (bottom) to permit the quantitative analysis of the levels of 19 functional proteins secreted from phenotypically defined single T cells, based on 10 parameter (for FACS/SCBC) or 1 surface specificity (NACS/SCBC). For each sample, ~1400 experiments are conducted simultaneously. The FACS/SCBC permits study of highly refined phenotypically defined T cell populations, whereas NACS/SCBC assays select only for tumor-antigen-specific TCRs on the T cells, and so constitute a less-refined study.

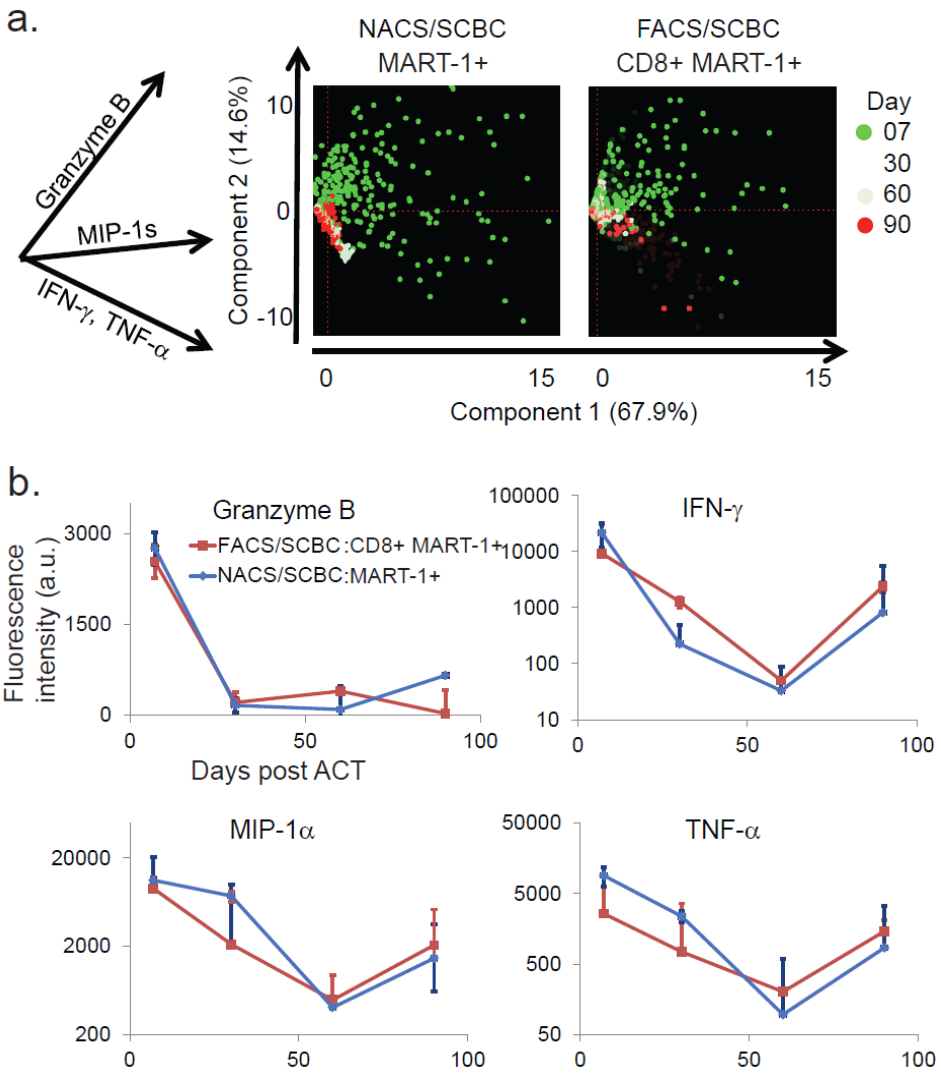

Supplementary Figure 2. Comparison of results from NACS/SCBC and FACS/SCBC protocols for multiplexed single cell functional proteomic analysis. a. PCA analysis showing the plot of the first two components of the time-dependent changes of CD8+ MART-1+ T cells (FACS/SCBC) and MART-1+ T cells (NACS/SCBC) from F5-8. b. Mean intensity for each protein from the polyfunctional T cells of CD8+ MART-1+ T cells (FACS/SCBC) and MART-1+ T cells (NACS/SCBC) from F5-8 over time. These plots indicate that the two experimental protocols revealed similar trends.

Supplementary Table 1. Antibody panel.

Antibody	Manufacturer
IFN-γ	R&D
IL-10	R&D
TNF-β	R&D
IL-4	eBioscience
IL-5	R&D
IL-1β	eBioscience
TGF-β1	R&D
GM-CSF	eBioscience
TNF-α	eBioscience
IL-17A	eBioscience
Eotaxin	R&D
Granzyme B	R&D
IL-13	R&D
IL-22	R&D
MIP-1α	R&D
IL-2	R&D
MIP-1β	R&D
IL-6	R&D
TGF-β2	R&D

Supplementary Table 2. Single cell cytokine panel and groupings of the functional protein identified by clustering.

	CD8+ MART-1+	CD8+ MART-1-negataive	CD4+ MART-1-negative	CD4+ MART-1+

Proliferative	IL-2	IL-2	IL-2	IL-2
	GM-CSF	GM-CSF	GM-CSF	GM-CSF
		IL-17A	TNF-a	IL-17A
			IL-4	TNF-a
Th2	IL-4			IL-4
	IL-5			IL-5
Regulatory	IL-10	IL-10	IL-10	IL-10
	TGF-b2	TGF-b2	TGF-b2	TGF-b2
	IL-17A	IL-22		
Inflammatory	IL-6	IL-6	IL-6	IL-6
	IL-1b	IL-1b	IL-1b	IL-1b
	IL-22	CCL-11	IL-17A	IL-22
		IL-5	IL-5	
Non-specific	IL-13	IL-13	IL-13	IL-13
	TGF-b1	TGF-b1	TGF-b1	TGF-b1
	TNF-b	TNF-b	TNF-b	TNF-b
	CCL-11		CCL-11	CCL-11
				Granzyme B
Antitumor Effector	IFN-g	IFN-g	IFN-g	IFN-g
	MIP-1a	MIP-1a	MIP-1a	MIP-1a
	MIP-1b	MIP-1b	MIP-1b	MIP-1b
	Granzyme B	Granzyme B	Granzyme B	
	TNF-a	TNF-a		
		IL-4	IL-22	

Supplementary Table 3. Melanoma antigen specific T cell populations studied.

$Tyrosinase_{1}$	NY-Eso1	MELOE-1
$Tyrosinase_{368}$	MAGE-A1	$PRAME_{100}$
$MART\text{-}1_{26}$	$MAGE\text{-}C2_{191}$	$PRAME_{300}$
$MART\text{-}1_{32}$	$MAGE\text{-}C2_{336}$	MMP-2
$gp100_{154}$	MAGE-3	Adipophilin
$gp100_{177}$	MAGE-A4	Survivin
$gp100_{209}$	MAGE-A10	
$gp100_{280}$	CAMEL	
$gp100_{457}$	HERV	
$gp100_{476}$	SSX-2	
$gp100_{619}$	TAG-1	
$gp100_{639}$	NA-17	
$TRP\text{-}2_{180}$	CDK-4	
$TRP\text{-}2_{360}$	Prdx-5	
RAB38		

General properties of T cell functional changes observed in ACT

The 19 measured cytokines and chemokines studied represent a broad range of T cell functions (**Figure 2b**). In order to capture general trends, we performed hierarchical clustering of each T cell type studied based on SCBC data from the three patients and all time points (**Figure 2b and Supplementary Table 2**). For the CD8+ MART-1+ T cells, we observed a primary clustering into antitumor effector functions (granzyme B, TNF-α, IFN-γ, etc.). Additional functions, such as regulatory (IL-10, TGF-β2) and pro-inflammatory (IL-6, IL-1β) are resolved with additional clustering (**Figure 2b**). Further analysis revealed that proteins within the same functional group exhibited a higher correlation than with proteins outside that group (**Figure 2b bottom panel**). These functional groupings are largely conserved across the four cell types studied (**Supplementary Table 2**). Thus, the T cells that we studied tend to exhibit coordinated behaviors.

The cytokine readouts that we measured reflect the kinetics of the immune response process. As an example, **Figure 2c and Supplementary Figures 3** present one-dimensional scatterplots of the cytokine production intensity of single CD8+ MART-1+ T cells from patient F5-1 over time. **Supplementary Figure 4** show such changes for patients F5-2 and F5-8. Gates that separate protein secreting- and non-secreting cells are identified by comparing signals from empty chambers and 1-cell chambers. The percentage and mean fluorescence intensity (MFI) of granzyme B-producing cells decreased sharply within the first 30 days after ACT, whereas IFN-γ (**Figure 2c**) and TNF-α (**Supplementary Figure 3**) were most abundant at day 60. The chemokines MIP-1a (**Figure 2c**) and MIP-1b (**Supplementary Figure 3**) reflected time course features of both granzyme B and IFN-γ. Of note, IL-2 secretion remained low (< 3% positive cells) across all time points (**Supplementary Figure 3**). The total functional intensity for a given cytokine (defined as the % of positive cells × MFI, and plotted as the black line in **Figure 2c**) reveals again these two waves of the immune response after ACT, characterized by the production of granzyme B, IFN-γ and TNF-α, respectively. Additionally, unique functional

properties of the cell types studied are reflected in the cytokine measurements: three out of the four cell types studied could be easily distinguished based upon their cytokine profiles (**Supplementary Figure 5**).

We noted that higher protein production levels were associated with cells that exhibit a higher polyfunctionality (**Figure 2c**). This feature is also quantitatively summarized in **Figure 2d and Supplementary Table 4** for all measured cytokines, where we defined a polyfunctional cell as one producing 5 or more cytokines upon stimulation. Such cells typically make up only 10% of the population of a given cell type, but on average they secrete 100 times more copies of a given protein than do the remaining 90% of the population (**Figure 2d**). The inference is that the highly functional T cells dominate (by about 10-fold) the anti-tumor immune response.

Based upon the importance of the polyfunctional T cells, we defined a polyfunctional strength index (pSI) to summarize the observed T cell functional changes. For a given cell type, the pSI is calculated as the percentage of polyfunctional T cells relative to all CD3+ T cells, multiplied by the sum of the mean fluorescence intensity (MFI) of each of the 19 assayed cytokines from the polyfunctional subset. This index represents the total functional intensity contributed by all polyfunctional T cells of a given cell type, at a specific time-point. We further characterized pSI according to the types of coordinated functions that are revealed by hierarchical clustering.

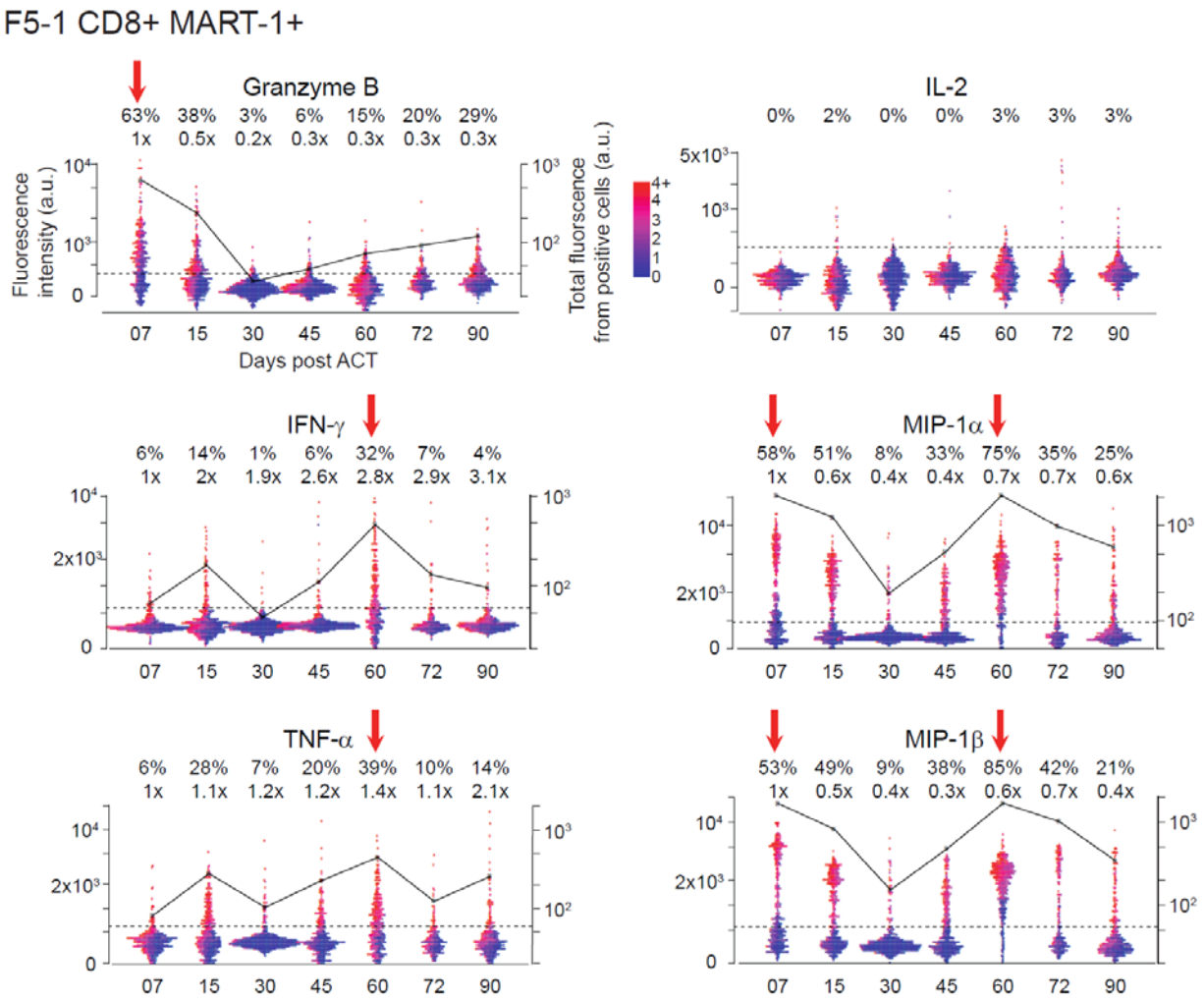

Supplementary Figure 3. Changes of selected cytokines secreted by CD8+ MART-1+ T cells from F5-1. One-dimensional scatterplots of six representative cytokines produced by single cells, separated by time points. The dotted line represents the gate that separates cytokine producing and non-producing cells. The percentages given above the plots denote the frequency of positive cells and the relative mean fluorescence intensity (MFI) of those cells relative to day 07. Each point represents a single cell assay. Those points are color encoded (from purple to red) to represent the numbers of different proteins produced by each cell. The black line shows the total functional intensity of the positive cells for the specific cytokine plotted, computed as the frequency of positive cells, times their MFI.

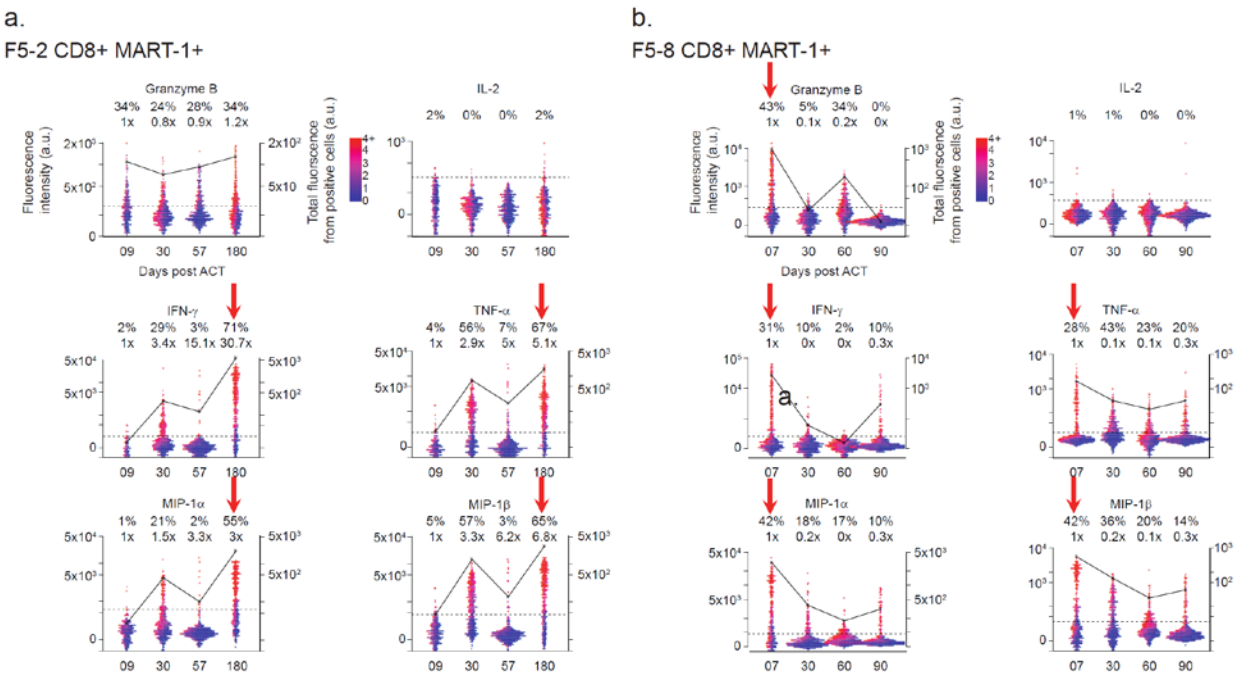

Supplementary Figure 4. Changes of selected cytokines secreted by CD8+ MART-1+ T cells from Patients F5-2 and F5-8. a-b. One-dimensional scatterplots of six representative cytokines produced by single cells, separated by time points for F5-2 and F5-8, respectively. The dotted line represents the gate that separates cytokine producing and non-producing cells. The percentages given above the plots denote the frequency of positive cells and the relative mean fluorescence intensity (MFI) of those cells relative to day 07. Each point represents a single cell assay. Those points are color encoded (from purple to red) to represent the numbers of different proteins produced by each cell. The black line shows the total functional intensity of the positive cells for the specific cytokine plotted, computed as the frequency of positive cells, times their MFI.

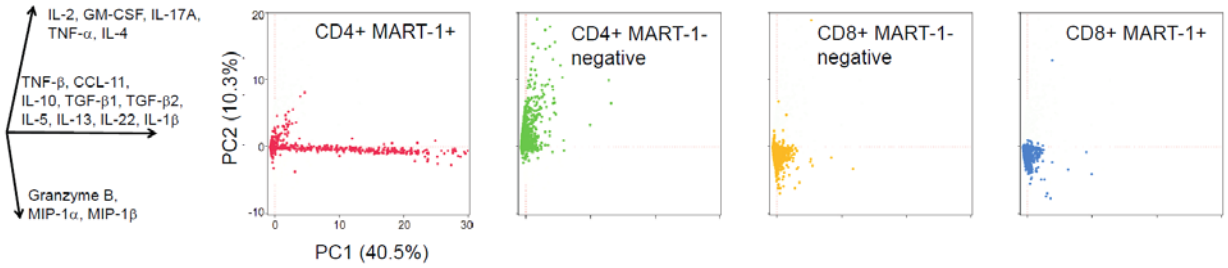

Supplementary Figure 5. Differences between different cell types studied. Cytokine secretion florescence intensity data, collected from the single cells functional assays, and collated for all time points and all three patients, was analyzed by principal component analysis. The first two components that jointly explain >50% of the data are plotted as the x- and y-axis. The four scatter plots highlight the individual single cell assays for each assayed T cell types. For each cell type, the points lie primarily along one direction. These different directions represent specific set of functions, which are given in the key at left. The ability of PCA to resolve the various phenotypes argues for the validity of the FACS/SCBC approach.

Supplementary Table 4. Functional differences of polyfunctional T cells and the rest T cells.

In mean fluorescence intensity

	IL2	IL17A	IFNg	TNFa	IL13	TNFb	CCL11	GB	TGFb1	IL4	IL5	IL6	IL10	GMCSF	TGFb2	MIP1a	MIP1b	IL22	IL1b	**Mean**	**Median**
MFI of polyfunctional	299	434	5220	6096	222	236	1546	4104	105	222	284	2742	189	1472	424	10922	9723	324	478	**2371**	**434**
MFI of the rest	36	39	152	227	35	47	195	789	36	23	68	38	15	7	36	1330	1358	63	48	**239**	**47**
Ratio	**8**	**11**	**34**	**27**	**6**	**5**	**8**	**5**	**3**	**10**	**4**	**71**	**12**	**211**	**12**	**8**	**7**	**5**	**10**	**10**	**9**

In mean molecular number

	IL2	IL17A	IFNg	TNFa	IL13	TNFb	CCL11	GB	TGFb1	IL4	IL5	IL6	IL10	GMCSF	TGFb2	MIP1a	MIP1b	IL22	IL1b	**Mean**	**Median**
Mean molecule number of polyfunctional	2.3E+05	4.8E+05	6.9E+07	9.4E+07	1.2E+05	1.4E+05	6.0E+06	4.3E+07	2.8E+04	1.2E+05	2.0E+05	1.9E+07	9.0E+04	5.5E+06	4.5E+05	3.0E+08	2.4E+08	2.7E+05	5.8E+05	**4.1E+07**	**4.8E+05**
Mean molecule number of the rest	2.4E+03	2.8E+03	4.3E+04	9.6E+04	2.2E+03	4.0E+03	7.1E+04	1.2E+06	2.4E+03	9.4E+02	8.5E+03	2.8E+03	4.3E+02	9.0E+01	2.4E+03	3.3E+06	3.4E+06	7.5E+03	4.2E+03	**4.3E+05**	**4.0E+03**
Ratio	**93**	**168**	**1599**	**978**	**55**	**35**	**85**	**37**	**11**	**132**	**24**	**6909**	**209**	**60546**	**192**	**92**	**70**	**36**	**137**	**96**	**118**

Time-dependent functional changes

We analyzed the samples from the three patients to compare the functional dynamics of the CD8+ MART-1+ T cells (using the pSI) against the frequency and phenotypic changes of these cells, as well as changes in tumor burden (**Figure 3**). All three patients exhibited an initial reduction in tumor volume, followed by tumor regrowth, but with different times to tumor relapse (**Figure 3a**). On the other hand, the patients had evidence of engraftment of the TCR engineered cells (**Figure 3b**). The cells proliferated briskly following ACT by at least one log expansion in total cell numbers, and then diminished gradually. At least 10^9 MART-1+ T cells, which accounted for >10% of blood T lymphocytes, remained in circulation out to day 90 post-ACT. The cellular phenotyping, based upon cell surface marker expression, revealed relatively uniform changes among the three patients, from an early differentiation phenotype (naïve, central memory and effector memory) to a later differentiation phenotype (effector memory RA and effector) (**Figure 3c, Methods and Supplementary Table 5**).

These observations contrast with the functional changes recorded for the polyfunctional T cells, as represented by the pSI plots of **Figure 3d**. These plots reveal large amplitude functional changes, as well as clear differences between the patients. For F5-1, at day 7 post-ACT, the CD8+ MART-1+ T cells predominately produced the cytotoxic molecule granzyme B, which accounted for >70% of the total functional intensity. However, by day 30, the pSI of these cells declined by around 100-fold. The functional strength of these cells begins to recover by day 45, but that recovery is accompanied by a different set of functions, including TNF-α, IFN-γ and inflammatory cytokines (such as IL-6), with no cytotoxic granule production. For F5-2, the CD8+ MART-1+ T cells only exhibited high antitumor effector functions (IFN-γ and TNF-α) after day 30. Patient F5-8 exhibited strong antitumor functions (granzyme B, IFN-g and TNF-a) initially that rapidly declined by day 30 post-ACT.

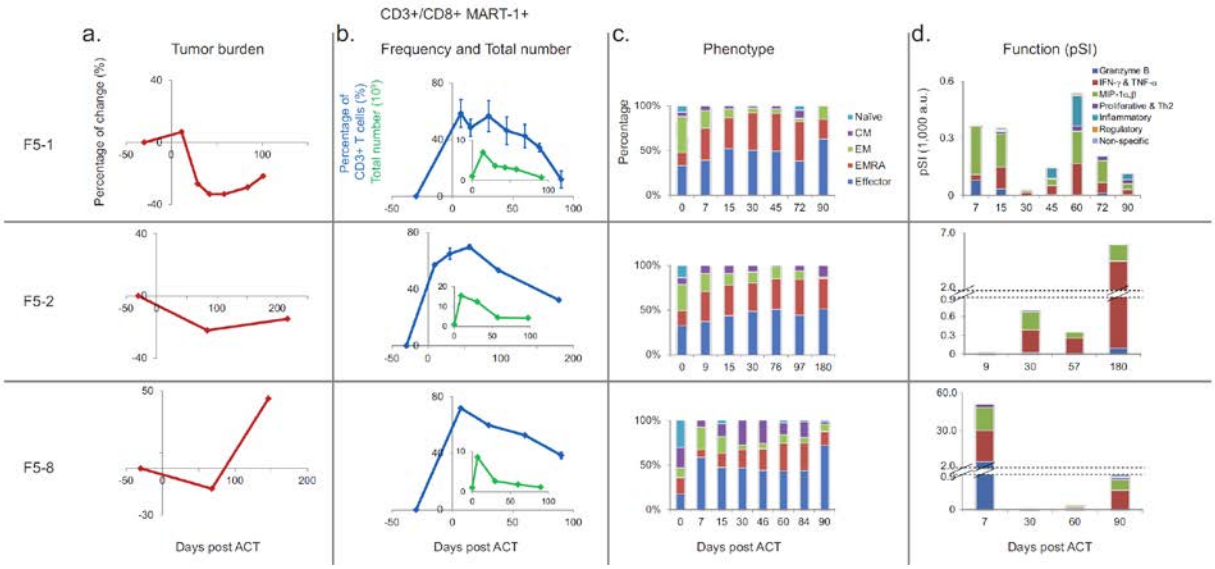

Figure 3. Time-dependent changes in tumor burden, and in number, phenotype, and function of CD8+ MART-1+ T cells. Each row provides results for a different patient (F5-1, F5-2, and F5-8). **a.** Changes in tumor burden, as measured by a modified RECIST method (Methods). **b.** Changes of frequency (blue) and total number (green insert) of CD8+ MART-1+ T cells. **c.** Phenotypic changes of CD8+ MART-1+ T cells. The percentage of each T cell phenotype (naïve, central memory, effector memory, effector memory RA, effector) is represented by a different color. **d.** Functional changes (in pSI) of CD8+ MART-1+ T cells. Each cytokine function group is represented by a different color. For F5-2 and F5-8, the y-axis is discontinuous to allow for large functional differences to be represented on the same graph.

Supplementary Table 5. Antibody panel used for flow cytometry immunophenotyping analysis.

Fluorchrome	Tube a	Tube b	Tube c
Pacific Blue	CD8 (3B5)*		
FITC	CD45RO (UCHL1)**	CD279 [PD1] (MHH4)**	CD28 (CD28.2)**
PE	Mart1 Tetramer***		
Dump Channel	7AAD***		

ECD	HLA-DR (Immu-357)***	CD45RA (2H4DHIILDB9)***	CD62L (DREG56)***
APC/AlexaFluor647	CD127 (hIL07R-M21)**	CCR7 (3D12)**	CD44 (G44-26)**
AlexaFluor700	CD3 (UCHT-1)*		
APC-Cy7	CD25 (M-A251)**	CD195[CCR5] (2D7/CCR5)**	CD27 (M-T271)**
PE-Cy7	CD4 (RPA-T4)$		

In parenthesis the clone used for detecting the CDs. * Life Science; ** BDbioscience;*** Beckman Coulter; $ Biolegend.

The functional behavior of the other profiled T cell types also exhibited sharp time-dependent changes. We present such data for patient F5-1 in **Figure 4a-f**. Functional changes for patients F5-2 and F5-8 are shown in **Supplementary Figures 6 and 7**. A table that summarizes changes between day 60 and day 07 for the three patients is provided in **Figure 4g**. The pSI of CD4+ MART-1+ T cells drops by ~100-fold at day 7 post ACT and shows an unstable functional profile, switching from proliferative-dominant (IL-2) at day 0 to antitumor effector-dominant (IFN-γ, TNF-α) on day 7, to inflammatory, regulatory and non-specific-dominant on day 30 (**Figure 4a**). We also recorded an accelerated disappearance of these cells, comparing to the CD8+ MART-1+ T cells (**Figure 4b**). A similar decrease in the pSI with functional shifting was observed for patient F5-8 (**Supplementary Figures 7 and Figure 4g**). For F5-2, no cytokine production was detected from this T cell population. Thus, this group of unnatural T cells -CD4+ T cells expressing TCRs recognizing a MHC class I-restricted antigen- lacked the ability to proliferate and perform stable functions *in vivo*.

The lymphodepletion and subsequent recovery process is reflected in the time-dependent functional changes of the MART-1-negative T cells (**Figure 4c-f**). For CD8+ MART-1-negative T cells from patient F5-1, the composition of the pSI is relatively unchanged across the 90 day period post-ACT, and exhibits cytotoxic and other anti-tumor functions throughout (**Figure 4c**). At around day 30 post-ACT, four populations attributable to epitope spreading were detected (**Figure 4d**). The presence of these populations was transient, diminishing again by day 72 post-ACT. Patient F5-2 presented similarities to F5-1. For example, a similar epitope spreading event and a durable, antitumor effector function-dominant pSI were both recorded for the CD8+ MART-1-negative T cell population of F5-2 (**Figure 4g and Supplementary Figure 6**). By contrast, patient F5-8, who had the lowest level of antitumor response, as well as a rapid tumor relapse (**Table 1 and Figure 4g**), presented no evidence for epitope spreading, and only a transient, anti-tumor pSI that had diminished by day 30 post-ACT (**Figure 4g and Supplementary Figure 7**).

In patient F5-1, the pSI of the CD4+ MART-1-negative T cells diminished during the lymphodepletion preconditioning and recovered by day 45. In absolute amplitude, the functional composition of these cells was relatively constant, and was dominated by proliferative functions (such as IL-2 and GM-CSF) (**Figure 4e**). However, starting around days 30-45, regulatory functions (TGF-β and IL-10) increased most significantly (by 27-fold relative to day 7) (**Figure 4f and g**). This strong increase of regulatory functions in these non-TCR transgenic T cells was also noted in samples from patient F5-8 as well at around day 60 (**Figure 4g and Supplementary Figure 7**).

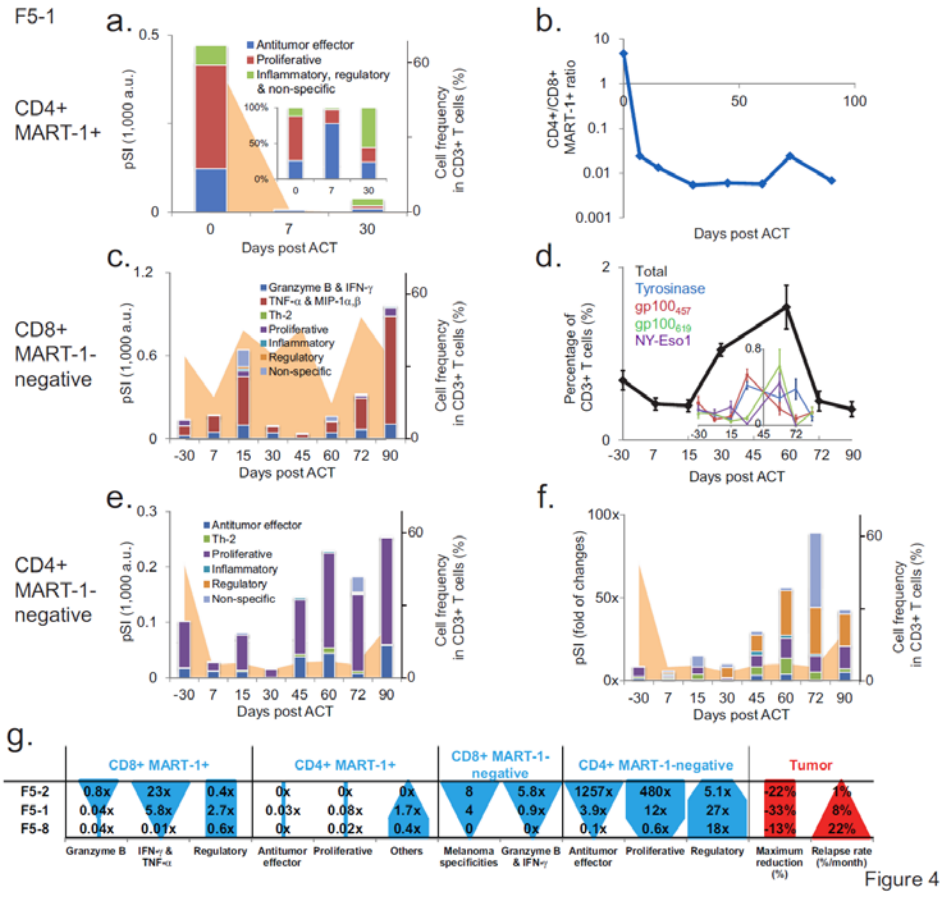

Figure 4

Figure 4. Functional changes of other T cell types for patient F5-1 over time and a summary of functional changes for all the three patients. a. Functional changes of the CD4+ MART-1+ T cells, plotted as a bar graph in pSI. The total frequency of this phenotype is plotted as the orange background.

Each cytokine function group is represented by a different color. The percent composition of the functions is provided in the insert. **b.** The frequency ratio of CD4+ MART-1+ to CD8+ MART-1+ T cells. **c.** Functional changes of the CD8+ MART-1-negative T cells, with cell frequency presented as the orange background. **d.** Frequency of antigen-specific T cells recognizing melanoma antigen other than MART-1 over the course of the therapy. The total frequency is plotted as the black line to provide an overall view of epitope spreading. The frequency of each antigen specificity detected is provided in the insert, denoted by different colors. **e.** Functional changes of the CD4+ MART-1-negative T cells, with cell frequency presented as the orange background. **f.** Relative functional changes of the CD4+ MART-1-negative T cells normalized to those observed at day 7 by each cytokine group, along with cell frequency. **g.** A summary of functional changes for each T cell type analyzed across three patients. The ratio is calculated by the pSI for a cytokine functional group at day 60 relative to that at day 7. The patients are ordered according to increasing tumor relapse rate. The differences between patients in cell function (solid blue shapes) and in tumor burden (red shapes) are shown graphically in the table.

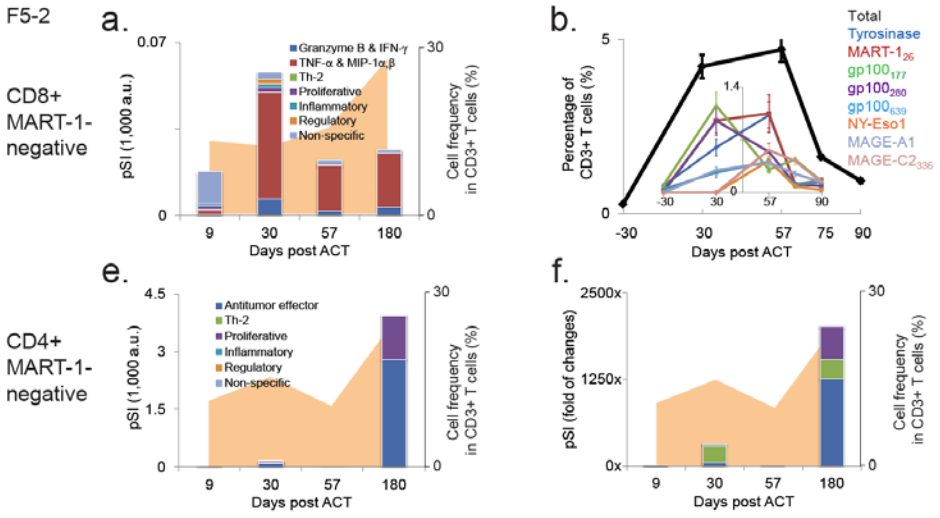

Supplementary Figure 6. Functional changes of other T cell phenotypes for patient F5-2 over time. **a.** Functional changes of the CD8+ MART-1-negative T cells, with cell frequency presented as the orange background. **b.** The frequency of antigen-specific T cells recognizing melanoma antigen other than

MART-1 over the course of the therapy. The total frequency is plotted as the black line to provide an overall view of epitope spreading. The frequency of each antigen specificity detected is provided in the insert, denoted by different colors. **c.** Functional changes of the CD4+ MART-1-negative T cells, with cell frequency presented as the orange background. **d.** Relative functional changes of the CD4+ MART-1-negative T cells normalized to those observed at day 07, along with cell frequency.

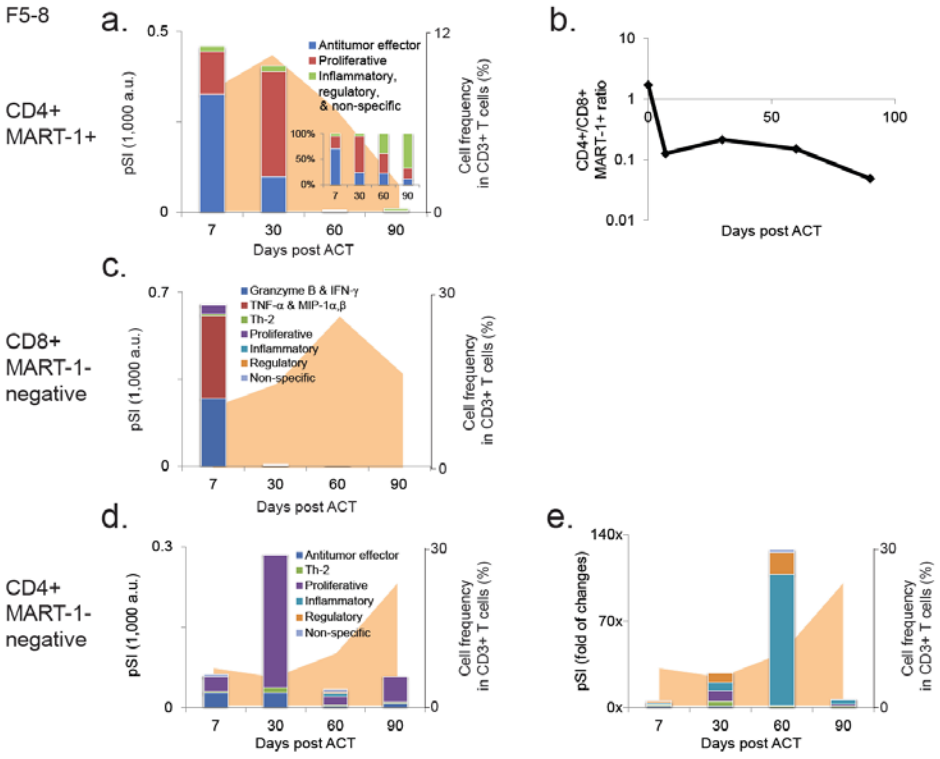

Supplementary Figure 7. Functional changes of other T cell phenotypes for patient F5-8 over time. **a.** Functional changes of the CD4+ MART-1+ T cells, plotted as a bar graph in pSI. The total frequency of this phenotype is plotted as the orange background. Each cytokine function group is represented by a different color. The percent composition of the functions is provided in the insert. **b.** The frequency ratio of CD4+ MART-1+ to CD8+ MART-1+ T cells. **c.** Functional changes of the CD8+ MART-1-negative T cells, with cell frequency presented as the orange background. **d.** Functional changes of the CD4+

MART-1-negative T cells, with cell frequency presented as the orange background. **e.** Relative functional changes of the CD4+ MART-1-negative T cells normalized to those observed at day 07, along with cell frequency.

Discussion

Little is known about the mechanisms that lead to tumor progression after a response in patients receiving ACT immunotherapy. For many years the prevailing concepts were based on the outgrowth of tumor escape variants that down regulated the expression of tumor antigens or molecules of the antigen expressing machinery, or the pre-existence of mutant clones that were insensitive to immune cell attack (76). More recently, several experiences are pointing to direct adaptive responses of tumor resultant from the T cells themselves modulating the tumor target, with the tumors changing through a variety of mechanisms to become insensitive to CTL attack. Examples include the up-regulation of PD-L1 (B7-H1) in response to interferons produced by tumor infiltrating T cells (77), or the antigen-specific T cells producing cytokines (i.e. TNF-α) that result in melanoma cells that express melanosomal antigens to dedifferentiate to escape (78). These are cancer cell-intrinsic mechanisms of resistance in response to adequately activated tumor antigen-specific T cells with full effector functions. A series of cancer cell-extrinsic mechanisms of resistance to immunotherapy have also been postulated, with a major focus on the presence of immune suppressive cells in tumors. The role of regulatory T cells, indoleamine-2.3-dyoxigenase (IDO) positive dendritic cells, and myeloid-derived suppressor cells (MDSC) in dampening immune responses in tumors has been well established in animal model systems and in patient-derived samples (79). Some of these immune suppressive cells are attracted or activated by the tumor-mediated secretion of immune suppressive factors, such as the transforming growth factor beta (TGF-β), vascular endothelial growth factor (VEGF) and certain other chemokines.

The study of immune cell-intrinsic mechanisms of resistance has been limited by the complexity of repeatedly assaying immune functions over time, and has typically relied on assays quantifying the frequency of tumor-specific T cells, or through analysis of a single effector molecule, or through the analyses of surface proteins for identifying different T cell phenotypes. However, T cells produce a large amount of coordinated proteins in response to antigen recognition, and the breadth and depth of that immune response is guided by the spectrum and level of the proteins being produced (17). For example, it

has been previously shown in mouse models that the functional behavior of polyfunctional T cells best reflects the overall quality of an immune response (80), presumably because multiple T cell functions are needed to orchestrate a successful immune response.

In the current studies we interrogated T cell responses to cancer by applying new generation, multiplexed immune monitoring assays. These assays yield an unprecedented high resolution view of T cell functional dynamics in patient-derived samples. These are highly involved studies, and so we focused on extensively analyzing samples from three patients that exhibited different degrees of tumor response after ACT immunotherapy. Our studies suggest that there is an initial wave of cytotoxicity-dominated antitumor functions from adoptively transferred CD8+ MART-1-specific T cells. This leads to initial melanoma tissue destruction as detected by the decrease in the size of the metastatic lesions. As has been noted in autoimmune diseases, this initial tissue destruction can lead to the expansion of T cells with specificity for other melanoma antigens, or epitope spreading (75). Epitope spreading within the population of the CD8+ MART-1-negative T cells was detected around day 30 in the two patients who had the best tumor responses, and that population of T cells retained robust antitumor functions out to at least day 90. However, the frequency of tumor-specific CTLs induced by epitope spreading was not maintained. One possibility, consistent with the data reported here, is that the CD4+ T cells, as they recover from the lymphodepletion regimen, may regulate and inhibit the anti-tumor immune response. This is also consistent with a report indicating that a deeper lymphodepletion regimen can improve the outcome for melanoma patients participating in TIL-based ACT trials (81).

A number of factors based on properties of cell phenotype and persistence have been identified to associate with ACT therapy efficacy (67, 82). Our study supports the notion that T cell function is another important aspect that requires close scrutiny, since even when T cells show similar persistence and phenotypic changes *in vivo*, they can exhibit dramatically different functional profiles. Although the number of patients in this study was limited, each of the patients was very thoroughly investigated, to the extent that we can begin to associate some of the functional changes with differences in tumor relapse

between patients. As showed in **Figure 4g**, a strong gain (day 60 compared to day 7) of IFN-γ and TNF-α for CD8+ MART-1+ T cells, granzyme B and IFN-γ for CD8+ MART-1-negative T cells, antitumor effector and proliferative functions for CD4+ MART-1-negative T cells and a wider epitope spreading are, at least for this study, associated with a slower tumor relapse. By contrast, a strong gain of regulatory functions in CD4+ MART-1-negative T cells following their recovery from the lymphodepletion regimen appears to be associated with a corresponding faster tumor relapse (**Figure 4g**).

These results suggest the need to incorporate strategies to maintain the functional properties of the TCR transgenic cells used for ACT therapies. These may include modifications of the culturing system to foster the generation of TCR transgenic cells with improved ability to persist functionally over time (83), pharmacological manipulations to provide more prolonged gamma-chain cytokine support (such as protracted low dose IL-2 administration), blockage of negative co-stimulatory signaling like CTLA4 or PD-1, or additional genetic engineering of the TCR transgenic cells to include cytokines or transcription factors that could maintain their function *in vivo*. It is also clear that the endogenous T cells can expand and boost the antitumor immune response and can regulate or otherwise influence the function of the infused T cells. Understanding this biology, and learning to control it, appears to be an important research direction for ACT therapy. A broader application of these single cell functional analyses may prove valuable for probing the successes and failures across the spectrum of cellular immunotherapies. In particular, recent ACT trials that have utilized either engineered TCRs or CARs directed against antigens with better tumor selectivity than MART-1, have resulted in cases with complete regressions (62, 70). Directing the tools described herein towards analyzing those successes may provide powerful insights into how best to design such therapies.

Methods

Clinical trial conduct Patients were enrolled in the clinical trial after signing a written informed consent approved by the UCLA IRB (#08-02-020 and #10-001212**)** under an investigator new drug (IND) filed with the US Food and Drug Administration (IND# 13859). The study had the clinical trial registration number NCT00910650. Eligible patients had MART-1 positive metastatic melanoma by immunohistochemistry (IHC) and were HLA-A*0201 positive by intermediate resolution molecular HLA testing. Objective clinical responses were recorded following a modified Response Evaluation Criteria in Solid Tumors (RECIST) (84), where tumor burden is quantified by the sum of the largest diameter of each tumor lesion measured either by PET/CT scan or physical exam. Skin and subcutaneous lesions evaluable only by physical exam were considered measurable if adequately recorded using a photographic camera with a measuring tape or ruler; there was no minimum size restriction for these lesions.

Immunophenotyping and immunohistochemistry (IHC) Calculation of the absolute number of blood circulating MART-1-tetramer-specific T cells was performed by a dual platform method, combining the readout from flow cytometry and automated hematology analyzer (85). The flow cytometry-based MHC tetramer assay studies and the adaptation of a multicolor flow cytometry have also been previously described (86-88). T cells were classified using a panel of antibodies as described in Supplementary Table 5. Naïve cells were classified as CD45+/CCR7+/CCR5-/PD1-, CD27+/CD28-/CD62L+, and CD45+/CCR7+/CCR5-/PD1+; central memory (CM) as CD45RO-/CD25-/HLA-DR-/CD127+; effector memory (EM) as CD45-/CCR7-/CCR5+/PD1+, CD45-/CCR7-/CCR5-/PD1+, CD45-/CCR7-/CCR5-/PD1-, CD45-/CCR7-/CCR5-/PD1-, and CD27-/CD28-/CD62L-; effector memory RA (EMRA) in CD8+ as CD45RA+/CCR7-/CCR5-/PD1+, CD45RA+/CCR7-/CCR5+/PD1+; and effector as CD45RO+/CD25+/HLA-DR+/CD127-, CD45RO+/CD25+/HLA-DR-/CD127-, CD45RO+/CD25-/HLA-DR-/CD127- (31, 89). Immunohistochemistry staining was performed following standard methods as previously described (48, 90).

Enumeration of antigen-specific T cells Our previously described peptide/MHC tetramer cell sorting approach (NACS) was used to enumerate antigen-specific T cells from cryopreserved PBMC obtained from patients through peripheral blood draws and leukaperesis as we have previously described (73). Briefly, NACS chips were generated by incubating p/MHC tetramer-ssDNA conjugate cocktail for 1 hour. Then 1 million PBMC were added on chip in RPMI medium for 20 minutes. Afterwards the slide was washed with RPMI medium and stained with CD3, CD4 and CD8 antibody cocktail for 30 minutes. Then the sample was fixed with PFA/PBS buffer for imaging with a Nikon TI florescence microscope (Melville, NY). The p/MHC tetramer was manufactured in-house. The method was shown to have good assay performance in comparison with flow cytometry analysis (73) (**Supplementary Figure 8**). The sensitivity of these NACS arrays to detect a particular tumor-antigen specific T cell population from all CD3+ T cells is about ~0.1% (73).

Purification of phenotypically defined T cells We used two methods to purify T cells for SCBC functional assays. For the NACS/SCBC protocol, the MART-1+ or CD3+ cells were purified using p/MHC tetramer or CD3 antibody as described above. Then cells were released and loaded on the SCBC chip within 30 minutes with MART-1 tetramer/CD28 antibody (10^{-7}M and 2ug/ml, respectively) (91) or CD3/CD28 antibody (10ug/ml and 2ug/ml, respectively) stimulation.

For the FACS/SCBC protocol, the T cells were sorted using a BD ARIA II machine (Franklin Lakes, NJ). Cells were gated on FSC-A, FSC-H, SSC-A (for singlet, lymphocytes identification), 7-AAD (viability), CD3 (clone: UCHT-1), CD4 (OKT-4), CD8 (HIT8a), MART-1 tetramer, CD45RA (HI100), CCR7 (G043H7). The machine was calibrated with BD positive and negative CompBeads before usage. Before sorting, PBMC had a viability of >80% and the four collected T cell populations were gated to achieve >95% viability and purity. The following cell populations were sorted and analyzed: CD3+CD4+MART-1+, CD3+CD8+MART-1+, CD3+CD4+ non-naïve MART-1-negative and CD3+CD8+ non-naïve MART-1-negative. Naïve T cells were classified as CD45RA+ and CCR7+. Then the cells were washed before stimulation with MART-1 tetramer/CD28 antibody, MART-1 tetramer, CD3/CD28 antibodies or

CD3 antibody, respectively. The concentration used are: MART-1 tetramer (10^{-7}M) (91), CD3 antibody (10ug/ml), and CD28 antibody (2ug/ml). All cell samples were also non-specifically stimulated with PMA (5ng/ml) and ionomycin (500ng/ml) given the long time and low-concentration staining required for FACS cell sorting before on chip functional assays that may lead to a low level of spontaneous cytokine production. However, these could be recovered by mitogen stimulation, as showed in **Supplementary Figure 2**.

Integrated functional assays of single T cells We integrated upstream cell purification techniques with the SCBC (10) to enable the study of the functional proteomics from phenotypically defined single cells. The chips used here had a capacity of 1360 microchambers, and permitted the simultaneous measurement of 19 cytokines from single cells. The chip was first blocked with 3% BSA/PBS buffer, before hybridized with antibody-DNA cocktails (10). Each step takes an hour. After PBMC was stimulated and loaded onto an SCBC chip, the chip was imaged using high resolution bright field microscopy. Cells were incubated on chip for 12 hours at 37 degree in 5% CO_2 cell incubator. Then they were rapidly washed out. The assay was completed by applying secondary biotinylated antibodies, streptavidin-cy3 and a final wash with 3% BSA/PBS buffer in sequence. Every step takes an hour. Finally, the slide was washed with PBS and 50/50 PBS/DI water in sequence before spin dried and scanned by a Molecular Devices GenePix 4400A scanner (Sunnyvale, CA). Detailed calibration and validation has been provided previously, where the measurement accuracy (coefficient of variation) of any given protein within a single cell assay is ~10% (10), and the assay sensitivity is several hundred molecules (10).

Computational algorithm and statistical analysis Custom routines written in the R software package were used to process, analyze and visualize the single cell functional assay results. The algorithm converts original scanned fluorescence images into data files containing the fluorescence intensities for each assayed protein within a given microchamber, and then matched them with the number of cells counted from videos of the chip collected. Data from empty chambers is used to measure the background level for each protein. This data was used to generate protein abundance histograms, which is fitted by

normal distributions and non-parametric methods, judged by Goodness of fit (92). The mean of the histogram, identified by the best fit, is used as the background level. Single cell data was then normalized by subtracting this background, so that different samples can be compared. The single cell data was then fitted by finite mixture models and the gate that separates the cytokine-producing and cytokine-non-producing cells is identified (92, 93). To ensure robustness, the results were individually checked. These data were then used for subsequent hierarchical clustering and principal component analysis (93), as well as the analysis of the pSI of the cells. Statistics and visual presentation was automatically generated by the algorithm.

The polyfunctional strength index (pSI) is defined as total functional intensity contributed by all polyfunctional T cells of a given cell type, at a specific time point. Therefore, for a given cell type, the pSI is calculated as the percentage (%) of polyfunctional T cells relative to all CD3+ T cells, multiplied by the sum of the mean fluorescence intensity (MFI) of each of the 19 assayed cytokines from the polyfunctional subset, i.e.

$$pSI\ for\ a\ cell\ type\ at\ a\ time\ point = \%\ of\ polyfunctional\ T\ cells\ within\ T\ cells \times \sum_{i=1}^{19} MFI\ of\ cytokine\ i\ of\ the\ polyfunctional\ T\ cells$$

Then, we further plot pSI as a segmented bar showing the contribution of each group of cytokines identified by hierarchical clustering. When comparing polyfunctional T cells with other T cells, fluorescence intensity is converted into molecular number using the calibration curves provided in (10).

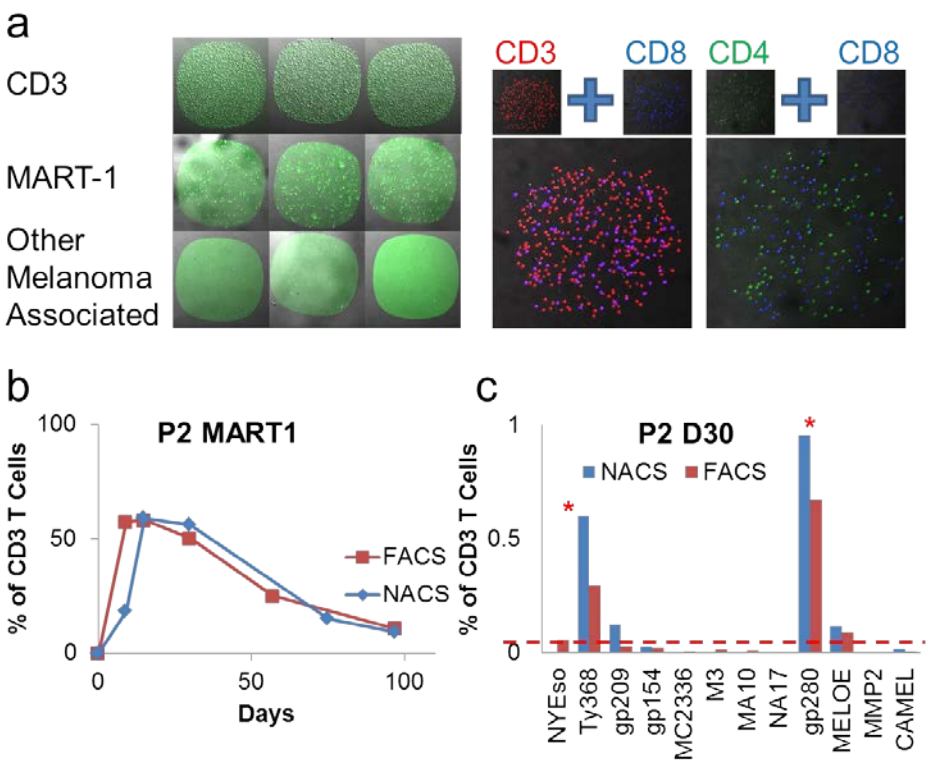

Supplementary Figure 8. Validation of melanoma antigen specific T cell population enumeration assays. a. Images of cells captured by CD3 antibody, MART-1/HLA-A0201 tetramer, and other melanoma-antigen/MHC tetramer on a multiplex microarray (left). Micrographs of immunofluorescence staining of CD3, CD4 and CD8 conducted after the cell capture (right). b. Comparison of the p/MHC tetramer microarray approach (NACS) with flow cytometry p/MHC tetramer staining for determining the abundance, over time, of the MART-1 T cells from patient F5-2. c. A comparison of NACS and FACS assays for the quantitation of the populations of other melanoma associated antigen-specific T cells from patient F5-2 on day 30 post-ACT.

References

1. Ribas A, Camacho LH, Lopez-Berestein G, Pavlov D, Bulanhagui CA, Millham R, et al. Antitumor Activity in Melanoma and Anti-Self Responses in a Phase I Trial With the Anti-Cytotoxic T Lymphocyte–Associated Antigen 4 Monoclonal Antibody CP-675,206. J Clin Oncol. 2005;23:8968-77.

2. Porter DL, Levine BL, Kalos M, Bagg A, June CH. Chimeric Antigen Receptor–Modified T Cells in Chronic Lymphoid Leukemia. New England Journal of Medicine. 2011;365:725-33.

3. Rosenberg SA, Restifo NP, Yang JC, Morgan RA, Dudley ME. Adoptive cell transfer: a clinical path to effective cancer immunotherapy. Nat Rev Cancer. 2008;8:299-308.

4. Restifo NP, Dudley ME, Rosenberg SA. Adoptive immunotherapy for cancer: harnessing the T cell response. Nat Rev Immunol. 2012;12:269-81.

5. Hunder NN, Wallen H, Cao J, Hendricks DW, Reilly JZ, Rodmyre R, et al. Treatment of Metastatic Melanoma with Autologous CD4+ T Cells against NY-ESO-1. New England Journal of Medicine. 2008;358:2698-703.

6. June C, Rosenberg SA, Sadelain M, Weber JS. T-cell therapy at the threshold. Nat Biotech. 2012;30:611-4.

7. Turtle CJ, Riddell SR. Genetically retargeting CD8+ lymphocyte subsets for cancer immunotherapy. Curr Opin Immunol. 2011;23:299-305.

8. Rosenberg SA, Yang JC, Sherry RM, Kammula US, Hughes MS, Phan GQ, et al. Durable Complete Responses in Heavily Pretreated Patients with Metastatic Melanoma Using T-Cell Transfer Immunotherapy. Clinical Cancer Research. 2011;17:4550-7.

9. Rosenberg SA, Morgan RA, Dudley ME, Wunderlich JR, Hughes MS, Yang JC, et al. Cancer regression in patients after transfer of genetically engineered lymphocytes. Science. 2006;314:126-9.

10. Rosenberg SA, Johnson LA, Morgan RA, Dudley ME, Cassard L, Yang JC, et al. Gene therapy with human and mouse T-cell receptors mediates cancer regression and targets normal tissues expressing cognate antigen. Blood. 2009;114:535-46.

11. Robbins PF, Morgan RA, Feldman SA, Yang JC, Sherry RM, Dudley ME, et al. Tumor Regression in Patients With Metastatic Synovial Cell Sarcoma and Melanoma Using Genetically Engineered Lymphocytes Reactive With NY-ESO-1. J Clin Oncol. 2011;29:917-24.

12. Seder RA, Darrah PA, Roederer M. T-cell quality in memory and protection: implications for vaccine design. Nat Rev Immunol. 2008;8:247-58.

13. Appay V, Douek DC, Price DA. CD8+ T cell efficacy in vaccination and disease. Nat Med. 2008;14:623-8.

14. Betts MR, Nason MC, West SM, De Rosa SC, Migueles SA, Abraham J, et al. HIV nonprogressors preferentially maintain highly functional HIV-specific CD8+ T cells. Blood. 2006;107:4781-9.

15. Ma C, Fan R, Ahmad H, Shi Q, Comin-Anduix B, Chodon T, et al. A clinical microchip for evaluation of single immune cells reveals high functional heterogeneity in phenotypically similar T cells. Nat Med. 2011;17:738-43.

16. Kwong GA, Radu CG, Hwang K, Shu CJ, Ma C, Koya RC, et al. Modular Nucleic Acid Assembled p/MHC Microarrays for Multiplexed Sorting of Antigen-Specific T Cells. J Am Chem Soc. 2009;131:9695-703.

17. Koya RC, Mok S, Comin-Anduix B, Chodon T, Radu CG, Nishimura MI, et al. Kinetic phases of distribution and tumor targeting by T cell receptor engineered lymphocytes inducing robust antitumor responses. Proceedings of the National Academy of Sciences. 2010;107:14286-91.

18. Ribas A, Timmerman JM, Butterfield LH, Economou JS. Determinant spreading and tumor responses after peptide-based cancer immunotherapy. Trends in Immunology. 2003;24:58-61.

19. Ferrone S, Marincola FM. Loss of HLA class I antigens by melanoma cells: molecular mechanisms, functional significance and clinial relevance. Immunology Today. 1995;16:487-94.

20. Taube JM, Anders RA, Young GD, Xu H, Sharma R, McMiller TL, et al. Colocalization of Inflammatory Response with B7-H1 Expression in Human Melanocytic Lesions Supports an Adaptive Resistance Mechanism of Immune Escape. Science Translational Medicine. 2012;4:127ra37.

21. Landsberg J, Kohlmeyer J, Renn M, Bald T, Rogava M, Cron M, et al. Melanomas resist T-cell therapy through inflammation-induced reversible dedifferentiation. Nature. 2012;490:412-6.

22. Chow MT, Möller A, Smyth MJ. Inflammation and immune surveillance in cancer. Seminars in Cancer Biology. 2012;22:23-32.

23. Seder RA, Darrah PA, Patel DT, De Luca PM, Lindsay RWB, Davey DF, et al. Multifunctional T(H)1 cells define a correlate of vaccine-mediated protection against Leishmania major. Nat Med. 2007;13:843-50.

24. Dudley ME, Yang JC, Sherry R, Hughes MS, Royal R, Kammula U, et al. Adoptive Cell Therapy for Patients With Metastatic Melanoma: Evaluation of Intensive Myeloablative Chemoradiation Preparative Regimens. J Clin Oncol. 2008;26:5233-9.

25. Klebanoff CA, Gattinoni L, Palmer DC, Muranski P, Ji Y, Hinrichs CS, et al. Determinants of Successful CD8+ T-Cell Adoptive Immunotherapy for Large Established Tumors in Mice. Clinical Cancer Research. 2011;17:5343-52.

26. Gattinoni L, Klebanoff CA, Restifo NP. Pharmacologic Induction of CD8+ T Cell Memory: Better Living Through Chemistry. Science Translational Medicine. 2009;1:11ps2.

27. Therasse P, Arbuck SG, Eisenhauer EA, Wanders J, Kaplan RS, Rubinstein L, et al. New Guidelines to Evaluate the Response to Treatment in Solid Tumors. Journal of the National Cancer Institute. 2000;92:205-16.

28. Hultin LE, Chow M, Jamieson BD, O'Gorman MRG, Menendez FA, Borowski L, et al. Comparison of interlaboratory variation in absolute T-cell counts by single-platform and optimized dual-platform methods. Cytometry Part B: Clinical Cytometry. 2010;78B:194-200.

29. Comin-Anduix B, Gualberto A, Glaspy JA, Seja E, Ontiveros M, Reardon DL, et al. Definition of an Immunologic Response Using the Major Histocompatibility Complex Tetramer and Enzyme-Linked Immunospot Assays. Clinical Cancer Research. 2006;12:107-16.

30. Comin-Anduix B, Lee Y, Jalil J, Algazi A, de la Rocha P, Camacho L, et al. Detailed analysis of immunologic effects of the cytotoxic T lymphocyte-associated antigen 4-blocking monoclonal antibody tremelimumab in peripheral blood of patients with melanoma. Journal of Translational Medicine. 2008;6:22.

31. Tumeh PC, Koya RC, Chodon T, Graham NA, Graeber TG, Comin-Anduix B, et al. The Impact of Ex Vivo Clinical Grade Activation Protocols on Human T-cell Phenotype and Function for the Generation of Genetically Modified Cells for Adoptive Cell Transfer Therapy. Journal of Immunotherapy. 2010;33:759-68 10.1097/CJI.0b013e3181f1d644.

32. Appay V, van Lier RAW, Sallusto F, Roederer M. Phenotype and function of human T lymphocyte subsets: Consensus and issues. Cytometry Part A. 2008;73A:975-83.

33. Sallusto F, Lenig D, Forster R, Lipp M, Lanzavecchia A. Two subsets of memory T lymphocytes with distinct homing potentials and effector functions. Nature.

34. Ribas A, Comin-Anduix B, Chmielowski B, Jalil J, de la Rocha P, McCannel TA, et al. Dendritic Cell Vaccination Combined with CTLA4 Blockade in Patients with Metastatic Melanoma. Clinical Cancer Research. 2009;15:6267-76.

35. Huang RR, Jalil J, Economou JS, Chmielowski B, Koya RC, Mok S, et al. CTLA4 Blockade Induces Frequent Tumor Infiltration by Activated Lymphocytes Regardless of Clinical Responses in Humans. Clinical Cancer Research. 2011;17:4101-9.

36. Cochran JR, Cameron TO, Stern LJ. The Relationship of MHC-Peptide Binding and T Cell Activation Probed Using Chemically Defined MHC Class II Oligomers. Immunity. 2000;12:241-50.

37. Reynolds DA, Rose RC. Robust text-independent speaker identification using Gaussian mixture speaker models. Speech and Audio Processing, IEEE Transactions on. 1995;3:72-83.

38. Johnson R, Wichern DW. Applied Multivariate Statistical Analysis. 6 ed: Pearson; 2007.

Chapter 5

KIR genes modify Crohn's Disease susceptibility by reprogramming human natural killer cell function

Summary

Crohn's Disease (CD) is a common chronic inflammatory disorder of the gastrointestinal tract. Killer cell Immunoglobulin-like receptors (KIRs) and Human Leukocyte Antigen (HLA) class I ligands are combinatorially associated with risks to CD and other chronic inflammatory diseases, but the underlying cellular mechanisms remain unknown. Here we show that the specific genetic combinations of KIR and HLA result in functional reprogramming of natural killer (NK) cells, known as 'licensing', that permits them to modulate the $CD4^+$ T cell activation threshold *ex vivo*. Single cell multiplex functional proteomics reveal that genetically licensed NK cells are polarized to robustly produce pro-inflammatory cytokines and chemoattractants, and these cytokines account for NK cell augmentation of $CD4^+$ T cell proliferation. Our findings revealed a new biologic paradigm to understand KIR-associated susceptibility to CD and other chronic inflammatory syndromes.

In summary, KIR educated human NK cells promote a unique profile of cytokine production and T cell activation that indicate a mechanism for the Crohn's Disease susceptibility.

Chapter 6

Functional Heterogeneity Among Apparently Undifferentiated Hematopoietic Cells

Summary

The pool of hematopoietic stem and progenitor cells (HSPCs) in the bone marrow are multipotent progenitors of the mature hematopoietic cells in the tissues of an animal's body. The most immature but longest–lived of the bone marrow cells are the long-term HSCs, while the rest, including short-term HSCs and multipotent progenitor cells (MPPs), are shorter lived(94, 95). However, other than being progenitors of mature cells that have functional activities, little is known about the effector function properties of HSPCs. Here we combine transgenic and genetic knockout mouse models with a microchip based single cell proteomics platform to show that, although long-term hematopoietic stem cells (HSCs) (defined as $Lineage^{-}cKit^{+}Sca1^{+}CD150^{+}CD48^{-}$) do not secrete cytokines upon toll-like receptor (TLR) stimulation, LKS cells (defined as $Lineage^{-}cKit^{+}Sca1^{+}$), a population including short-term HSCs and MPPs, can produce cytokines upon direct TLR-4 and TLR-2 stimulation. Within the population of LKS cells, we detect multiple functional subsets of cells, specialized in producing myeloid-like or lymphoid-like cytokine combinations. Moreover, we show that cytokine production by LKS cells is regulated by NF-κB activity, because p50-deficient LKS cells show reduced cytokine production while microRNA-146a (miR-146a)-deficient LKS cells show significantly enhanced cytokine production. Our results demonstrate a remarkable ability of phenotypically undifferentiated HSPCs to function as cytokine-producing cells following activation of TLR/NF-κB signaling. Importantly, a portion of the LKS cells show a clear signature of myeloid/lymphoid differentiation branching even though they lack any known distinguishing surface markers.

References

1. Hodi FS, O'Day SJ, McDermott DF, Weber RW, Sosman JA, Haanen JB, et al. Improved Survival with Ipilimumab in Patients with Metastatic Melanoma. New England Journal of Medicine. 2010;363:711-23.
2. Rosenberg SA. Raising the Bar: The Curative Potential of Human Cancer Immunotherapy. Science Translational Medicine. 2012;4:127ps8.
3. Liu C, Peng W, Xu C, Lou Y, Zhang M, Wargo JA, et al. BRAF Inhibition Increases Tumor Infiltration by T cells and Enhances the Antitumor Activity of Adoptive Immunotherapy in Mice. Clinical Cancer Research. 2013;19:393-403.
4. Hunder NN, Wallen H, Cao J, Hendricks DW, Reilly JZ, Rodmyre R, et al. Treatment of Metastatic Melanoma with Autologous CD4+ T Cells against NY-ESO-1. New England Journal of Medicine. 2008;358:2698-703.
5. Kantoff PW, Higano CS, Shore ND, Berger ER, Small EJ, Penson DF, et al. Sipuleucel-T Immunotherapy for Castration-Resistant Prostate Cancer. New England Journal of Medicine. 2010;363:411-22.
6. Bendall SC, Simonds EF, Qiu P, Amir E-aD, Krutzik PO, Finck R, et al. Single-Cell Mass Cytometry of Differential Immune and Drug Responses Across a Human Hematopoietic Continuum. Science. 2011;332:687-96.
7. Bendall SC, Nolan GP, Roederer M, Chattopadhyay PK. A deep profiler's guide to cytometry. Trends in Immunology. 2012;33:323-32.
8. Bodenmiller B, Zunder ER, Finck R, Chen TJ, Savig ES, Bruggner RV, et al. Multiplexed mass cytometry profiling of cellular states perturbed by small-molecule regulators. Nat Biotech. 2012;30:858-67.
9. Newell Evan W, Sigal N, Bendall Sean C, Nolan Garry P, Davis Mark M. Cytometry by Time-of-Flight Shows Combinatorial Cytokine Expression and Virus-Specific Cell Niches within a Continuum of CD8+ T Cell Phenotypes. Immunity. 2012;36:142-52.
10. Ma C, Fan R, Ahmad H, Shi Q, Comin-Anduix B, Chodon T, et al. A clinical microchip for evaluation of single immune cells reveals high functional heterogeneity in phenotypically similar T cells. Nat Med. 2011;17:738-43.
11. Ma C, Cheung AF, Chodon T, Koya RC, Wu Z, Ng C, et al. Multifunctional T Cell Analyses to Study Response and Progression in Adoptive Cell Transfer Immunotherapy. Cancer Discovery. 2013.
12. Wang J, Tham D, Wei W, Shin YS, Ma C, Ahmad H, et al. Quantitating Cell–Cell Interaction Functions with Applications to Glioblastoma Multiforme Cancer Cells. Nano Letters. 2012;12:6101-6.
13. Varadarajan N, Julg B, Yamanaka YJ, Chen H, Ogunniyi AO, McAndrew E, et al. A high-throughput single-cell analysis of human CD8+ T cell functions reveals discordance for cytokine secretion and cytolysis. The Journal of Clinical Investigation. 2011;121:4322-31.
14. Han Q, Bagheri N, Bradshaw EM, Hafler DA, Lauffenburger DA, Love JC. Polyfunctional responses by human T cells result from sequential release of cytokines. Proceedings of the National Academy of Sciences. 2012;109:1607-12.
15. Varadarajan N, Kwon DS, Law KM, Ogunniyi AO, Anahtar MN, Richter JM, et al. Rapid, efficient functional characterization and recovery of HIV-specific human CD8+ T cells using microengraving. Proceedings of the National Academy of Sciences. 2012;109:3885-90.
16. Darrah PA, Patel DT, De Luca PM, Lindsay RWB, Davey DF, Flynn BJ, et al. Multifunctional T(H)1 cells define a correlate of vaccine-mediated protection against Leishmania major. Nature Medicine. 2007;13:843-50.
17. Seder RA, Darrah PA, Roederer M. T-cell quality in memory and protection: implications for vaccine design. Nat Rev Immunol. 2008;8:247-58.

18. Gordon S, Taylor PR. Monocyte and macrophage heterogeneity. Nat Rev Immunol. 2005;5:953-64.
19. O'Shea JJ, Hunter CA, Germain RN. T cell heterogeneity: firmly fixed, predominantly plastic or merely malleable? Nat Immunol. 2008;9:450-3.
20. Kaech SM, Wherry EJ. Heterogeneity and cell-fate decisions in effector and memory CD8(+) T cell differentiation during viral infection. Immunity. 2007;27:393-405.
21. Lee PP, Yee C, Savage PA, Fong L, Brockstedt D, Weber JS, et al. Characterization of circulating T cells specific for tumor-associated antigens in melanoma patients. Nature Medicine. 1999;5:677-85.
22. Seder RA, Darrah PA, Roederer M. T-cell quality in memory and protection: implications for vaccine design (vol 8, pg 247, 2008). Nat Rev Immunol. 2008;8.
23. Re F, Strominger JL. Heterogeneity of TLR-induced responses in dendritic cells: from innate to adaptive immunity. Immunobiology. 2004;209:191-8.
24. Chattopadhyay PK, Yu J, Roederer M. A live-cell assay to detect antigen-specific CD4(+) T cells with diverse cytokine profiles. Nature Medicine. 2005;11:1113-7.
25. Zak DE, Aderem A. Systems biology of innate immunity. Immunological Reviews. 2009;227:264-82.
26. Precopio ML, Betts MR, Parrino J, Price DA, Gostick E, Ambrozak DR, et al. Immunization with vaccinia virus induces polyfunctional and phenotypically distinctive CD8(+) T cell responses. Journal of Experimental Medicine. 2007;204:1405-16.
27. Mantovani A, Allavena P, Sica A, Balkwill F. Cancer-related inflammation. Nature. 2008;454:436-44.
28. Coussens LM, Werb Z. Inflammation and cancer. Nature. 2002;420:860-7.
29. Medzhitov R. Origin and physiological roles of inflammation. Nature. 2008;454:428-35.
30. Hagemann T, Balkwill F, Lawrence T. Inflammation and cancer: A double-edged sword. Cancer Cell. 2007;12:300-1.
31. Appay V, van Lier RAW, Sallusto F, Roederer M. Phenotype and Function of Human T Lymphocyte Subsets: Consensus and Issues. Cytometry Part A. 2008;73A:975-83.
32. Song KM, Rabin RL, Hill BJ, De Rosa SC, Perfetto SP, Zhang HH, et al. Characterization of subsets of CD4(+) memory T cells reveals early branched pathways of T cell differentiation in humans. Proceedings of the National Academy of Sciences of the United States of America. 2005;102:7916-21.
33. Kotecha N, Floress NJ, Irish JM, Simonds EF, Sakai DS, Archambeault S, et al. Single-cell profiling identifies aberrant STAT5 activation in myeloid malignancies with specific clinical and biologic correlates. Cancer Cell. 2008;14:335-43.
34. Bailey RC, Kwong GA, Radu CG, Witte ON, Heath JR. DNA-encoded antibody libraries: A unified platform for multiplexed cell sorting and detection of genes and proteins. Journal of the American Chemical Society. 2007;129:1959-67.
35. Fan R, Vermesh O, Srivastava A, Yen BKH, Qin LD, Ahmad H, et al. Integrated barcode chips for rapid, multiplexed analysis of proteins in microliter quantities of blood. Nature Biotechnology. 2008;26:1373-8.
36. Shin YS, Ahmad H, Shi QH, Kim H, Pascal TA, Fan R, et al. Chemistries for Patterning Robust DNA MicroBarcodes Enable Multiplex Assays of Cytoplasm Proteins from Single Cancer Cells. Chemphyschem. 2010;11:3063-9.
37. Wang J, Ahmad H, Ma C, Shi QH, Vermesh O, Vermesh U, et al. A self-powered, one-step chip for rapid, quantitative and multiplexed detection of proteins from pinpricks of whole blood. Lab Chip. 2010;10:3157-62.
38. Aderem A, Ulevitch RJ. Toll-like receptors in the induction of the innate immune response. Nature. 2000;406:782-7.

39. Fan J, Malik AB. Toll-like receptor-4 (TLR4) signaling augments chemokine-induced neutrophil migration by modulating cell surface expression of chemokine receptors. Nature Medicine. 2003;9:315-21.
40. Attig S, Hennenlotter J, Pawelec G, Klein G, Koch SD, Pircher H, et al. Simultaneous Infiltration of Polyfunctional Effector and Suppressor T Cells into Renal Cell Carcinomas. Cancer Res. 2009;69:8412-9.
41. De Rosa SC, Lu FX, Yu J, Perfetto SP, Falloon J, Moser S, et al. Vaccination in humans generates broad T cell cytokine responses. J Immunol. 2004;173:5372-80.
42. Makedonas G, Betts MR. Polyfunctional analysis of human t cell responses: importance in vaccine immunogenicity and natural infection. Springer Semin Immun. 2006;28:209-19.
43. Morgan RA, Dudley ME, Wunderlich JR, Hughes MS, Yang JC, Sherry RM, et al. Cancer regression in patients after transfer of genetically engineered lymphocytes. Science. 2006;314:126-9.
44. Kwong GA, Radu CG, Hwang K, Shu CJY, Ma C, Koya RC, et al. Modular Nucleic Acid Assembled p/MHC Microarrays for Multiplexed Sorting of Antigen-Specific T Cells. Journal of the American Chemical Society. 2009;131:9695-703.
45. Bachmann MF, Wolint P, Schwarz K, Jager P, Oxenius A. Functional properties and lineage relationship of CD8(+) T cell subsets identified by expression of IL-7 receptor alpha and CD62L. J Immunol. 2005;175:4686-96.
46. van Lier RAW, ten Berge IJM, Gamadia LE. Human CD8(+) T-cell differentiation in response to viruses. Nat Rev Immunol. 2003;3:931-8.
47. Pantaleo G, Koup RA. Correlates of immune protection in HIV-1 infection: what we know, what we don't know, what we should know. Nature Medicine. 2004;10:806-10.
48. Ribas A, Comin-Anduix B, Chmielowski B, Jalil J, de la Rocha P, McCannel TA, et al. Dendritic Cell Vaccination Combined with CTLA4 Blockade in Patients with Metastatic Melanoma. Clinical Cancer Research. 2009;15:6267-76.
49. Thorsen T, Maerkl SJ, Quake SR. Microfluidic large-scale integration. Science. 2002;298:580-4.
50. Comin-Anduix B, Lee Y, Jalil J, Algazi A, de la Rocha P, Camacho LH, et al. Detailed analysis of immunologic effects of the cytotoxic T lymphocyte-associated antigen 4-blocking monoclonal antibody tremelimumab in peripheral blood of patients with melanoma. Journal of Translational Medicine. 2008;6.
51. Comin-Anduix B, Gualberto A, Glaspy JA, Seja E, Ontiveros M, Reardon DL, et al. Definition of an immunologic response using the major histocompatibility complex tetramer and enzyme-linked immunospot assays. Clin Cancer Res. 2006;12:107-16.
52. Eisen MB, Spellman PT, Brown PO, Botstein D. Cluster analysis and display of genome-wide expression patterns. Proceedings of the National Academy of Sciences of the United States of America. 1998;95:14863-8.
53. Britten CM, Meyer RG, Kreer T, Drexler I, Wolfel T, Herr W. The use of HLA-A*0201-transfected K562 as standard antigen-presenting cells for CD8(+) T lymphocytes in IFN-gamma ELISPOT assays. J Immunol Methods. 2002;259:95-110.
54. Johnson LA, Morgan RA, Dudley ME, Cassard L, Yang JC, Hughes MS, et al. Gene therapy with human and mouse T-cell receptors mediates cancer regression and targets normal tissues expressing cognate antigen. Blood. 2009;114:535-46.
55. Ribas A, Comin-Anduix B, Chmielowski B, Jalil J, de la Rocha P, McCannel TA, et al. Dendritic cell vaccination combined with CTLA4 blockade in patients with metastatic melanoma. Clin Cancer Res. 2009;15:6267-76.
56. Thuillier G, Malek CK. Development of a low cost hybrid Si/PDMS multi-layered pneumatic microvalve. Microsystem Technologies-Micro-and Nanosystems-Information Storage and Processing Systems. 2005;12:180-5.

57. Michel B, Bernard A, Bietsch A, Delamarche E, Geissler M, Juncker D, et al. Printing meets lithography: Soft approaches to high-resolution patterning. Chimia. 2002;56:527-42.
58. Lange SA, Benes V, Kern DP, Horber JKH, Bernard A. Microcontact printing of DNA molecules. Analytical Chemistry. 2004;76:1641-7.
59. Delamarche E, Bernard A, Schmid H, Michel B, Biebuyck H. Patterned delivery of immunoglobulins to surfaces using microfluidic networks. Science. 1997;276:779-81.
60. Bernard A, Michel B, Delamarche E. Micromosaic immunoassays. Analytical Chemistry. 2001;73:8-12.
61. Ribas A, Camacho LH, Lopez-Berestein G, Pavlov D, Bulanhagui CA, Millham R, et al. Antitumor Activity in Melanoma and Anti-Self Responses in a Phase I Trial With the Anti-Cytotoxic T Lymphocyte–Associated Antigen 4 Monoclonal Antibody CP-675,206. J Clin Oncol. 2005;23:8968-77.
62. Porter DL, Levine BL, Kalos M, Bagg A, June CH. Chimeric Antigen Receptor–Modified T Cells in Chronic Lymphoid Leukemia. New England Journal of Medicine. 2011;365:725-33.
63. Rosenberg SA, Restifo NP, Yang JC, Morgan RA, Dudley ME. Adoptive cell transfer: a clinical path to effective cancer immunotherapy. Nat Rev Cancer. 2008;8:299-308.
64. Restifo NP, Dudley ME, Rosenberg SA. Adoptive immunotherapy for cancer: harnessing the T cell response. Nat Rev Immunol. 2012;12:269-81.
65. June C, Rosenberg SA, Sadelain M, Weber JS. T-cell therapy at the threshold. Nat Biotech. 2012;30:611-4.
66. Turtle CJ, Riddell SR. Genetically retargeting CD8+ lymphocyte subsets for cancer immunotherapy. Curr Opin Immunol. 2011;23:299-305.
67. Rosenberg SA, Yang JC, Sherry RM, Kammula US, Hughes MS, Phan GQ, et al. Durable Complete Responses in Heavily Pretreated Patients with Metastatic Melanoma Using T-Cell Transfer Immunotherapy. Clinical Cancer Research. 2011;17:4550-7.
68. Rosenberg SA, Morgan RA, Dudley ME, Wunderlich JR, Hughes MS, Yang JC, et al. Cancer regression in patients after transfer of genetically engineered lymphocytes. Science. 2006;314:126-9.
69. Rosenberg SA, Johnson LA, Morgan RA, Dudley ME, Cassard L, Yang JC, et al. Gene therapy with human and mouse T-cell receptors mediates cancer regression and targets normal tissues expressing cognate antigen. Blood. 2009;114:535-46.
70. Robbins PF, Morgan RA, Feldman SA, Yang JC, Sherry RM, Dudley ME, et al. Tumor Regression in Patients With Metastatic Synovial Cell Sarcoma and Melanoma Using Genetically Engineered Lymphocytes Reactive With NY-ESO-1. J Clin Oncol. 2011;29:917-24.
71. Appay V, Douek DC, Price DA. CD8+ T cell efficacy in vaccination and disease. Nat Med. 2008;14:623-8.
72. Betts MR, Nason MC, West SM, De Rosa SC, Migueles SA, Abraham J, et al. HIV nonprogressors preferentially maintain highly functional HIV-specific CD8+ T cells. Blood. 2006;107:4781-9.
73. Kwong GA, Radu CG, Hwang K, Shu CJ, Ma C, Koya RC, et al. Modular Nucleic Acid Assembled p/MHC Microarrays for Multiplexed Sorting of Antigen-Specific T Cells. J Am Chem Soc. 2009;131:9695-703.
74. Koya RC, Mok S, Comin-Anduix B, Chodon T, Radu CG, Nishimura MI, et al. Kinetic phases of distribution and tumor targeting by T cell receptor engineered lymphocytes inducing robust antitumor responses. Proceedings of the National Academy of Sciences. 2010;107:14286-91.
75. Ribas A, Timmerman JM, Butterfield LH, Economou JS. Determinant spreading and tumor responses after peptide-based cancer immunotherapy. Trends in Immunology. 2003;24:58-61.
76. Ferrone S, Marincola FM. Loss of HLA class I antigens by melanoma cells: molecular mechanisms, functional significance and clinial relevance. Immunology Today. 1995;16:487-94.

77. Taube JM, Anders RA, Young GD, Xu H, Sharma R, McMiller TL, et al. Colocalization of Inflammatory Response with B7-H1 Expression in Human Melanocytic Lesions Supports an Adaptive Resistance Mechanism of Immune Escape. Science Translational Medicine. 2012;4:127ra37.
78. Landsberg J, Kohlmeyer J, Renn M, Bald T, Rogava M, Cron M, et al. Melanomas resist T-cell therapy through inflammation-induced reversible dedifferentiation. Nature. 2012;490:412-6.
79. Chow MT, Möller A, Smyth MJ. Inflammation and immune surveillance in cancer. Seminars in Cancer Biology. 2012;22:23-32.
80. Seder RA, Darrah PA, Patel DT, De Luca PM, Lindsay RWB, Davey DF, et al. Multifunctional T(H)1 cells define a correlate of vaccine-mediated protection against Leishmania major. Nat Med. 2007;13:843-50.
81. Dudley ME, Yang JC, Sherry R, Hughes MS, Royal R, Kammula U, et al. Adoptive Cell Therapy for Patients With Metastatic Melanoma: Evaluation of Intensive Myeloablative Chemoradiation Preparative Regimens. J Clin Oncol. 2008;26:5233-9.
82. Klebanoff CA, Gattinoni L, Palmer DC, Muranski P, Ji Y, Hinrichs CS, et al. Determinants of Successful CD8+ T-Cell Adoptive Immunotherapy for Large Established Tumors in Mice. Clinical Cancer Research. 2011;17:5343-52.
83. Gattinoni L, Klebanoff CA, Restifo NP. Pharmacologic Induction of CD8+ T Cell Memory: Better Living Through Chemistry. Science Translational Medicine. 2009;1:11ps2.
84. Therasse P, Arbuck SG, Eisenhauer EA, Wanders J, Kaplan RS, Rubinstein L, et al. New Guidelines to Evaluate the Response to Treatment in Solid Tumors. Journal of the National Cancer Institute. 2000;92:205-16.
85. Hultin LE, Chow M, Jamieson BD, O'Gorman MRG, Menendez FA, Borowski L, et al. Comparison of interlaboratory variation in absolute T-cell counts by single-platform and optimized dual-platform methods. Cytometry Part B: Clinical Cytometry. 2010;78B:194-200.
86. Comin-Anduix B, Gualberto A, Glaspy JA, Seja E, Ontiveros M, Reardon DL, et al. Definition of an Immunologic Response Using the Major Histocompatibility Complex Tetramer and Enzyme-Linked Immunospot Assays. Clinical Cancer Research. 2006;12:107-16.
87. Comin-Anduix B, Lee Y, Jalil J, Algazi A, de la Rocha P, Camacho L, et al. Detailed analysis of immunologic effects of the cytotoxic T lymphocyte-associated antigen 4-blocking monoclonal antibody tremelimumab in peripheral blood of patients with melanoma. Journal of Translational Medicine. 2008;6:22.
88. Tumeh PC, Koya RC, Chodon T, Graham NA, Graeber TG, Comin-Anduix B, et al. The Impact of Ex Vivo Clinical Grade Activation Protocols on Human T-cell Phenotype and Function for the Generation of Genetically Modified Cells for Adoptive Cell Transfer Therapy. Journal of Immunotherapy. 2010;33:759-68 10.1097/CJI.0b013e3181f1d644.
89. Sallusto F, Lenig D, Forster R, Lipp M, Lanzavecchia A. Two subsets of memory T lymphocytes with distinct homing potentials and effector functions. Nature.
90. Huang RR, Jalil J, Economou JS, Chmielowski B, Koya RC, Mok S, et al. CTLA4 Blockade Induces Frequent Tumor Infiltration by Activated Lymphocytes Regardless of Clinical Responses in Humans. Clinical Cancer Research. 2011;17:4101-9.
91. Cochran JR, Cameron TO, Stern LJ. The Relationship of MHC-Peptide Binding and T Cell Activation Probed Using Chemically Defined MHC Class II Oligomers. Immunity. 2000;12:241-50.
92. Reynolds DA, Rose RC. Robust text-independent speaker identification using Gaussian mixture speaker models. Speech and Audio Processing, IEEE Transactions on. 1995;3:72-83.
93. Johnson R, Wichern DW. Applied Multivariate Statistical Analysis. 6 ed: Pearson; 2007.
94. Seita J, Weissman IL. Hematopoietic stem cell: self-renewal versus differentiation. Wiley Interdiscip Rev Syst Biol Med. 2010;2:640-53.

95. Forsberg EC, Serwold T, Kogan S, Weissman IL, Passegue E. New evidence supporting megakaryocyte-erythrocyte potential of flk2/flt3+ multipotent hematopoietic progenitors. Cell. 2006;126:415-26.

Abbreviation list: ACT: Adoptive cell transfer; MFI: Mean fluorescence intensity; pSI: polyfunctional strength index; TCR: T cell receptor; CTL: cytotoxic T lymphocyte; TIL: tumor infiltrating T lymphocyte; CAR: chimeric antigen receptor; SCBC: single cell barcode chip; DEAL: DNA encoded antibody library; NACS: nucleic acid cell sorting; PBMC: peripheral blood mononuclear cell; IND: investigator new drug; DC: dendritic cell; FACS: fluorescence activated cell sorting;